

Scuola Internazionale Superiore di Studi Avanzati
International School for Advanced Studies

Solar Neutrinos and Neutrino Properties

Thesis submitted for the degree of
“Doctor Philosophiæ”

CANDIDATE

Mauro Moretti

SUPERVISORS

Prof. R. Barbieri

Prof S.T. Petcov

October 1993

SOLAR NEUTRINOS AND NEUTRINO PROPERTIES

INTRODUCTION

CHAP. 1 NEUTRINO OSCILLATIONS IN VACUUM AND IN MATTER

§1.1 The relevant lagrangean for neutrinos

§1.2 Propagation of a flavour neutrino state in vacuum

§1.3 Relevance of vacuum neutrino oscillations for the solar neutrino problem

§1.4 Matter induced neutrino oscillations

§1.4.1 The propagation of a neutrino in a dense medium

§1.4.2 Forward scattering amplitudes

§1.4.3 Neutrino evolution equations in matter

§1.4.4 The MSW effect

CHAP. 2 SOLAR NEUTRINO EXPERIMENTS AND DETERMINATION OF THE NEUTRINO OSCILLATION PARAMETERS

§2.1 The calculation

§2.2 Confidence regions for neutrino oscillation parameters

§2.3 Energy spectra

§2.4 Charged and neutral current interactions.

§2.5 Berillium neutrinos

§2.6 Conclusions

§2.7 Appendix

CHAP. 3 NEUTRINO SPIN PRECESSION IN A MAGNETIC FIELD

§3.1 The effective lagrangean accounting for neutrino electromagnetic properties

§3.2 Neutrino evolution equations in a magnetic field

§3.3 General properties of neutrino spin precession in a magnetic field and their possible implications for solar neutrinos.

§3.4 The VVO and the hybrid models

§3.5 Do $\bar{\nu}_e$ come out from the sun?

§3.5.1 Bounds on the $\bar{\nu}_e$ flux from kamiokande II background data

§3.5.2 Hybrid models with large mixing angle and solar $\bar{\nu}_e$ flux

CHAP. 4 NEUTRINO OSCILLATION AND MAGNETIC MOMENT TRANSITION IN A MODEL WITH A CONSERVED LEPTON NUMBER

§4.1 The model

§4.2 Flavour oscillations and spin flip in the absence of coherent weak interaction

§4.3 Inclusion of coherent weak interaction

§4.3.1 The adiabatic and the sudden regions

§4.3.2 The adiabatic and the sudden solutions

§4.3.3 Discussion

§4.4 Conclusions

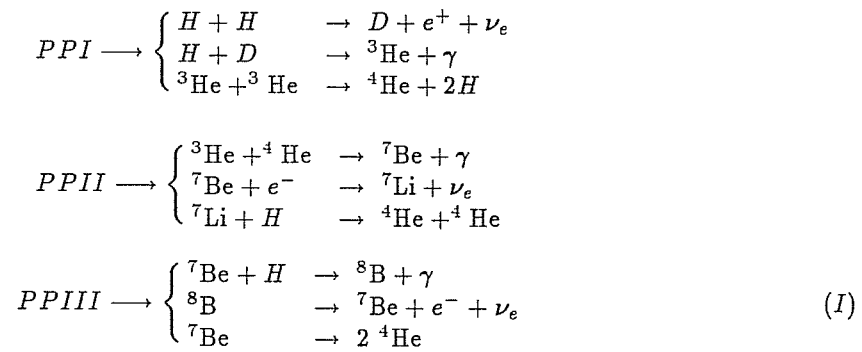
CHAP. 5 NEUTRINO DECAY

§5.1 The Decay Solution to the Solar Neutrino Problem

§5.1.1 Neutrino decay with majoron emission	
§5.1.2 The decay solution to the SNP revisited	-
§5.1.3 Solar antineutrino signal	
§5.1.4 Other mechanisms of solar antineutrino production	
§5.2 Matter induced neutrino decay and solar antineutrinos	
§5.2.1 Dynamics of matter-induced decay	
§5.2.2 Neutrino decay in solar medium	
§5.2.3 Antineutrino signal	

INTRODUCTION

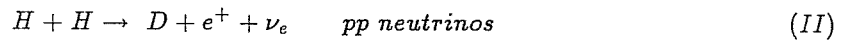
It is commonly accepted that stars, due to their long mean lifetime, are systems in hydrostatic * equilibrium. Since stars continuously emit energy (in the form of radiation or particles, with velocity higher than the escape velocity) a mechanism for the energy production must be active in the star. The other key ingredients to describe the stellar evolution are nuclear combustions, which provide energy, and the energy transport mechanism. If we limit our attention to stars being in an evolutive stage which is typical of the sun, the main contribution to the energy production is due to the so called PP chains of reactions



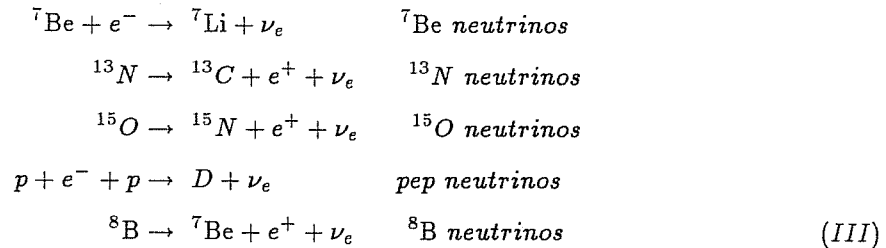
The relative importance of each of these chains depends on the temperature in the core of the star.

Once the mechanisms for energy transport are known, the evolution equation for the state of the star can be determined. This equation links together the macroscopic variables of the system (luminosity, mass, temperature, pressure) and the microscopic mechanisms which determine them (energy transport and nuclear reactions). Given the equation of state and the initial conditions (luminosity, mass, the temperature at the surface of the sun) it is possible to determine the complete state of the system. In particular it is possible to determine the reaction rates for (I) and consequently the neutrino fluxes.

The main source of the solar neutrino flux is the reaction:



Electron neutrinos are produced also in the following reactions:



* For a description of the theoretical models of stellar evolution see, for example, [1]

The reactions (III) are essentially negligible from the point of view of energy production, and the corresponding neutrino fluxes are much smaller in comparison with those due to reaction (II). However, ${}^7\text{Be}$ and ${}^8\text{B}$ neutrinos are easier to detect due to their higher energies. The spectra of the different components of the solar neutrino flux are shown on fig. I.1. Notice that the total fluxes of the pp , ${}^7\text{Be}$, ${}^8\text{B}$, pep and CNO neutrinos depend on the conditions in the neutrino production region in the sun [2]. On the contrary, the shape of the spectra of pp , ${}^8\text{B}$ and CNO neutrinos is independent of the solar physics: it is determined only by the nuclear processes in which the corresponding neutrinos are produced and it is known with a very good accuracy.

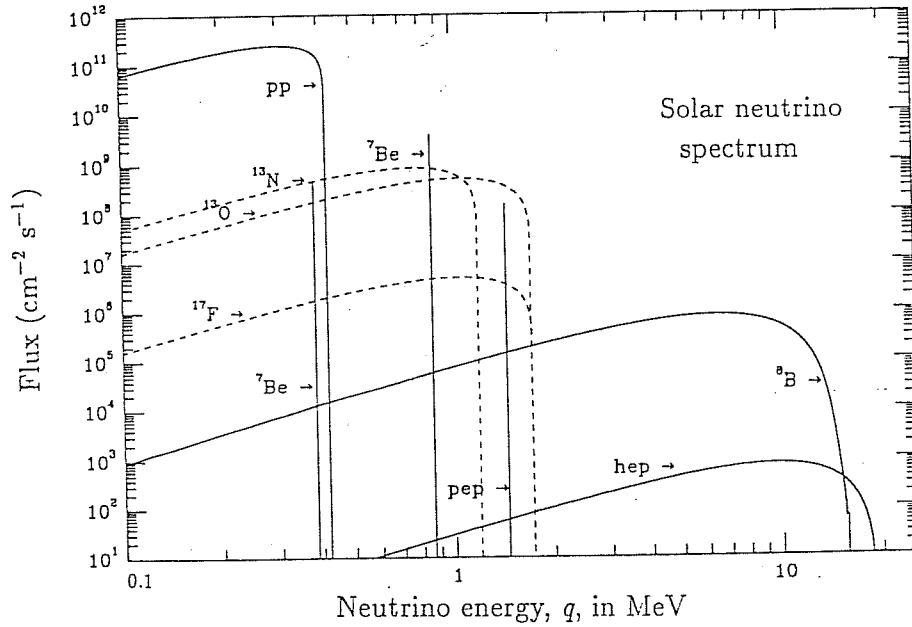


Fig. I.1 Solar neutrino spectrum. The neutrino fluxes from continuous sources are given as number per cm^2 per second per MeV. The line fluxes are given as number per cm^2 per second [3].

The predicted total fluxes are [2]:

$$\begin{aligned}
 \Phi_{pp} &= 6.00(1 \pm 0.02) 10^{10} \text{cm}^{-2} \text{sec}^{-1} \\
 \Phi_{{}^7\text{Be}} &= 4.89(1 \pm 0.18) 10^9 \text{cm}^{-2} \text{sec}^{-1} \\
 \Phi_{{}^8\text{B}} &= 5.69(1 \pm 0.43) 10^6 \text{cm}^{-2} \text{sec}^{-1} \\
 \Phi_{pep} &= 1.43(1 \pm 0.04) 10^8 \text{cm}^{-2} \text{sec}^{-1} \\
 \Phi_{{}^{15}\text{O}} &= 4.26(1 \pm 0.58) 10^8 \text{cm}^{-2} \text{sec}^{-1} \\
 \Phi_{{}^{13}\text{N}} &= 4.92(1 \pm 0.51) 10^8 \text{cm}^{-2} \text{sec}^{-1}
 \end{aligned}
 \tag{IV}$$

where all the errors are estimated to be effective 3σ errors in [2].

According to the present day views about how the sun "works", embodied in the standard solar model (SSM), neutrinos are produced in spherical regions centered around the solar center. The dimensions of these regions are different for the different neutrinos: pp neutrinos are produced in a region with a radius $R \simeq 0.20R_{\odot}$, $R_{\odot} = 6.95 \times 10^5$ km being the solar radius, ${}^7\text{Be}$ neutrinos in a region of radius $R \simeq 0.13R_{\odot}$ and ${}^8\text{B}$ neutrinos in a region of radius $R \simeq 0.08R_{\odot}$. The differential rates of productions of the pp , ${}^7\text{Be}$ and ${}^8\text{B}$ neutrinos as functions of the distance from the centre of the sun are shown on fig. I.2.

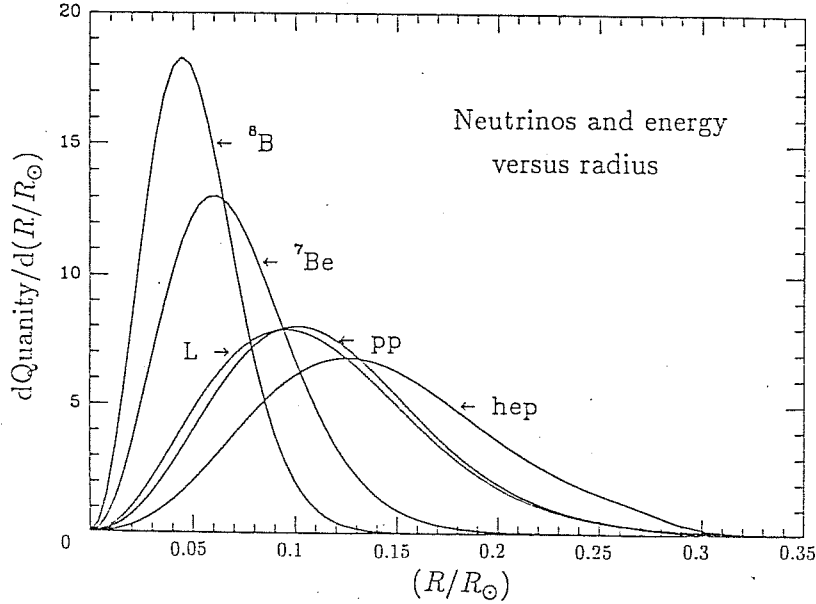
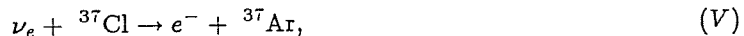


Fig. I.2. Neutrino and Energy production as a function of radius. The fraction of neutrinos that originate in each fraction of the solar radius is $[d\text{Flux}/d(R/R_{\odot})]d(R/R_{\odot})$. The figure illustrates the production fraction for ${}^8\text{B}$, ${}^7\text{Be}$, pp and hep neutrinos. The fraction of solar luminosity that is produced at each radius is denoted by L [3].

To our knowledge, the story of solar neutrinos begins in 1946 with the famous Chalk River Laboratory report PD-205 by B. Pontecorvo [4]. In it Pontecorvo suggested that the nuclear reactors and the sun are powerful sources of neutrinos. On the basis of flux and cross section estimates he concluded that the experimental detection of the reactor neutrinos is feasible, while the detection of solar neutrinos might be very difficult, but not impossible. In the same article the radioactive methods of neutrino detection in general and, more specifically, the Cl-Ar method, were proposed. As it is well known, neutrinos indeed were first detected in an experiment performed at a nuclear reactor by Reines and Cowan in 1956 [5]. It took much longer time preparing and beginning an experiment to detect the solar neutrinos.

At Homestake R. Davis together with his collaborators are performing an experiment running since 1968 [6]. This experiment exploits the Cl-Ar radiochemical method for detection of solar neutrinos of Pontecorvo. The method is based on the reaction



which has a threshold energy of 0.816 MeV. Due to the energy threshold and to the fact that the cross-section is strongly increasing with the neutrino energy, the Homestake experiment is predicted to be sensitive mainly to ${}^8\text{B}$ (about 75 % of the signal) and ${}^7\text{Be}$ (about 15 % of the signal) neutrinos. Notice that this experiment is not sensitive at all to the most abundant pp neutrinos whose end-point energy is 0.420 MeV.

The experimental set up consists of a tank of 615 tons of liquid tetrachloroethylene, C_2Cl_4 , placed underground to reduce background from cosmic radiation at an acceptable level. The overall shielding corresponds to about 4400 m of water equivalent. The ${}^{37}\text{Ar}$ atoms counting is performed removing the atoms from the tank and observing the radioactive decay of ${}^{37}\text{Ar}$ (with an half-life of 35 days) in a small proportional counter chamber. The half-life of ${}^{37}\text{Ar}$ determines the exposure time which is about 60 days.

The average ${}^{37}\text{Ar}$ production rate, $R_{exp}(\text{Ar})$, in the Homestake experiment, during 20 years of measurements, reads [7]:

$$R_{exp}(\text{Ar}) = 2.33 \pm 0.25 \text{ SNU} \quad (VI)$$

(1 SNU is 10^{-36} captures per target atom per second) which corresponds to approximately half an atom of ${}^{37}\text{Ar}$ produced per day and to a counting of 10-15 atoms per run. In more than 20 years of operation Homestake experiment collected about 750 ${}^{37}\text{Ar}$ atoms.

The predicted capture rate in the Cl-Ar experiment has been calculated by many authors. We give below the results obtained within the SSM by Bahcall and Pinsonneault [2], R^{BP} , and by S. Turk-Chieze et al. [8], R^T ,

$$\begin{aligned} R^{BP}(\text{Ar}) &= 8.0 \pm 3.0 \\ R^T(\text{Ar}) &= 6.4 \pm 4.2 \end{aligned} \quad (VII)$$

where the quoted errors are estimated to be effective 3σ errors taking into account both theoretical uncertainties and uncertainties in the experimentally determined quantities which enter in the computation.

The difference between the predicted rates gives an idea about the astrophysical uncertainties in the calculations. We have chosen to quote this two particular results since all the other existent results [9, 10] give predictions which lie in between the quoted (VI) one. Let us add that in the calculation performed in [2] the helium diffusion in the sun was taken into account. This is the only existent calculation which embodies this effect in the evolutionary code (the typical effect is to increase the calculated ${}^8\text{B}$ neutrino flux by about 10 %)

The discrepancy between the theoretical prediction (VII) and the experimental result (VI) constitutes the essence of the so called "Solar Neutrino Problem" (SNP).

It was suggested that the Homestake data are anticorrelated with the eleven years solar semicycle [7]. One way to see the correlation is to compare the signals at the maxima and minima of the solar activity. Averaging over the two semicycles, during which Homestake detector has taken data, the reported signals are [7]:

$$\begin{aligned} S_M^{(D)} &= 0.8 \pm 0.3 \text{ SNU} \\ S_m^{(D)} &= 4.1 \pm 0.6 \text{ SNU} \end{aligned} \quad (VIII)$$

where $S_{M,m}^{(D)}$ is the signal detected at the maximum (minimum) of solar activity

In 1986 another experiment begun a systematic measurements of the solar neutrino flux. The Kamiokande II collaboration [11] developed a water Cherenkov detector which can detect the elastic scattering of solar neutrinos on electrons,

$$\nu_e e^- \rightarrow \nu_e e^- \quad (IX)$$

The reaction (VI) is always kinematically allowed. However for technical reasons an effective threshold of 7.5 MeV (it was 9.3 MeV in the earlier stage of the experiment [12]) is used in the analysis of the data. Due to the large threshold energy only ^8B neutrinos contribute to the signal in the Kamiokande detector.

The experimental set up consists of a 3,000 tons water Cherenkov detector surrounded by 950 photomultipliers. Only the most inner 680 tons of the detector are used as fiducial volume for the solar neutrino detection. The neutrino counting proceeds through the collection of the Cherenkov light emitted by the scattered electrons. The amount of produced Cherenkov light is proportional to the energy of the emitting electron and this allows to measure also the electron energy. Moreover, the Cherenkov light keeps track of the direction of the momentum of emitting electron giving the possibility to reconstruct the direction of the electron momentum. Since the electron momentum is correlated with the incoming neutrino momentum it is possible to measure also the neutrino momentum.

The result of the first and second period of data taking (Kamiokande II collaboration) starting from January 1987 to March 1990 is [13]:

$$\Phi_{^8\text{B}} = 2.67 \pm 0.29 \text{ (stat.)} \pm 0.35 \text{ (sist.) } 10^6 \text{ cm}^{-2} \text{ sec}^{-1}, \quad (X)$$

where $\Phi_{^8\text{B}}$ is the integral ^8B neutrino flux and the value is obtained assuming the SSM prediction for the neutrino spectrum. The result (VII) corresponds to the detection of about 240 neutrinos from the sun. The detector was subsequently upgraded (to become Kamiokande III) and the combined Kamiokande II and Kamiokande III * result is [14]

$$\Phi_{^8\text{B}} = 2.84 \pm 0.29 \text{ (stat.)} \pm 0.35 \text{ (sist.) } 10^6 \text{ cm}^{-2} \text{ sec}^{-1} \quad (XI)$$

* The Kamiokande III collaboration reported results based on data taken December 1990 to August 1992

In total about 350 solar neutrino induced events have been collected.

The predictions for the ${}^8\text{B}$ neutrino flux are

$$\begin{aligned}\Phi_{\text{sB}}^{BP} &= 5.7(1 \pm 0.43) 10^6 \text{cm}^{-2} \text{sec}^{-1} \\ \Phi_{\text{sB}}^T &= 4.4 \pm 3.3 10^6 \text{cm}^{-2} \text{sec}^{-1}\end{aligned}\quad (XII)$$

where, again, the BP subscript refer to Bahcall and Pinsonneault calculation, the T subscript refer to S. Turk-Chieze et al. calculation, and the error is an estimated effective 3σ error. Therefore we can conclude that the Kamiokande experiments have reinforced the case of the Solar Neutrino Problem.

The Kamiokande II-III collaboration have searched for an eventual correlation of the solar neutrino flux with the solar activity. They do not observe such an anticorrelation within a 30% accuracy [13, 14] Finally two collaboration, SAGE [15] and GALLEX [16], begun two different radiochemical experiments, based on the detection of the same reaction



which has a threshold energy of 0.233 MeV. The low energy threshold implies that these experiments are mainly sensitive to the most abundant pp neutrinos (about 55 % of the predicted signal) and ${}^7\text{Be}$ neutrinos (about 25 % of the predicted signal), with a small contribution coming from ${}^8\text{B}$ neutrinos (about 10 % of the predicted signal). Let us recall here that the predictions for the pp neutrino flux are essentially free from theoretical uncertainties being directly related to a measured quantity, the solar luminosity.

The SAGE experiment uses 60 tons (30 in the first stage of operation) of metal gallium placed in a tunnel under Mount Andyrchi in Caucasus region. The overall shielding is about 4700 m of water equivalent. The ${}^{71}\text{Ge}$ is removed by a weak hydrochloridric acid solution mixed with the gallium in the presence of hydrogen peroxide, which results in extraction of germanium in the aqueous phase. The extracted solution containing ${}^{71}\text{Ge}$ is placed in a proportional counter where the low-energy K- and L-shell Auger electrons and X rays produced during the decay are detected. The experiment begun in may 1988. However, due to a strong contamination of ${}^{68}\text{Ge}$ produced by cosmic rays when the gallium was on the earth surface, the data taking begun in January 1990, after almost all the ${}^{68}\text{Ge}$ atoms decayed. The result S_5^{90} for the period January 1990 - July 1990 (published at the end of 1991) is [17]:

$$S_5^{90} = 20_{-20}^{+15} \text{ (stat)} \pm 32 \text{ (syst)}. \quad (XIV)$$

It was obtained using 30 tons of gallium and analyzing only the data in the K peak (the background in the L peak being larger than the signal). In August 1992, after the publication of the first GALLEX result, the SAGE collaboration announced a new, preliminary, result based on data taken the period June-December 1991. The announced result is [18]:

$$S_5^{91} = 85_{-32}^{+22} \text{ (stat)} \pm 20 \text{ (syst)} \quad (XV)$$

and combining the two sets of data the following average value is obtained

$$S_S = 58_{-24}^{+17} \text{ (stat)} \pm 14 \text{ (syst)}. \quad (XVI)$$

The measurements in 1991 were performed using 57 tons of metal gallium and again using only the data from the K peak. The whole set of data correspond to the observation of 25 ^{71}Ge atoms.

The GALLEX experiment uses 30 tons of an aqueous solution of gallium acidified with HCl , placed in the underground Laboratori Nazionali del Gran Sasso. The volatility of GeCl_4 allows it to be separated from the non-volatile GaCl_3 by bubbling an inert gas through the solution. The extracted germanium is then placed in a proportional counter and its quantity is measured. An important feature is that both L and K peak data can be used for the analysis essentially allowing a double number of counts. The result, S_G , obtained by the GALLEX collaboration after eleven months of data taking (May 1991 March 1992, altogether 14 runs) was published in June 1992 and reads [19]:

$$S_G^a = 84 \pm 19 \text{ (stat)} \pm 8 \text{ (syst)}. \quad (XVII)$$

This result is remarkable since it provides the first observation of the neutrinos from the pp chain, which, as we have already discussed, is the source of the energy of the sun. In this manner, the GALLEX observations confirm a basic element in the theory of stellar evolution.

Subsequently [20] in ~~1993~~ ^(August-February) the result for additional six months ~~(??)~~ of data taking was announced. The average result reads:

$$S_G = 87 \pm 13 \text{ (stat)} \pm 8 \text{ (syst)}, \quad (XVIII)$$

which corresponds to about 75 ^{71}Ge counts.

Let us notice here that the two collaboration plan to perform calibration experiments in 1994 using calibration sources of one megacurie of ^{51}Cr . This will allow a direct measurement of the extraction efficiency.

The predicted signal according to the SSM is [2, 8]:

$$\begin{aligned} S_{Ga}^B &= 132_{-17}^{+15} \text{ SNU} \\ S_{Ga}^T &= 123 \pm 21 \text{ SNU} \end{aligned} \quad (XIX)$$

where the meaning of the subscripts and of the quoted errors is the same as in eq. (XII). Notice that the uncertainty in the predicted signal is much lower than for the other experiments since, as we have already emphasized, the prediction for the pp neutrinos flux is almost free from theoretical uncertainties.

The first results of the Ga-Ge experiments published in 1991-1992 made it clear that the data of the first generation of solar neutrino detectors (Homestake, Kamiokande II-III, GALLEX, SAGE) will not be sufficient to resolve the solar neutrino problem which exists since the second half of 70ies. In principle, there can be two, very different, potential sources of the discrepancy between the solar neutrino observations and the corresponding predictions based on the SSM. First, it is impossible, at present, to exclude the possibility that the current SSMs do not predict correctly the ^8B and

${}^7\text{Be}$ fluxes (this possibility is conventionally referred to as astrophysical solution). However, it was shown recently, on the basis of very general arguments, that, if the solar neutrino data (VI), (XI) and (XVIII) are correct, an astrophysical solution of the solar neutrino problem is very unlikely (if not excluded) [10, 21]. Second, the SNP can be ascribed to the existence of unconventional neutrino properties (neutrino physics solutions). This second possibility is the main subject of investigation in the present thesis.

If neutrinos have unconventional properties, the solar electron neutrinos can take part in a number of physically rather different processes when they travel from the central part of the sun to the surface of the Earth. They can undergo:

- i) Neutrino Oscillations in Vacuum into different weak eigenstate neutrinos (ν_μ and/or ν_τ and/or sterile neutrinos ν_s), on their way from the surface of the sun to the earth [22-24],
- ii) Matter-Enhanced Transitions, $\nu_e \rightarrow \nu_\mu, \nu_\tau, \nu_s$ while they propagate from the center to the surface of the Sun [25, 26],
- iii) Spin or Spin-Flavour Precession in the magnetic field of the sun [27-29],
- iv) Decay into a lighter neutrino and a very light or massless scalar particle $\nu_e \rightarrow \nu' + \varphi$ [30].

The vacuum oscillations $\nu_e \leftrightarrow \nu_{\mu, (\tau, s)}$ and the matter-enhanced (MSW) transitions $\nu_e \rightarrow \nu_{\mu, (\tau, s)}$ can take place if neutrinos have nonzero masses and lepton mixing occurs in the weak charged lepton current. The matter-enhanced transitions of the solar neutrinos can be generated by neutrino changing neutral current interaction and flavour diagonal but flavour nonsymmetric neutrino interactions with the ordinary matter [31] even in the absence of lepton mixing [32, 33] and neutrino masses [32]. Neutrino decay is possible only if neutrinos are massive, lepton mixing occurs and if neutrinos are coupled to an almost massless scalar.

All these possibilities have been thoroughly studied in the literature and they appeal to physics beyond the Standard Theory of Strong and Electroweak Interaction or Standard Model (SM) and most of them imply that neutrinos are massive and that lepton mixing exists.

The existence of nonzero neutrino masses and lepton mixing is closely associated, according to the gauge theory of electroweak interactions and its possible extensions, with the non conservation of the global lepton charges L_e, L_μ, L_τ .

The hypothesis of massive neutrinos can be implemented with only minor modification of the SM, namely with the introduction of right-handed neutrino states. However, this option leaves unexplained the smallness of neutrino mass with respect to the quark and the lepton masses of the same family. Basically only two known mechanism of neutrino mass generation provide an explanation of the smallness of neutrino mass: the see-saw mechanism [34] and the radiative one (a well known example of the second one is the Zee model [35]). In many extension of the SM and in particular Grand Unified Theories (GUT) like SO(10), non minimal SU(5) and string inspired low energy effective theories these mechanisms are naturally implemented and a small neutrino mass appears.

In the see-saw mechanism the active neutrinos are supposed to mix with sterile partners. The smallness of neutrino masses is connected to the existence of a fundamental scale M much large than the electroweak scale (M can be either the scale of the unification of strong and electroweak

interactions or some intermediate scale of the theory like the left-right symmetry breaking scale). The typical size of the active neutrino mass appearing in these models is M_W^2/M . In the radiative mechanism of neutrino mass generation it is assumed that neutrino masses are zero at the tree-level. They arise only as radiative corrections which are vanishing in the limit of zero mass of the charged lepton (or more seldomly of the quarks). This naturally implies a hierarchy among the neutrino masses and the charged lepton masses.

In addition to massive neutrinos, the hypothesis that neutrinos have a magnetic moment large enough to affect the evolution of solar neutrinos requires the introduction either of new spontaneously broken gauge symmetries [36], addressing therefore the issues of the hierarchy of lepton masses and of the family structure of the SM, and/or the introduction of a non trivial pattern of scalar particles with masses quite close to the electroweak scale [37].

Finally, the neutrino decay hypothesis requires again massive neutrinos. In addition an almost massless scalar is needed. Barring fine tuning of the parameters the only possible candidate is a Goldstone boson [38] which can typically be associated with the spontaneous breaking of the lepton number symmetry. Therefore in this case also a spontaneous breaking of a global symmetry plays an important role.

From the previous discussion it should be clear that the solar neutrino experiments are testing the fundamental symmetries of the electroweak interactions and are searching for effects beyond these predicted by the Standard Model. As it was indicated earlier, our hopes for understanding the origin of the SNP are associated with the next generation of solar neutrino experiments, some of which will become operative in 1995-1996. We shall next briefly discuss the planned capabilities of three of these experiments: SNO, Super Kamiokande and Borexino. The next generation detectors have all the common feature to be high-statistic experiments with respect to the first generation experiments (Chlorine, Kamiokande, Gallium) for which a few hundreds of events have been collected in several years of operations. Moreover all these three experiments are real time experiments in contrast to to the radiochemical experiments (Cl-Ar and Ga-Ge).

At the end of 1995 two experiments, SNO [39] and Super Kamiokande [40], are expected to be operative and to have the capability to measure the neutrino spectra. Super Kamiokande is essentially an enlarged (50,000 tons of water, corresponding to about 22,000 tons of fiducial volume) version of the existent Kamiokande detector. SNO will be a Cherenkov detector using 1,000 tons of heavy water designed for the detection of e^- from the reaction $\nu_e + D \rightarrow e^- + p + H$. Both collaboration plan to have an effective threshold for the electron kinetic energy of about 5 MeV and therefore they will be sensitive to ^8B neutrinos only. The predicted events rate for this two detector is approximately 10^4 neutrino scattering per year. Since we already know from Kamiokande II-III results that the observed capture rate cannot be lower than $2 \div 3$ times the predicted one we are left with at least a few thousands events per year.

At the end of 1996 Borexino [41] detector is expected to be operative. The aim of this detector is the measurement of the strength of the Berillium line with an impressive statistic (the predicted rate is 50,000 events per year). The neutrino counting is again performed through the detection of scattered e^- which are however revealed trough their scintillator light. Borexino is expected to

detect the electron from $\nu_e e^-$ elastic scattering up to a recoil electron energy of about 250 KeV. Due to the large number of events this detector is expected to have a strong capability to reveal neutrino mixing in vacuum in the case of large mixing angles for Δm^2 in the range $10^{-7} \div 10^{-11}$ (eV)². In principle one expects that the information about the ⁷Be line strength measurements will have a great impact also in the analysis of the matter induced neutrino oscillations. In fact in combination with SNO and Super Kamiokande, which determine the ⁸B neutrino flux and with GALLEX and SAGE which measure a combination of pp , ⁷Be and ⁸B neutrino fluxes, the determination of ⁷Be neutrino flux should allow the determination of the pp component of the spectra which is almost completely independent of the solar model (only 2 % h).

Finally in a second stage SNO detector will also attempt to measure the total content of active neutrinos coming from the sun irrespective of their flavour exploiting the reaction $\nu_x + D^2 \rightarrow \nu_x + n + H$ which is mediated by the Z boson exchange and require only the presence of an active neutrino. The detection will be performed through the observation of the γ rays released in the capture of the free neutron by the target material. This reaction is conventionally referred as neutral current reaction in literature while the previously discussed $\nu_e + D \rightarrow e^- + p + p$, being mediated by the W^+ boson, is usually referred as charged current reaction. The predicted rate for the neutral current reaction is about 2×10^3 events per year.

The present thesis is mainly devoted to the analysis of the neutrino physics solutions of the solar neutrino problems.

In CHAPTER 1 we review the theory of the neutrino oscillations in vacuum [22] and the theory of neutrino oscillations in matter (MSW effect) [25, 26]. These theories represent the basic technical ingredients of the original results described in the subsequent chapters. We discuss also the current status of the vacuum oscillation solutions of the SNP and review, qualitatively, the solutions based on the idea of matter-enhanced neutrino transitions.

In CHAPTER 2 we analyze [42] the MSW solution of the SNP. The system of evolution equations for neutrinos crossing the solar matter is solved numerically. We determine the regions of values of the relevant parameters, characterizing the neutrino transition in the sun, for which the predicted signals agree with the experimental data (Homestake, Kamiokande, GALLEX and SAGE results). The computation is repeated using both Bahcall and Pinsonneault and Turk-Chieze et al. prediction to study the effect of the theoretical uncertainties. We then concentrate on the expected results from the future detectors with particular emphasis on the measurements of the neutrino spectra, of the ⁷Be line and of the neutral to charged current ratio.

Using χ^2 analysis we compute the region of parameters where a detectable distortion of the spectrum will take place. This information is completely independent from the standard model and therefore it allows to study neutrino properties without any reference to the source strength.

We then study the impact of the measure of ⁷Be neutrinos flux in testing the MSW hypothesis. To this end we assume for the experimental errors the ultimate errors which are expected in 1997 for the Kamiokande, Chlorine and Gallium experiments.

Finally we concentrate our attention on the neutral to the charged current ratio. We determine the region of parameters where a charged to neutral current ratio significantly (larger than the detectors sensitivity) different from one arises.

Particular emphases is given to the relevance of these signal in the region of parameters allowed for the solution of the SNP.

In CHAPTER 3 we discuss the hypothesis that neutrinos have unusual electromagnetic properties, such as an electric dipole moment or a magnetic moment. In this case the interaction of neutrinos with the solar magnetic field can induce the transition of the left-handed electron neutrino into a right-handed neutrino state either sterile (right-handed electron neutrino) or active (right-handed muon or tau antineutrino) [27, 28]. The main interest in this effect is due to the fact that it can explain the suggested correlation of the signal with the solar activity [28].

To understand if neutrino spin-flip can be effective in the sun it is crucial to determine the magnitude of the neutrino magnetic moment and the solar magnetic field which are required in order that observable effects can occur. The answer to this problem is connected with the magnetic field spatial shape which is unknown and in principle arbitrarily complicated. This has lead in the past to some conceptual misunderstanding. We derive [43] a rigorous lower bound on the magnitude of the product of neutrino magnetic moment and the solar magnetic field which is required in order that a given spin-flip precession takes place for solar neutrinos.

The solar neutrino data can be described in particular using the so called "hybrid models" where it is assumed that the spin-flavour conversion is assisted by vacuum oscillations or the MSW effect. A very important predictions of this class of models is the existence of a $\bar{\nu}_e$ component in the solar neutrino flux. It arises as a result of the interplay of flavour $\nu_e \rightarrow \nu_x$ transitions and spin-flip $\nu_e \rightarrow \bar{\nu}_x$ transitions. Using the data of Kamiokande II experiment which can detect $\bar{\nu}_e$ via the reaction $\bar{\nu}_e + p \rightarrow n + e^+$, we derive [44] a stringent upper limit on the $\bar{\nu}_e$ component of the solar ν_e flux. This upper bound rules out the class of two neutrinos hybrid models which require large lepton mixing in vacuum.

In CHAPTER 4 we propose [45] an alternative hybrid model which is qualitatively compatible with the data and is free from some internal theoretical inconsistency typically characterizing the hybrid models. We consider all the three neutrino flavors and we assume that the lepton number $L_e + L_\tau - L_\mu$ is conserved. The particle spectrum of this model consists of one massive Dirac neutrino and one massive Weyl neutrino. An unquenched spin flip can occur between the left and right helicity states of the Dirac neutrino while oscillation, can occur between the Dirac neutrino and the Weyl one. The model we propose requires only one mass scale and does not predict $\bar{\nu}_e$ production.

Then we study the neutrino evolution problem postulating that the magnetic field is present only in the convective zone. We examine in detail the evolution equations for the neutrinos looking in particular at the condition under which the neutrino evolution is adiabatic or non adiabatic. This discussion is valid also beyond the specific contest in which is made.

In CHAPTER 5 we consider the possibility that solar neutrinos decay on the way to the earth [30]. Since the fast radiative decay is excluded both from particle physics and astrophysical arguments, one has to consider "fast" invisible neutrino decay.

The observation of the $\bar{\nu}_e$ pulse from SN1987A [11, 46] rules out the neutrino decay solution of SNP with negligible neutrino mixing [30], which requires a ν_e (we remark that, in vacuum, the decay properties of ν_x and $\bar{\nu}_x$ are the same, namely $\Gamma_\nu = \Gamma_{\bar{\nu}}$) decay length adjusted to the sun-earth distance. However, the case [47, 48] when the neutrino mixing angle α is substantial remains an open possibility.

We determine [49] the allowed region of parameters which could explain the Homestake and Kamiokande solar neutrino data. We obtain also the prediction for Gallium detectors. The comparison of this prediction with the recent GALLEX results shows that this scenario is strongly disfavoured. One of the central phenomenological feature of this scenario is the appearance of a substantial flux of solar $\bar{\nu}_e$. We examine the perspective for the detection of this signal.

Matter effects can drastically alter the properties of neutrino decay [47]. In particular in matter the $\nu_e \rightarrow \bar{\nu}_e + \chi$ (χ is a light scalar) decay become possible. In the second half of CHAPTER 5 we revisit [50] in great detail the characteristic of the matter induced neutrino decay (decay amplitudes, kinematics, energy distribution of the decay products) and we examine the perspective for the possibility to detect this interesting signal.

CHAP. 1

NEUTRINO OSCILLATIONS IN VACUUM AND IN MATTER

We now consider the possibility that neutrinos are massive. Generally neutrino flavour eigenstates do not coincide with mass eigenstates. Neutrinos produced in weak processes, therefore, are linear superpositions of neutrinos with different masses. During the propagation the mass splitting among the different neutrinos induces a phase shift among the neutrinos with different masses. Due to this phase shift the flavour content of the initial neutrino depends on time. This physical possibility is called neutrino oscillations [22].

If neutrinos are moving inside a dense medium neutrino evolution can be substantially modified. Even neglecting neutrino scattering, the coherent interference of the forward scattering amplitude with the unscattered wave modifies the dispersion relations for the neutrino. This can induce an effective mixing angle in matter strongly different from the vacuum mixing angle [25].

The occurrence of both type of oscillations can influence the flavour content of neutrinos coming from the sun.

In the case of vacuum oscillations two quite different possibilities can occur:

a) if the oscillation length is adjusted to be of the same order of magnitude of the sun earth distance (just-so oscillation) [23, 52, 53], it is possible to observe the oscillations with energy of the flavour content of the incoming neutrinos. The survival probability for the flavour of the initial neutrino can be as small as zero. In this case the modification of the spectrum of electron neutrino coming from the sun depends on the neutrino energy and experiment with different thresholds are expected to detect different signals [53].

b) for oscillation length smaller than the sun earth distance the energy resolution of the detectors average over the oscillating term and its net contribution to the signal is negligible. In this case it is expected an energy independent modification of the spectrum and the survival probability for the flavour of the initial neutrino is fixed and larger than $1/N$, N being the number of neutrinos involved in the oscillations. The only possible difference arises among the experiments which employ different reactions to reveal neutrinos due to the contribution of neutral current interactions. In this case no oscillation at all is observed, however, also this case is almost always referred as neutrino oscillation in the literature.

In matter, for squared mass splitting in the range $10^{-4} \div 10^{-8 \div 9}$ (eV)² the effective mixing become maximal in some region inside the sun core independently of the vacuum mixing angle [26]. The $\nu_e \rightarrow \nu_x$ transition probability is energy dependent and even with small vacuum mixing angle can be large. Also in this case experiments with different threshold energies are expected to give different results.

Given the present experimental situation and understanding of the solar dynamic both the hypothesis can explain the solar neutrino problem and are compatible with the experimental results. Vacuum oscillations require large mixing angle and just-so oscillations, in addition, require a very specific mass splitting. On the contrary matter oscillations can occur with both large and small

vacuum mixing angles and for a rather wide mass range, avoiding the fine tuning of the relevant parameters.

Neutrinos can be either Dirac or Majorana particles. For relativistic neutrinos the description of neutrino oscillation is the same in both cases (neglecting correction of order m_ν/E_ν , m_ν and E_ν being the neutrino mass and energy respectively); therefore we shall consider for definiteness Majorana neutrinos.

§1.1 The Relevant Lagrangean for Neutrinos

For simplicity we limit the discussion to only two neutrinos since the extension to three (or more) neutrinos is straightforward. In terms of the flavour neutrino fields, the kinetic term of the lagrangean density for neutrinos is

$$\begin{aligned} \mathcal{L} = & i\bar{\nu}_e(x)\gamma_\alpha\partial_\alpha\nu_e(x) + i\bar{\nu}_\mu(x)\gamma_\alpha\partial_\alpha\nu_\mu(x) \\ & + \frac{1}{2}(m_{ee}\nu_e^T(x)C\nu_e(x) + m_{e\mu}\nu_e^T(x)C\nu_\mu(x) \\ & + m_{\mu e}\nu_\mu^T(x)C\nu_e(x) + m_{\mu\mu}\nu_\mu^T(x)C\nu_\mu(x) + h.c.) \end{aligned} \quad (1.1)$$

where C is the charge conjugation matrix and ν_x are left-handed spinor fields. Due to the relation $C = -C^T$ and to the anticommutation of the spinor fields we get $m_{e\mu} = m_{\mu e}$. Out of the three complex phases in m_{ee} , $m_{\mu\mu}$ and $m_{e\mu}$ two can be reabsorbed redefining the phases of ν_e and ν_μ and these phases can be eliminated from the lagrangean of the standard model using the freedom of redefining the phases of the electron and muon fields which are unobservable. Only one phase is physically relevant in the lagrangean (1.1) [54]. This CP violating phase does not exist in the case of Dirac neutrinos, however as we shall see it is irrelevant in the description of neutrino oscillations. For convenience we redefine the mass parameters in (1.1) as follows:

$$\begin{aligned} m_{ee} &= m_e e^{2i\delta} \\ m_{\mu\mu} &= m_\mu e^{-2i\delta} \\ m_{e\mu} &= m \end{aligned} \quad (1.2)$$

where m_e , m_μ , m and δ are real positive parameters.

Given the lagrangean (1.1) the neutrino mass eigenstates are the Majorana fields ν_1, ν_2 :

$$\begin{aligned} \nu_1 &= e^{i\delta}(\cos\alpha\nu_e + \sin\alpha\nu_\mu) \\ \nu_2 &= e^{-i\delta}(-\sin\alpha\nu_e + \cos\alpha\nu_\mu) \end{aligned} \quad (1.3)$$

where

$$\begin{aligned} \cos 2\alpha &= \frac{m_e - m_\mu}{\sqrt{(m_{ee} - m_{\mu\mu})^2 + 4m^2}} \\ \sin 2\alpha &= \frac{-2m}{\sqrt{(m_{ee} - m_{\mu\mu})^2 + 4m^2}} \end{aligned} \quad (1.4)$$

The Lagrangean (1.1) can be rewritten as:

$$\begin{aligned} \mathcal{L} = & \bar{i}\psi_1(x)\gamma_\alpha\partial_\alpha\nu_1(x) + \bar{i}\psi_2(x)\gamma_\alpha\partial_\alpha\nu_2(x) \\ & + \frac{1}{2}[m_1\nu_1^T(x)C\nu_1(x) + m_2\nu_2^T(x)C\nu_2(x) + \text{h.c.}] \end{aligned} \quad (1.5)$$

where

$$\begin{aligned} m_1 = & \frac{1}{2}(m_{ee} + m_{\mu\mu} - \sqrt{(m_{ee} - m_{\mu\mu})^2 + 4m^2}) \\ m_2 = & \frac{1}{2}(m_{ee} + m_{\mu\mu} + \sqrt{(m_{ee} - m_{\mu\mu})^2 + 4m^2}) \end{aligned} \quad (1.6)$$

§1.2 Propagation of a Flavour Neutrino State in Vacuum

We now study the propagation in the vacuum of an electron neutrino produced in a weak process. If this neutrino has been created at the point \mathbf{x}_ν and time $t_0 = 0$, the neutrino wave packet is:

$$|\psi_\nu(\mathbf{x})\rangle = \int d\mathbf{p} [a(\mathbf{p}) |\nu_{1\mathbf{p}}\rangle e^{i\mathbf{p}(\mathbf{x}-\mathbf{x}_\nu)} + b(\mathbf{p}) |\nu_{2\mathbf{p}}\rangle e^{i\mathbf{p}(\mathbf{x}-\mathbf{x}_\nu)}] \quad (1.7a)$$

where $a(\mathbf{p})$ and $b(\mathbf{p})$ are momentum distribution peaked around the momenta \mathbf{p}_1 and \mathbf{p}_2 respectively and with widths Δp_1 and Δp_2 and $|\nu_{j\mathbf{p}}\rangle$ is a j -type neutrino with definite momentum \mathbf{p} and the usual normalization

$$\begin{aligned} \int d\mathbf{p} |a(\mathbf{p})|^2 &= 1 \\ \int d\mathbf{p} |b(\mathbf{p})|^2 &= 1 \\ \langle \nu_{m\mathbf{q}} || \nu_{j\mathbf{p}} \rangle &= \delta_{jm}\delta(\mathbf{p}-\mathbf{q}) \\ \langle \mathbf{x} || \nu_{j\mathbf{p}} \rangle &= e^{i\mathbf{p}\mathbf{x}}. \end{aligned} \quad (1.7b)$$

In the relativistic limit we can neglect term of order m/p_0 and $\mathbf{p}_1 \simeq \mathbf{p}_2 = \mathbf{p}_0$, $a(\mathbf{p}) \simeq \cos\alpha a_0(\mathbf{p})e^{i\delta}$ and $b(\mathbf{p}) \simeq -\sin\alpha a_0(\mathbf{p})e^{-i\delta}$. After a time t the neutrino propagates in the following way

$$|\psi_e(\mathbf{x}, t)\rangle = \int d\mathbf{p} [a(\mathbf{p}) |\nu_{1\mathbf{p}}\rangle e^{i[\mathbf{p}(\mathbf{x}-\mathbf{x}_0)-E_1t]} + b(\mathbf{p}) |\nu_{2\mathbf{p}}\rangle e^{i[\mathbf{p}(\mathbf{x}-\mathbf{x}_0)-E_2t]}] \quad (1.8)$$

where $E_j(\mathbf{p}) = \sqrt{p^2 + m_j^2}$. Therefore at time t the wave packet will be located around a point \mathbf{x}_1 at a distance $d = vt$, v denoting the velocity of the neutrino wave packet. For a relativistic neutrino $v \simeq c$ and so $\mathbf{p}(\mathbf{x}_0 - \mathbf{x}_1) \simeq pt$.

The probability amplitude for the emitted neutrino to be detected at a time t as an electron neutrino located around \mathbf{x}_1 is $\mathcal{A}_{ee} = \langle \psi_e(\mathbf{x}_1) | \psi_e(\mathbf{x}_0, t) \rangle$. Using eqs. (1.7) and (1.8) we obtain

$$\mathcal{A}_{ee} = \int d\mathbf{p} [\cos^2\alpha |a_0(\mathbf{p})|^2 e^{i[\mathbf{p}(\mathbf{x}_1-\mathbf{x}_0)-E_1t]} + \sin^2\alpha |a_0(\mathbf{p})|^2 e^{i[\mathbf{p}(\mathbf{x}_1-\mathbf{x}_0)-E_2t]}] \quad (1.9)$$

For small m/p we get $E_j(\mathbf{p}) = p + m_j^2/2p$. In this limit we obtain from (1.9)

$$\mathcal{A}_{ee} = \int dp [\cos^2 \alpha |a_0(\mathbf{p})|^2 e^{-im_1^2 t/2p} + \sin^2 \alpha |a_0(\mathbf{p})|^2 e^{-im_2^2 t/2p}] \quad (1.10)$$

If the width Δp of the wave packet is small in comparison with the neutrino momentum p_0 , for all the relevant momentum p we get

$$\begin{aligned} \frac{m^2}{2p} &= \frac{m^2}{2p_0} + \frac{m^2}{2p_0^2} q + O\left(\frac{q^2}{p_0^2}\right) \\ p &= p_0 + q \end{aligned} \quad (1.11)$$

Exactly in the same way taking for the ν_μ state the orthogonal one to ν_e state we get $\mathcal{A}_{e\mu}$. The probability P_{ex} to detect the original ν_e as a ν_x is the square of the probability amplitude, from (1.10) and (1.11) we get:

$$\begin{aligned} P_{ee}(t) &= 1 - \frac{1}{2} \sin^2 2\alpha (1 - C \cos \Phi) \\ P_{e\mu}(t) &= \frac{1}{2} \sin^2 2\alpha (1 - C \cos \Phi) \end{aligned} \quad (1.12a)$$

where

$$\Phi = \frac{m_2^2 - m_1^2}{2p_0} t \quad (1.12b)$$

and

$$C = \left| \int dq |a(p_0 + q)|^2 \exp i \frac{m_2^2 - m_1^2}{2p_0^2} q t \right| \quad (1.12c)$$

When $C = 1$ eqs. (1.12) describe the phenomenon known as neutrino oscillations * [22]. It is a typical quantum mechanical phenomenon and, as it follows from eqs. (1.9-1.10), is due to the interference of the two neutrinos wave packets. Let's we remark here that, as we anticipated the CP violating phase δ has disappeared from the expression of P_{ex} and it is therefore irrelevant [54].

As we have already outlined, for relativistic neutrinos time and distance are equivalent and in the previous equation we can substitute t with R where R is the distance between the points \mathbf{x}_0 and \mathbf{x}_1 . It is therefore useful to define an oscillation length $L_0 = 4\pi E / (m_1^2 - m_2^2)$ which is the distance after which the phase Φ takes the value 2π .

When $C = 0$ the interference phenomenon disappears. The neutrinos emitted in the process under consideration are two distinct particles with different probability to be produced and with distinct interactions. In particular, in scattering process these neutrinos do not conserve separately the family lepton numbers L_e , L_μ and have different probabilities to produce leptons of a given flavour. (If neutrinos are Majorana particle no lepton number at all is conserved, however for scattering process involving relativistic neutrinos the total lepton number is almost conserved, the deviation from this approximate conservation law being of order m_ν^2/E_ν^2).

* For a description of neutrino oscillations using wave packets see [55]

The value of C is strongly dependent on the behaviour of the oscillating term in the integral. If the phase is nearly constant over a momentum interval $\delta\mathbf{q} \geq \Delta\mathbf{p}$ then $C \simeq 1$ and neutrino oscillations holds; in contrast if the phase varies strongly over a momentum interval $\delta\mathbf{q} \leq \Delta\mathbf{p}$ its net effect is to average to zero the integral and then $C \simeq 0$ and no oscillatory behaviour can be observed in the detected signal. Therefore

$$\begin{aligned} C &= 1 & \text{if } D(t)\Delta p &\ll 1 \\ C &= 0 & \text{if } D(t)\Delta p &\gg 1 \\ D(t) &= \frac{m_1^2 - m_2^2}{2p_0^2} t \end{aligned} \quad (1.13)$$

The meaning of $D(t)$ is straightforward. If ϵ_1 and ϵ_2 are the energies of the two neutrinos then

$$D(t) = \frac{p}{\epsilon_2} - \frac{p}{\epsilon_1} \simeq \frac{m_1^2 - m_2^2}{2p_0^2} t = v_{rel} t \quad (1.14)$$

where v_{rel} is the relative velocity among the two neutrino wave packets. From eq. (1.14) it follows that $D(t)$ is the mean spatial separation among the wave packets. Since $\Delta p = 1/\delta x$, δx being the spatial spread of the wave packets, from (1.13) one gets that $C \simeq 1$ until when the wave packets overlap and $C \simeq 0$ when they do not overlap [22, 24]. This is in agreement with the fact that the term proportional to $\cos \Phi$ in the expression for the probability (1.12) is due to the interference among the two wave packets; it disappears when the two wave packets no more overlap. According to (1.13-1.14) we can define a decoupling time t_d as

$$t_d = \frac{2p^2}{m_1^2 - m_2^2} \delta x \quad (1.15)$$

If $t > t_d$ holds, no interference occurs between ν_1, ν_2 and $C = 0$ in eqs. (1.12). Let's we notice here that in this case the probabilities P_{ex} do not depend on the energy of the neutrino.

§1.3 Relevance of Vacuum Neutrino Oscillations for the Solar Neutrino Problem

We shall now assume that vacuum neutrino oscillations occur between the sun and the earth and we shall examine briefly their implication for the signal which is detected by solar neutrino experiments. The signal S_D in the Chlorine experiment is

$$S_D = TN\epsilon \int_{E_{th}}^{E_{end}} dE \Phi(E) \sigma(E) P_{ee}(E) \quad (1.16)$$

where $\Phi(E)$ is the differential flux of solar neutrinos, $\sigma(E)$ is the absorption cross section for the reaction $\nu_e + Cl^{37} \rightarrow e^- + Ar^{37}$, E_{th} is the threshold energy for the detection of the signal, E_{end} is the end point energy of the spectrum, T is the detection time, N is the number of scatterers and ϵ

is the efficiency for the extraction of Ar^{37} from the detector. The signal S_K in Kamioka experiment is

$$S_K = TN \int_{E_{th}}^{E_{end}} dE \Phi(E) \epsilon(E) [(\sigma_e(E) P_{ee}(E) + \sigma_\mu(E) P_{e\mu}(E))] \quad (1.17)$$

where σ_x is the elastic cross section for $\nu_x e$ scattering. The signal in the SAGE and GALLEX experiments is again given by (1.16) where now $\sigma(E)$ is the cross section for the reaction $\nu_e + Ga^{71} \rightarrow e^- + Ge^{71}$.

Assuming both Φ and σ to be known in (1.16-17) the signal in the various detectors are determined once P_{ex} is known. In the standard model neutrino are massless and $P_{ex} = \delta_{ex}$. If neutrino oscillations indeed occur it is important to notice that if P_{ex} is energy dependent than the amount of deviation of the signal with respect to the standard model prediction is a function of energy and it is expected a different behaviour among the three experiments due to the different thresholds. If instead P_{ex} is energy independent than the radiochemical experiments which are sensible only to electron neutrinos are expected to give the same deviation with respect to the standard model prediction while the Cerenkov experiment is expected to show a somewhat smaller deviation due to the contribution of μ neutrinos (if they are active neutrinos) whose cross section in the detector is about 1/7 of the cross section for electron neutrinos. These considerations are quite general and can be extended in an obvious manner also to the expected future experiments.

To understand the possible difference among the various experiments it is therefore important to understand if the probability P_{ex} depends on energy. It is useful to define $\Delta = m_1^2 - m_2^2$. There are three points to take into account

a) the condition for spatial overlapping (see 1.13) of the two wave packets.

This problem was investigated in [55]. The two wave packets are still spatially overlapped when they reach the earth if

$$\frac{\Delta}{E_\nu^2} \leq 10^{-21} \quad (1.18)$$

If condition (1.18) is not satisfied the interference term in eq. (1.12) goes to zero before neutrinos reach the earth and neutrino oscillations disappear.

b) If the oscillation length is not larger than the solar core averaging over the region of production of the neutrinos is equivalent to average over the oscillating term which gives zero contribution [22, 24]. If

$$\frac{E_\nu}{\Delta} \geq 10^{-2} R_\odot \quad (1.19)$$

where R_\odot is the solar radius, than vacuum oscillation length is larger than the production zone. This case, in principle, is quite different from the previous one. If condition (1.18) is not satisfied individual neutrinos wave packet can indeed oscillate among different neutrino flavors, however due to the size of the production region the oscillatory phase (Φ in eq. (1.12)) can acquire all the possible values for neutrinos produced in distinct process. Since from the experimental point of view it is impossible to follow the evolution of an individual neutrino the net effect of the oscillatory phase is averaged to zero. Therefore in this case the oscillations are present but they cannot be observed

due to experimental limitation. In the case of the sun the parameters are such that condition a and b are equivalent [24].

c) If the product $R_{se}(m_1^2 - m_2^2)/4$, where R_{se} is the sun-earth distance, is much larger than the typical energy of neutrinos which are detected the contribution of the oscillating term is again averaged to one half, due to the finite energy resolution of the detectors [52]. If

$$3 \times 10^{-10} \leq \Delta \leq 3 \times 10^{-12} \text{eV}^2 \quad (1.20)$$

than the detector energy resolution does not average the oscillating term. In other words looking at eqs. (1.16-1.17) one can realize that if the product $\phi(E)\epsilon(E)\sigma_x(E)$ varies slowly during an oscillation period of P_{ex} the net effect of oscillation on the detected signal is negligible. The bound which comes from condition c is the stronger one.

One comment is in order. Condition c applies only if the spectrum for the production of neutrinos is continuous. In particular it does not apply for berillium neutrinos. In the case of large mixing angle, experiments like the planned Borexino/Borex with large statistics and whose main goal is the detection of berillium neutrinos, will be sensitive to mass square difference lower or equal to 10^{-7} (eV)^2 [41].

Finally oscillation are ineffective for oscillation length which are larger than the sun earth distance since in this case there is no time for the oscillations to develop and $P_{ee} = 1$ and $P_{\mu\mu} = 0$.

The region of parameters for which the probabilities are energy dependent has been investigated in [56]. For:

$$5 \times 10^{-11} \leq \Delta \leq 2.5 \times 10^{-10} \quad \sin^2 2\alpha \geq 0.7 \quad (1.21)$$

it is possible to reconcile, within the experimental errors, the data of the four experiments. The allowed parameter region at 95 % C.L. is shown in fig. 1.1

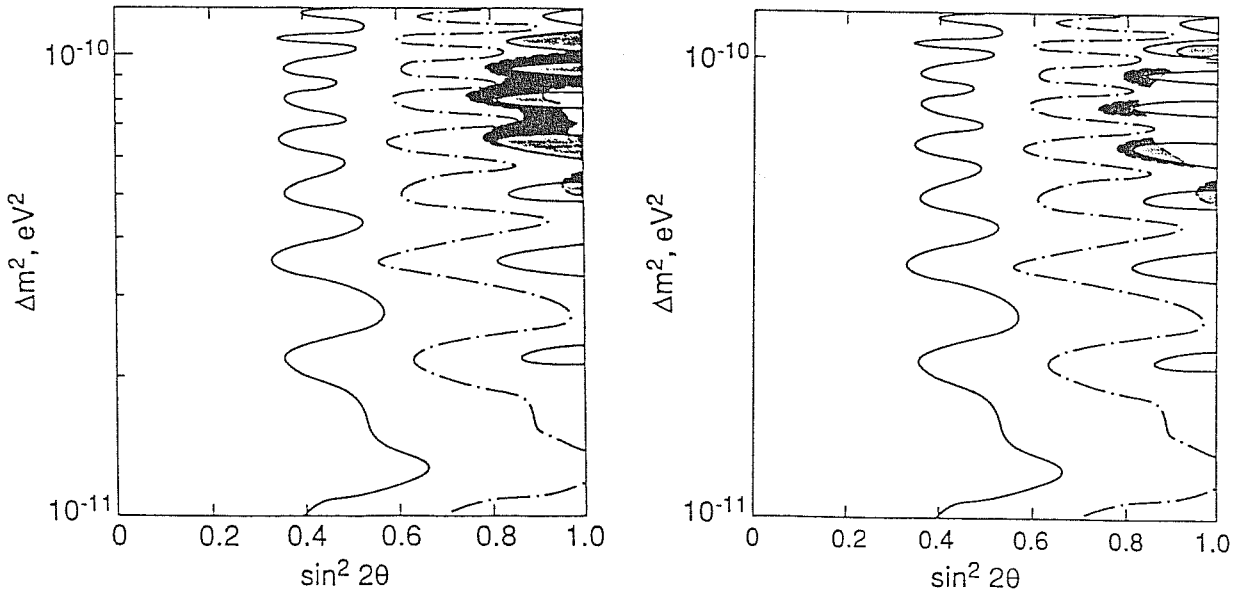


Fig. 1.1 (a) Region of values of the parameters Δm^2 and $\sin^2 \theta$ allowed by the Homestake, Kamiokande II and SAGE 1990 individual run data (grey+black area), and by the 68% C.L. (black area) and 95% C.L. (grey+black area) GALLEX results in the case of solar neutrino oscillations into active neutrinos: $\nu_e \leftrightarrow \nu_{\mu(\tau)}$. Shown are also the iso-SNU contours corresponding to an average rate of ${}^7\text{Li}$ production in the Ga-Ge experiments of 83 SNU (dash-dotted line), 104 SNU and (63) SNU (solid lines). (b) The same as in (a) but for solar neutrino oscillations into sterile neutrinos [56](Krastev and Petcov)

If just so oscillations are the main responsible for the SNP one expects a variation of the signal of monochromatic neutrinos with the variation of $R_{s,e}$ which is at least of order several per cent. Such an effect will probably be measured in the large statistic Borexino detector. Another important phenomenological feature of this scenario is the distortion of the neutrino spectrum which should be measurable in the future Kamiokande II and SNO detectors [56]. Finally, if oscillations occur among two active states, one expects the deviation of the ratio among neutral current and charged current from one. The size of this deviation is such that it will be certainly measured in SNO detector. Let's we notice that all these effects are completely independent from the standard model of the sun and therefore all these measures are unaffected by the theoretical uncertainties and will provide an unambiguous analysis of this hypothesis.

If the oscillating term can be averaged the probability can be taken out of the integral. If we assume that electron neutrino oscillates only in active neutrino we get (see (1.16-1.17))

$$\begin{aligned}
 R_D &= P_{ee} \\
 R_K &= [P_{ee} + (1 - P_{ee})\bar{\sigma}_\mu/\bar{\sigma}_e] \\
 \bar{\sigma}_x &= \int_{E_{th}}^{E_{end}} dE \Phi(E) \sigma_x(E)
 \end{aligned} \tag{1.22}$$

where R_D and R_K are the ratios of the detected signals and the theoretical expectation. Taking into account possible oscillations between all the three neutrino flavors it must be $P_{ee} \geq 1/3$ (if a neutrino is a linear superposition of n neutrino mass eigenstates, $\nu_e = \sum_{i=1}^n a_i \nu_i$, averaging the oscillating terms in the probabilities we get $P_{ee} = \sum_{i=1}^n |a_i|^4$ and for the three neutrino system the minimum value for P_{ee} is $1/3$). Having in mind this restriction to reconcile the two signals require

$$0.413 \leq P_{ee} \leq 0.442 \quad \Delta > 3 \times 10^{-10} (\text{eV})^2 \tag{1.23}$$

where we have considered 2σ intervals for all the experiments and we have used the Turk-Chieze's theoretical prediction [8]. Using instead Bahcall prediction [2] this possibility is excluded. We therefore conclude that this possibility, although disfavoured, is still compatible with the experimental data.

§1.4 Matter Induced Neutrino Oscillations

The neutrinos we are considering are produced in the sun core and for a time of about two seconds travel inside the sun which is a relatively dense medium. Matter density in the sun is not enough to provide significant cross section for neutrino scattering, however the interference of the forward scattering amplitude with the the unscattered neutrino wave modifies the dispersion relation for neutrinos. Due to the contribution of charged current interaction of electron neutrino with electrons in the sun the dispersion relation are differently modified for ν_e and ν_μ . This induce an effective level splitting among neutrinos of different flavors. In general this level splitting has the effect to quench the oscillations in the flavour space. However, if this level splitting compensates the splitting due to the mass difference, it has the effect to produce maximal mixing among the neutrino states. Therefore, even in presence of small vacuum mixing angle, the effective mixing in the sun interior can be large and large conversion probabilities are possible.

§1.4.1 The propagation of a neutrino in a dense medium

The neutrino travelling in the medium is a coherent superposition of states $|\nu_{jP}\rangle$ as in (1.7). We now want to understand the time evolution of the system. We follow the evolution of a j-type neutrino, neglecting scattering and absorption (for the typical matter density in the sun it is a very good approximation). In a background medium of electrons the neutrino state is:

$$|\nu_j(x, t)\rangle = \int d\mathbf{p}_e d\mathbf{x}_e \rho(\mathbf{p}_e, \mathbf{x}_e) \int d\mathbf{p} d\mathbf{q} a_{\nu j}(\mathbf{p}) a_e(\mathbf{q}, \mathbf{p}_e) e^{-i[(E_\nu + E_e)t + \mathbf{p}(\mathbf{x} - \mathbf{x}_n) + \mathbf{q}(\mathbf{x} - \mathbf{x}_e)]} |\nu_{jP}\rangle |e_q\rangle \quad (1.24)$$

where $a_{\nu j}$ and a_e are the wave function in momentum space for j-type neutrino and electron respectively and ρ is the electron density. The evolution of the $|\nu_j\rangle$ state at a time $t + \Delta t$ is given by,

$$|\psi_j(x, t + \Delta t)\rangle = \int d\mathbf{p}_e d\mathbf{x}_e \rho(\mathbf{p}_e, \mathbf{x}_e) \int d\mathbf{p} d\mathbf{q} d\mathbf{k} a_{\nu j}(\mathbf{p}) a_e(\mathbf{q}, \mathbf{p}_e) e^{-i[(E_\nu + E_e)t + \mathbf{p}(\mathbf{x} - \mathbf{x}_n) + \mathbf{q}(\mathbf{x} - \mathbf{x}_e)]} e^{-iE_X \Delta t} [\delta(\mathbf{p} + \mathbf{q} - \mathbf{k}) \delta_{\psi_j X} + S_{\mathbf{p} \mathbf{q} \mathbf{k}}^{\psi_j X} \Delta t] |X_k\rangle \quad (1.25)$$

where $|X_k\rangle$ is any final state of neutrino electron interaction, $S_{\mathbf{p} \mathbf{q} \mathbf{k}}^{\psi_j X}$ is the scattering amplitude for unit time and volume for the process $|\nu\rangle |e\rangle \rightarrow |X\rangle$. Since weak interactions are short range interactions one immediately realize from (1.24) that only electrons for which $\mathbf{x}_e \sim \mathbf{x}_n$ are relevant and therefore for sufficiently rarified medium we can forget the integration over electron densities and consider only individual scattering. It is now crucial to understand what are, among the $|X\rangle$ states the states which can coherently interfere with the initial neutrino states. We are interested in states $|X\rangle$ which can evolve back to the initial neutrino states with non negligible amplitude ($O(G_F)$, G_F being the Fermi coupling constant). To avoid a negligible scatterers density this states

have to be the product of the initial electron state times an arbitrary neutrino state. We shall therefore study the evolution of the state,

$$|X(t)\rangle = \int d\mathbf{p}d\mathbf{q}b_{\nu m}(\mathbf{p})a_e(\mathbf{q}, \mathbf{p}_e)e^{-i[(E_\nu+E_e)t+\mathbf{p}(\mathbf{x}-\mathbf{x}_n)+\mathbf{q}(\mathbf{x}-\mathbf{x}_e)]} |\nu_{m\mathbf{p}}\rangle |e_{\mathbf{q}}\rangle. \quad (1.26)$$

The time evolution of the state $|\nu_m(\mathbf{x}, t)\rangle$ is described by $|\psi_m(\mathbf{x}, t)\rangle$ and it can be directly read from eq. (1.25). Given

$$|X(\mathbf{x}, t + \Delta t)\rangle = \alpha(t) |\nu_j(\mathbf{x}, t)\rangle \Delta t + |Y\rangle + O((\Delta t)^2) \quad (1.27)$$

we want to understand what are the $|\nu_m(\mathbf{x}, t)\rangle$ states for which α is non negligible.

From (1.25) and (1.26) we get

$$\alpha(t) = \int d\mathbf{p}d\mathbf{q}d\mathbf{k}d\mathbf{u}a_e(\mathbf{u})a_e(\mathbf{q})a_{\nu j}(\mathbf{p})b_{\nu m}(\mathbf{k})S_{\mathbf{p}\mathbf{q}\mathbf{k}\mathbf{u}}^{\nu_j\nu_m} e^{i\{[E_\nu(\mathbf{p})+E_e(\mathbf{q})-E_\nu(\mathbf{k})+E_e(\mathbf{u})]t+(\mathbf{p}-\mathbf{k})(\mathbf{x}-\mathbf{x}_n)+(\mathbf{q}-\mathbf{u})(\mathbf{x}-\mathbf{x}_e)\}} \quad (1.28)$$

If the initial neutrino and electron have a well defined momentum (if S is nearly constant over the wave packets widths) $a_x(\mathbf{p}) \sim \mathcal{N}_x \delta(\mathbf{p} - \mathbf{p}_x)$ and from (1.28) one gets

$$\alpha(t) \simeq \mathcal{N}_e^2 S_{\mathbf{p}_e \mathbf{p}_\nu \mathbf{p}_e \mathbf{p}_\nu}^{\nu_j \nu_m} \int d\mathbf{q} a_{\nu j}(\mathbf{q}) b_{\nu j}(\mathbf{q}) \quad (1.29)$$

therefore α is non negligible only if $a_{\nu j}(\mathbf{p}) \simeq b_{\nu m}(\mathbf{p})$. From eq. (1.29) we obtain that only the forward scattered states can coherently interfere with the initial state.

§1.4.2 Forward scattering amplitudes

We can now determine the evolution equation for our system. The amplitude $S_{\psi\psi'}$ for a state $|\psi\rangle$ at a time t to become a state $|\psi'\rangle$ at a time $t + \Delta t$ is

$$S_{\psi\psi'} = \langle \psi' | T \exp(i \int_{t_0}^{t_0+\Delta t} dt L_{int}) | \psi \rangle$$

$$L_{int} = \int_{R^3} dx \mathcal{L}_{int} \quad (1.30)$$

where \mathcal{L}_{int} is the interacting sector of the lagrangean density. Since we want to compute the time evolution we need to consider the small Δt limit. Essentially we need Δt much less than the typical mean free path of neutrinos. On the other hand for (1.30) to be of any use (read calculable) Δt must be much larger than the typical collision time in order we can apply asymptotic states limit in the computation of the S matrix. In the case under consideration the typical mean free path is much larger than the sun and we can safely compute (1.30) with the ordinary methods.

The medium is constituted of ordinary matter and we will need to consider the elastic scattering off electrons, protons and neutrons. We shall now consider in detail the amplitude S for the process

$$\nu_1^L + e_q \rightarrow \nu_2^L + e_q \quad (1.31)$$

where with $\nu_j^{(L,R)}$ we denote ν_j neutrinos with left (right) handed polarization. From (1.30) and we get:

$$S = \langle 0 | a_{\nu_2 p}^{\dagger L} a_{e q}^{\dagger} [T i \int_{t_0}^{t_0 + \Delta t} dt \int dx - \frac{G}{\sqrt{2}} \sin \alpha \cos \alpha e^{-2i\delta} e^{-i(p_{01} - p_{02})t_0} \times \bar{\nu}_2(x) \gamma_\mu (1 + \gamma_5) e(x) \bar{e}(x) \gamma_\mu (1 + \gamma_5) \nu_1(x) + \dots + h. c.] a_{e q} a_{\nu_1 p}^L | 0 \rangle \quad (1.32)$$

where $a_{x p}^{\dagger}$ is the creation operator for a particle x with momentum p , and the factor $e^{-i(p_{01} - p_{02})t_0}$ takes into account that we are working in the interaction picture.

Normalizing properly at a density of one neutrino per unit volume and N_e electron per unit volume we get:

$$S = -i \frac{G}{2\sqrt{2}} \frac{\sin 2\alpha N_e}{4q_0 p_0} e^{-2i\delta} \bar{e}(q) \gamma_\mu (1 + \gamma_5) e(q) \int_{t_0}^{t_0 + \Delta t} dt e^{i(p_{02} - p_{01})t_0} \times [\bar{\nu}_2(p) \gamma_\mu (1 + \gamma_5) \nu_1(p) + \nu_1^T(p) C \gamma_\mu (1 + \gamma_5) C \nu_2^*(p) e^{-i\delta}] = -i \Delta t \frac{G \sin 2\alpha N_e}{8q_0 p_0} e^{-2i\delta} \bar{e} \gamma_\mu (1 + \gamma_5) e \times [\bar{\nu}_2 \gamma_\mu (1 + \gamma_5) \nu_1 + \nu_1^T C \gamma_\mu (1 + \gamma_5) C \nu_2^*] e^{i(p_{02} - p_{01})t_0} + O(\Delta^2 t) \quad (1.33)$$

For the evolution equation we need $\mathcal{N} = i \frac{\Delta}{\Delta t} \mathcal{S} e^{-i(p_{02} - p_{01})t_0}$, where the time dependent phase is needed to go back to the ?? representation. Averaging over the electron spin we get:

$$\mathcal{N}_{1,2}^L = i \frac{\Delta}{\Delta t} \mathcal{A} = -\frac{G \sin 2\alpha N_e}{4\sqrt{2}q_0 p_0} e^{-2i\delta} \times q_\mu [\bar{\nu}_2 \gamma_\mu (1 + \gamma_5) \nu_1 + \nu_1^T C \gamma_\mu (1 + \gamma_5) C \nu_2^* e^{-i\delta}] \quad (1.34)$$

in the rest frame of the medium $\langle q \rangle = 0$ and finally we get:

$$\mathcal{N}_{1,2}^L = -GN_e \sqrt{2} \sin 2\alpha e^{-2i\delta} \quad (1.35)$$

In the same way we get the other contributions

$$\begin{array}{c} \nu_1 \quad e \\ \hline \{W\} \\ \hline e \quad \nu_1 \end{array} + \begin{array}{c} \nu_1 \quad \nu_1 \\ \hline \{Z\} \\ \hline e \quad e \end{array} ; \quad \begin{array}{c} \nu_2 \quad e \\ \hline \{W\} \\ \hline e \quad \nu_2 \end{array} + \begin{array}{c} \nu_2 \quad \nu_2 \\ \hline \{Z\} \\ \hline e \quad e \end{array} \quad (1.36)$$

It follows

$$\begin{aligned}\mathcal{N}_{1,1}^L &= \frac{G}{\sqrt{2}}(2N_e \cos^2 \alpha - GN_n) \\ \mathcal{N}_{2,2}^L &= \frac{G}{\sqrt{2}}(2N_e \sin^2 \alpha - GN_n)\end{aligned}\quad (1.37)$$

Transition $|\nu_{1,2p}^L\rangle |e_q^{(\alpha)}\rangle \rightarrow |\nu_{1,2p}^R\rangle |e_q^{(\alpha)}\rangle$ are forbidden by angular momentum conservation and this can be verified explicitly, so we get

$$\mathcal{N}_{1,1}^{L,R} = \mathcal{N}_{1,2}^{L,R} = \mathcal{N}_{2,1}^{L,R} = \mathcal{N}_{2,2}^{L,R} = 0 \quad (1.38)$$

for transition of right handed polarized states we get in general $\mathcal{N}^L = -\mathcal{N}^{R*}$

$$\begin{aligned}\mathcal{N}_{1,1}^R &= -\frac{G}{\sqrt{2}}(2N_e \cos^2 \alpha - GN_n) \\ \mathcal{N}_{2,2}^R &= -\frac{G}{\sqrt{2}}(2N_e \sin^2 \alpha - GN_n) \\ \mathcal{N}_{1,2}^R &= GN_e \sqrt{2} \sin 2\alpha e^{2i\delta}\end{aligned}\quad (1.39)$$

§1.4.3 Neutrino evolution equation in matter

If the neutrino state at a time t is

$$|\nu^{L,R}(t)\rangle = d_1^{L,R}(t) |\nu_1\rangle^{L,R} + d_2^{L,R}(t) |\nu_2\rangle^{L,R} \quad (1.40)$$

the evolution equation in matter is

$$i \frac{\partial}{\partial t} d_j^{L,R} = H_{j,k}^{L,R} d_k^{L,R} \quad (1.41)$$

where * [25]

$$\begin{aligned}H^L &= \begin{pmatrix} E_1 + \mathcal{N}_{1,1}^L & \mathcal{N}_{1,2}^L \\ \mathcal{N}_{1,2}^{L*} & E_2 + \mathcal{N}_{2,2}^L \end{pmatrix} \\ H^R &= \begin{pmatrix} E_1 + \mathcal{N}_{1,1}^R & \mathcal{N}_{1,2}^R \\ \mathcal{N}_{1,2}^{R*} & E_2 + \mathcal{N}_{2,2}^R \end{pmatrix}\end{aligned}\quad (1.42)$$

We define

$$\begin{aligned}E^X &= (E_1 + E_2 + \mathcal{N}_{1,1}^X + \mathcal{N}_{2,2}^X)/2 \\ \epsilon &= (E_1 - E_2 + \mathcal{N}_{1,1}^X - \mathcal{N}_{2,2}^X)/2\end{aligned}$$

* We have given here our own derivation of the Wolfenstein equation, for the original derivation see [25], for alternative derivations see [57]

$$\theta^X = \mathcal{N}_{1,2}^X \quad (1.43)$$

The Hamiltonian is

$$H^X = \begin{pmatrix} E^X & 0 \\ 0 & E^X \end{pmatrix} + \begin{pmatrix} \epsilon^X & \theta^X \\ \theta^{X*} & -\epsilon^X \end{pmatrix} \quad (1.44)$$

The diagonal term can be reabsorbed in a redefinition of the amplitude $a_j(t)$. With

$$A_j(t) = e^{-iEt} a_j(t)$$

$$\mathcal{H} = \begin{pmatrix} \epsilon & \theta \\ \theta^* & -\epsilon \end{pmatrix} \quad (1.45)$$

we get

$$i \frac{\partial}{\partial t} A_j(t) = \mathcal{H}_{jk} A_k(t) \quad (1.46)$$

where we have dropped the X index. If $\theta = \theta_0 e^{i\theta_1}$ using the unitary transformation

$$U = \begin{pmatrix} \cos \beta e^{-i\theta_1/2} & \sin \beta e^{i\theta_1/2} \\ -\sin \beta e^{-i\theta_1/2} & \cos \beta e^{i\theta_1/2} \end{pmatrix}$$

$$\cos 2\beta = \frac{-\epsilon}{\sqrt{\epsilon^2 + \theta_0^2}}$$

$$\sin 2\beta = \frac{-\theta_0}{\sqrt{\epsilon^2 + \theta_0^2}} \quad (1.47)$$

we can diagonalize \mathcal{H}

$$\mathcal{H}_D = U \mathcal{H} U^\dagger$$

$$\mathcal{H}_D = \begin{pmatrix} -\sqrt{\epsilon_0^2 + \theta_0^2} & 0 \\ 0 & \sqrt{\epsilon_0^2 + \theta_0^2} \end{pmatrix} \quad (1.48)$$

If \mathcal{N} is constant in time following (1.48) the evolution problem is solved. Solar neutrinos, of interest for the experiment we are discussing, for masses below 1 MeV are relativistic. Since we are interested to discuss the effect of matter induced oscillation for solar neutrinos we give the relativistic limit for the previous equations. We choose, for convenience, to give the expression in the flavour basis.

$$\mathcal{H}_{(r)}^L = \begin{pmatrix} \frac{\Delta}{4E} \cos 2\alpha + \mathcal{N}_e & -\frac{\Delta}{4E} \sin 2\alpha \\ -\frac{\Delta}{4E} \sin 2\alpha & -\frac{\Delta}{4E} \cos 2\alpha + \mathcal{N}_\mu \end{pmatrix}$$

$$\mathcal{H}_{(r)}^R = \begin{pmatrix} \frac{\Delta}{4E} \cos 2\alpha - \mathcal{N}_e & \frac{\Delta}{4E} \sin 2\alpha e^{-i\delta} \\ \frac{\Delta}{4E} e^{i\delta} \sin 2\alpha & -\frac{\Delta}{4E} \cos 2\alpha - \mathcal{N}_\mu \end{pmatrix} \quad (1.49)$$

where

$$\mathcal{N}_e = G\sqrt{2}n_e - \frac{G}{\sqrt{2}}n_n$$

$$\mathcal{N}_\mu = -\frac{G}{\sqrt{2}}n_n \quad (1.49)$$

The matrix $\mathcal{H}_{(r)}^L$ is diagonalized by the transformation

$$\mathcal{H}_D = U_m \mathcal{H}^L U_m^\dagger$$

$$U_m = \begin{pmatrix} \cos \alpha_m & -\sin \alpha_m \\ \sin \alpha_m & \cos \alpha_m \end{pmatrix}$$

$$\begin{aligned} \cos 2\alpha_m &= -\frac{\frac{\Delta}{4E} \cos 2\alpha + \frac{G}{\sqrt{2}} n_e}{\sqrt{\left(\frac{\Delta}{4E} \cos 2\alpha + \frac{G}{\sqrt{2}} n_e\right)^2 + \left(\frac{\Delta}{4E}\right)^2 \sin^2 2\alpha}} \\ \sin 2\alpha_m &= \frac{\frac{\Delta}{4E} \sin 2\alpha}{\sqrt{\left(\frac{\Delta}{4E} \cos 2\alpha + \frac{G}{\sqrt{2}} n_e\right)^2 + \left(\frac{\Delta}{4E}\right)^2 \sin^2 2\alpha}} \end{aligned} \quad (1.50)$$

where

$$\mathcal{H}_D = \begin{pmatrix} -\bar{\lambda} & 0 \\ 0 & \bar{\lambda} \end{pmatrix} \quad (1.51)$$

and

$$\bar{\lambda} = \sqrt{\left(\frac{\Delta}{4E} \cos 2\alpha + \frac{G}{\sqrt{2}} n_e\right)^2 + \left(\frac{\Delta}{4E}\right)^2 \sin^2 2\alpha} \quad (1.52)$$

and similar expression with the obvious change are obtained for \mathcal{H}^R .

Since the equations we got are similar to the equations for the vacuum neutrino oscillations, in analogy with this case α_m is called the effective mixing angle in matter and $L_m = 2\pi/\bar{\lambda}$ is the effective mixing length in matter. Notice that also in the case of matter induced neutrino oscillations the CP violating phase disappear from the evolution hamiltonian and is therefore irrelevant [58].

§1.4.4 The MSW effect

The density, in the sun, is not constant and in its travel neutrino experience different densities and therefore a potential \mathcal{N} which is not constant in time. Neutrinos are relativistic and $R = t$ if R is the distance between the point in which the neutrino is emitted and the point it reaches at the time t . Equation (1.46) becomes

$$i \frac{\partial}{\partial R} A = \mathcal{H}_{(r)}(R) A \quad (1.53)$$

where the R dependence of $\mathcal{H}_{(r)}$ is completely described by the R dependence of electron and neutron densities $N_e(R)$, $N_n(R)$.

Micayev and Smirnov [26] noticed that, according to the sign of Δ , $\tan \alpha_m$ can share resonant behaviour. In fact for negative Δ we observe the following behaviour of α_m :

a) at large electron density ($G n_e \gg -\Delta/4E$) the mixing angle in matter is vanishing and the electron neutrino coincide with the higher energy eigenvalue of the hamiltonian

b) at the resonant density $n_r = -\sqrt{2}\Delta/(4E \cos^2 \alpha)G$ the mixing, in the flavour basis, becomes maximal and substantial $\nu_e \rightarrow \nu_\mu$ transition is possible

c) for small electron density ($Gn_e \ll -\Delta/4E$) the vacuum case is recovered and the higher energy eigenstate of the hamiltonian is $\nu_2 = \cos \alpha \nu_\mu - \sin \alpha \nu_e$.

Since the matter density in the sun is obviously varying from the density in the solar core to zero density, if condition *a* is fulfilled in the solar core, neutrinos will certainly meet the resonant density (see *b*) in their path to the detector. In this region an almost maximal admixture of flavour neutrino states occurs also for small vacuum mixing angle.

Using the diagonalization (1.50) and taking into account that α_m is a function of R we get

$$i \frac{\partial}{\partial R} \begin{pmatrix} B_1 \\ B_2 \end{pmatrix} = \begin{pmatrix} \lambda(R) & 0 \\ 0 & -\lambda(R) \end{pmatrix} \begin{pmatrix} B_1 \\ B_2 \end{pmatrix} + \begin{pmatrix} 0 & i \frac{\partial \alpha_m}{\partial R} \\ -i \frac{\partial \alpha_m}{\partial R} & 0 \end{pmatrix} \begin{pmatrix} B_1 \\ B_2 \end{pmatrix} \quad (1.54)$$

where $B_j = (U_m)_{jk} A_k$.

In general equation (1.55) is not exactly solvable. However two important limits are easily under control.

$$\dot{\alpha}_m(R) \gg \lambda(R) \quad (1.55)$$

which corresponds to the impulsive limit, the time variation is too fast and the state doesn't change.

$$\dot{\alpha}_m(R) \ll \lambda(R) \quad (1.55)$$

which corresponds to the adiabatic regime. In the limit in which $\dot{\alpha}_m$ is negligible we get for the evolution of a state $|\nu_{j,t=0}\rangle$ which at a time t is an eigenvector of \mathcal{H} with eigenvalue λ_j

$$|\nu_{j,t=0}(t)\rangle \rightarrow |\nu_{j,t}\rangle \exp -i \int_0^t ds \lambda_j(s) \quad (1.56)$$

where $|\nu_{j,t}\rangle$ are the instantaneous eigenstates of the hamiltonian $\mathcal{H}(t)$ at the time t .

If the evolution is adiabatic $|\nu_{j,t}\rangle$ evolves staying an instantaneous eigenstate $|\nu_{j,t}\rangle$ of the Hamiltonian. Let's we write the adiabatic condition for the hamiltonian $\mathcal{H}_{(r)}^L$,

$$\frac{\frac{dN_e}{dR} \frac{\Delta}{4E} \sin 2\alpha}{\bar{\lambda}^2(R)} \ll \bar{\lambda}(R) \quad (1.57)$$

which, at the resonant density, becomes

$$\frac{\frac{dN_e}{dR}}{(\frac{\Delta}{4E})^2 \sin^2 2\alpha} \ll 1 \quad (1.58)$$

The meaning of condition (1.59) is intuitively clear. The term $\bar{\lambda}(R)/(dN_e/dR)$ is the typical distance over which the diagonal elements of the hamiltonian is changing significantly, $\Delta/4E \sin 2\alpha$ is the oscillation length at the resonance. Looking at (1.60) one can therefore interpret (1.59) in the following way: if the oscillation length is much larger of the distance over which the hamiltonian is going to change there is plenty of time for the system to develop oscillations and therefore the instantaneous hamiltonian eigenstates evolve remaining eigenstates and acquiring a phase, if instead

the oscillation length is much larger than the typical time of evolution of the hamiltonian there is no time to develop any oscillations and the system does not change.

§1.4.5 Relevance of Neutrino Mixing in Matter for the Solar Neutrino Problem

If impulsive condition (1.56) holds the neutrino state is left unchanged and the evolution is the same as in vacuum. Conversely if adiabatic condition holds the picture is drastically altered. As we have already stressed, for relativistic neutrinos time and distance are completely equivalent and we can substitute the time t with the position R in the equation for the evolution of the neutrino.

If ν_{jm} are the instantaneous eigenstates in matter, the initial neutrino state, at the point R_i in the interior of the sun, is:

$$|\nu_e(R_i)\rangle = \cos \alpha_m(R_i) |\nu_{1m}\rangle + \sin \alpha_m(R_i) |\nu_{2m}\rangle \quad (1.61)$$

In a point R_f at the surface of the sun, the ν_e states becomes

$$\nu_e(R_f) = \cos \alpha_m(R_i) |\nu_1\rangle e^{-i \int_{R_i}^{R_f} ds \lambda_j(s)} + \sin \alpha_m(R_i) |\nu_2\rangle e^{i \int_{R_i}^{R_f} ds \lambda_j(s)} \quad (1.62)$$

Projecting the neutrino states $\nu_e(R_i)$ over the ν_e state in vacuum, we get the amplitude \mathcal{A}_{ee} for the emitted ν_e to emerge outside the sun as ν_x

$$\mathcal{A}_{ee} = \cos \alpha_m(R_i) \cos \alpha e^{-i \int_{R_i}^{R_f} ds \lambda_j(s)} + \sin \alpha_m(R_i) \sin \alpha e^{i \int_{R_i}^{R_f} ds \lambda_j(s)} \quad (1.63)$$

For the outcoming probability we get

$$\begin{aligned} P_{ee} &= \cos^2 \alpha_m(R_i) \cos^2 \alpha + \sin^2 \alpha_m(R_i) \sin^2 \alpha \\ &+ 2 \sin \alpha_m(R_i) \sin \alpha \cos \alpha_m(R_i) \cos \alpha \cos \int_{R_i}^{R_f} ds \lambda_j(s) \end{aligned} \quad (1.64)$$

Once one takes the average over the production region the term which is oscillating with the adiabatic phase in (1.64) is averaged to zero and the probability becomes

$$\langle P_{ee} \rangle = \frac{1}{2} (1 - \langle \cos 2\alpha_m \cos 2\alpha \rangle) \quad (1.65)$$

where $\langle \rangle$ denotes a quantity averaged over the neutrino production region.

Particularly simple is the small α limit: $\cos \alpha = 1$ and $\sin \alpha = O(\alpha)$. In this case we get, neglecting $O(\alpha)$ terms:

$$P_{ee} = \cos^2 \alpha_m(R_i) \cos^2 \alpha \quad (1.66)$$

where,

$$\cos^2 \alpha_m(R_i) = \frac{1}{2} \left(1 - \frac{\frac{\Delta \cos 2\alpha}{4E} + \frac{Gn_e}{\sqrt{2}}}{\sqrt{\frac{\Delta^2}{16E^2} + \sqrt{2}Gn_e \cos 2\alpha \frac{\Delta}{4E} + \frac{G^2 n_e^2}{2}}} \right) \quad (1.67)$$

If $\Delta < 0$ $\cos^2 \alpha_m(R_i)$ is a decreasing function of energy. This is a manifestation of the resonant condition, in fact if

$$\frac{Gn_e(R_i)}{\sqrt{2}} > -\frac{\Delta}{4E} \quad (1.68)$$

than neutrinos cross a resonance in their path to the detector, otherwise this is not possible. From (1.68) one can roughly say that only neutrinos with energy E_ν such that

$$E_\nu > -\frac{\Delta}{4} \frac{\sqrt{2}}{Gn_e(R_i)} \quad (1.69)$$

are significantly affected from matter effect. An additional constraint for matter effect to be significant is given from the adiabatic condition (1.59). Again qualitatively speaking the point at which this condition is more easily violated is at the resonance where $\bar{\lambda}$ get its minimum value. Defining the resonant point R_r as

$$n_e(R_r) = -\frac{\Delta}{2\sqrt{2}GE} \quad (1.70)$$

the adiabatic condition at the resonant point (1.70) can be rewritten as

$$\left| \frac{dN_e}{dR}(R_r) \right| \ll \left(\frac{\Delta}{4E} \sin 2\alpha \right)^2 \quad (1.71)$$

In general this condition has a complicated dependence on E since also R_r depends on E . However for the sun, if the resonance is not too close to the solar core, the matter density is exponentially varying with a very good approximation, $n_e \simeq n_0 e^{-10R/R_\odot}$, and therefore $dN/dR|_{R_r} = (10/R_\odot)(\Delta/4E) \sin 2\alpha$ and finally the resonant condition becomes

$$E \ll -\frac{R_\odot}{40} \Delta \sin 2\alpha \quad (1.72)$$

With a crude approximation in order to estimate at least qualitatively the possible influence of the matter effects on the flavour content of solar neutrinos we can assume, following (1.69-1.72), that

$$P_{ee} = 0 \quad \text{if} \quad -\frac{\Delta}{4} \frac{\sqrt{2}}{Gn_e(R_i)} < E_\nu < -\frac{R_\odot}{40} \Delta \sin 2\alpha \quad (1.73)$$

or

$$P_{ee} = 0 \quad \text{if} \quad \frac{-\Delta}{\chi} \cdot 7 \cdot 10^{12} (\text{eV})^{-1} < E_\nu < \Delta \sin 2\alpha \cdot 10^{15} (\text{eV})^{-1} \quad (1.74)$$

where E_ν is the neutrino energy and $\chi = n_e/n_A$, n_A being the Avogadro number. From (1.74) we can estimate the order of magnitude of all the relevant parameters which can give rise to a significant matter effect for solar neutrinos. We recall that the only neutrino fluxes which are important for solar neutrino experiments are ${}^8\text{B}$, ${}^7\text{Be}$ and pp neutrino fluxes. The end point energy for these fluxes are 15, 0.8, and 0.4 MeV respectively. Looking at (1.74) one can therefore immediately infer, taking into account that the maximum value of χ in the sun is around 150, that for $-\Delta$ above $2 \times 10^{-4} (\text{eV}^2)$, $2 \times 10^{-5} (\text{eV}^2)$ and $10^{-5} (\text{eV}^2)$ no matter effect is expected for ${}^8\text{B}$, ${}^7\text{Be}$ and pp neutrinos respectively. Taking the $\sin 2\alpha \rightarrow 1$ limit we can also infer a lower limit on Δ . For $-\Delta$

below 5×10^{-9} (eV^2), 10^{-9} (eV^2) and 5×10^{-10} (eV^2) ^8B , ^7Be and pp respectively are not affected. Finally one can also observe that for a given Δ there is also a lower limit on $\sin 2\alpha$ which has to be greater than $E_\nu/(-\Delta) \times 10^{-15}(\text{eV})^{-1}$ (one can assume $E_\nu = 3 - 5, 0.8, 0.3$ MeV for ^8B , ^7Be and pp respectively). This constraint can easily be understood qualitatively, in fact, in the limit of vanishing α no oscillation is possible in the flavour space, due to the absence of mixing both in matter and in vacuum, and therefore it must exist a lower limit on the non diagonal elements in the evolution hamiltonian below which oscillations are ineffective.

To go beyond these qualitative analysis an exact or almost exact solution of the evolution equation is needed. The evolution equation has been solved analytically assuming a linear density or an exponential density. The linear approximation [59] can be good only locally and must be used near the resonance, however it has the drawback to be not very accurate for large mixing angle due to the fact that in this case the length of the resonant region can be quite large. The exponential [60] density is a good representation of the solar density (at least not too close to the solar core) and it has not problems in the case of large mixing angle. These two approximation have been extensively used to analyze solar neutrino data [61-65].

In the following chapter we report the results of our analysis of solar neutrino data based on numerical solution of the evolution equations.

CHAPTER 2

SOLAR NEUTRINO EXPERIMENTS AND DETERMINATION OF THE NEUTRINO OSCILLATION PARAMETERS

The MSW matter enhanced neutrino oscillation mechanism [25, 26] offers an attractive possibility of reconciling the theory and the experimental results with a minimal change of the standard neutrino physics. We believe it is worthwhile investigating the quantitative impact that the forthcoming experiments will have in testing the MSW hypothesis.

We first address the numerical calculation of the solar neutrino signals in the different detectors as a function of the neutrino square mass difference and of the mixing angle. This computation has been repeated using both Bahcall best model with helium diffusion [2] and Turk-Chièze solar model [8] in order to estimate the impact of the theoretical uncertainties. This calculation determines the region of MSW parameters that reproduce the experimental data. We compare our results with the other existing computations [61-65] of the MSW effect to assess the importance of our more rigorous approach and try to explain small differences between calculations.

The other purpose of this chapter is to discuss the impact that future experiments, namely Super Kamiokande [40], SNO [39] and Borexino [41], are likely to have on the MSW effect. We individuated the following two key issues. The first question concerns the range of MSW parameters that can be tested independently of the SSM. We do not need to stress the importance of testing the MSW mechanism without dealing with the theoretical uncertainties on the neutrino fluxes. The second question addresses the possibility of restricting the MSW parameters to only one of the two disjointed regions of the parameter space that are allowed by the present experimental data (the so called large and small mixing angle solutions to the SNP).

Because of the correlation between the detected electron and the incoming neutrino energies, the SNO and Superkamiokande detectors will be able of measuring the ^8B neutrino spectrum. The shape of the neutrino spectra is determined only by the nuclear process responsible for the neutrino production and is independent of the solar model. Therefore, any spectral distortion would be an incontrovertible evidence of unconventional neutrino properties independently of the SSM. We compute the neutrino spectra as a function of the squared mass difference, Δm^2 , and the vacuum mixing angle θ . Using both Montecarlo simulation and theoretical analysis of the χ^2 distribution function we obtain a quantitative estimation of the possibility to appreciate the distortion. In this way we are able to precisely delimit the region of MSW parameters where a, say, 3σ effect will be detected (with a given probability).

The SNO detector has the unique possibility of measuring separately both the charged current contribution from solar neutrinos, through the reaction $\nu_e D \rightarrow p + p$, and the the neutral current contribution, through the reaction $\nu_e D \rightarrow n + p + e^-$. The ratio of these two signal is again independent of the solar model and its being different from the value expected in the case of no oscillation would be also evidence that ν_e are converted to ν_μ or ν_τ : unconventional neutrino properties would

be tested independently of the SSM. To this purpose, we report the isocontour plot of the ratio of the charged to the neutral current signal expected from the SNO detector on the MSW plane.

We also realize that an independent measurement of this same ratio can be extracted from the comparison of the SNO charged current and the Super Kamiokande mixed current signals. To our knowledge this is the first time that this possibility is noticed. Given the expected statistics in the two experiments, we estimate that this second measurement of the charged to neutral current ratio will have the same accuracy of the direct measure. Moreover, the comparison of the SNO charged current and Super Kamiokande mixed current signals will provide not only this ratio integrated over the energy, but also its differential value as function of the energy.

Finally, the Borexino experiment [41] is expected to measure with a large accuracy the ${}^7\text{Be}$ neutrino line. The knowledge of the ${}^7\text{Be}$ neutrino flux from this experiment, of the ${}^8\text{B}$ neutrino flux measured by Superkamiokande and SNO and of the combination of the pp , ${}^7\text{Be}$ and ${}^8\text{B}$ neutrino fluxes from the Gallex and Sage experiments should determine at least in principle, the various components of the neutrino flux: i. e. one can derive the total neutrino flux which can be compared with that inferred from the measured energy produced in the Sun (again a test independent of the SSM). We report the isoSNU contour plot for Borexino.

Before reporting the results of our analysis we believe useful to recall all the important points which have to be considered to obtain the correct answer.

1) Since neutrinos are produced over an extended region of the sun one has to average the conversion probability over the production region of the neutrinos.

2) Expecially in the case of large mixing angle large vacuum precession amplitudes are possible. However in the parameter range of interest this results in oscillations with the neutrino energy which cannot be resolved by the detector energy resolution, therefore one has to take only the average effect of these oscillations.

3) In a restricted range of parameters matter effects are important also inside the earth. Neutrinos converted to ν_μ can cross the earth and be regenerated as ν_e . This effect is extensively discussed in [66, 67]. This effect is obviously present only for neutrinos detected during night and therefore in the relevant range of parameters one expects to observe some difference among the signal detected during night and the signal detected during the day (day-night effect). On the basis of the non observation of this effect alone it has been possible to exclude a portion of the parameter space [14, 68]. Let's we notice here that this effect is completely independent from the solar model. In the future we expect that the sensitivity to this effect will be enlarged expecially for the large statistic detector Borexino [41]. In the computation of neutrino evolution one has therefore to include the path of neutrinos trough the earth and in the analysis one has to take into account the exclusion region obtained on the basis of the non observation of the day-night effect.

4) Finally it is evident from the resonant and adiabatic conditions (1.69) and (1.59) that the matter effect is energy dependent and therefore some deviation is expected from the original neutrino spectrum. Since this spectrum depends only on the involved nuclear reaction it is completely independent from the solar model. On the basis of the spectral information alone it has been possible to exclude a region in the parameter space [69]. This effect will be extremely important for some

of the future experiments (SNO [39], Superkamiokande [40]) which will measure the B^8 neutrino spectrum with large statistic.

§2.1 The Calculation

Neutrinos are produced as flavor eigenstates. If mass and flavor eigenstates do not coincide, flavor oscillations will occur. The practical relevance of this effect will depend on the neutrino mixing angle and mass difference. Neutrino interaction with matter can significantly change the oscillation pattern [25, 26]. The time dependent evolution hamiltonian depends on the neutrino energy, mass splitting and vacuum mixing angle, and on the matter density. Approximations are available that yield analytic solutions of the neutrino evolution equations and reproduce the numerical solution within a few percents for a given monotonic density profile [59, 60] For non monotonic density profiles, as the ones found on their path by part of the neutrinos, these solutions can be less accurate. We realized that the results from the next stage experiments, as we hope to show in this paper, will be accurate enough that even the small errors introduced by these approximations might matter. Therefore, we chose to numerically integrate the equations. To this end we developed a new numerical code completely independent from the one [67] used by the GALLEX group [61]. The main difficulty of numerically integrating this system of equations is due to the presence of two often widely different length-scales in the problem: the distance over which matter density changes and the wave-length associated with the energy difference between the two solutions. We use a combination of an adaptive-step Runge-Kutta method, which controls that the 1% required accuracy on the final amplitude is achieved, and exact diagonalization of the evolution hamiltonian at intermediate steps, which solves the problem for constant density and make the computation more efficient when the density is not constant. Sum over the production regions is performed using the radial distribution functions for the different neutrino fluxes given by Bahcall [3]; total fluxes and energy spectra are taken from the same source. Solar electron and neutron density profiles have been calculated by Castellani *et al.* [10]. To check the stability of the MSW suppression against changes of the electron and neutron density profiles, we have repeated the calculation with the electron and neutron density profiles for the best model of Ref. [2] with and without helium diffusion. A preliminary comparison of the suppression obtained with the three densities profiles, the one calculated by Castellani *et al.* [10] and the two calculated by Bahcall and Pinsonneault [2], shows no significant difference between the three models. Since we used about twice as many density points for the first profile, this lack of difference seems also to imply that the mesh used was adequate. We shall more carefully address these issues elsewhere. We took the terrestrial densities as tabulated by Poirier [70], and assumed a 0.5 ratio of neutrons to nucleons. We did not test the effect of changing the terrestrial densities, but the check made for the solar densities suggests that results are not very sensitive to the details of the density profile. We used the $^{71}\text{Ga}(\nu_e, e^-)^{71}\text{Ge}$ cross-section tabulated by Bahcall [3], and the $^{37}\text{Cl}(\nu_e, e^-)^{37}\text{Ar}$ cross section from Ref. [71]. Cross-sections for $^2\text{d}(\nu_e, e^-) \text{pp}$ have been taken from

Ref. [72]. All tabulated data, fluxes, densities and cross-sections, have been interpolated by cubic spline.

Solar neutrinos can undergo matter induced oscillations [25, ms] both inside the sun and inside the earth [66, 67], and vacuum oscillations on their way from the sun to the earth surface. Depending on the production point, on the time of the day, the time of the year and the position of the detector, neutrinos travel along different paths inside the sun, in the vacuum and inside the earth. Results reported in this paper are properly weighted averages over the neutrino production region and over the whole year: we selected 34 earth positions equally spaced in time on the exact orbit and 38 equally spaced times of the day for a total of 1292 different paths. The detector has been taken at a latitude of 45 degrees.

The whole calculation has been performed for a set of 6000 choices of the neutrino oscillation parameters: 60 logarithmically spaced values of $\sin^2 2\theta$ between 10^{-4} and 1, and 100 logarithmically spaced values of $\frac{\Delta m^2}{4E}$ between 1.25×10^{-23} MeV and 7.5×10^{-17} MeV. The already good resolution obtained by this grid has been improved by a two dimensional interpolation.

§2.2 Confidence regions for neutrino oscillation parameters

For each choice of the neutrino oscillation parameters Δm^2 and $\sin^2 2\theta$ there is a corresponding theoretical prediction for the probability P_{eX} of an electron neutrino ν_e , produced in the sun, to reach a detector as a different neutrino ν_X . In this paper we shall only consider mixing between ν_e and ν_μ . We calculate this conversion probability in the region of parameter space relevant for the MSW effect. The combination of the conversion probability and a theoretical prediction of the solar neutrino fluxes yields a theoretical prediction for any experiment whose neutrino detection cross-section is known. This prediction for the chlorine, νe -scattering and gallium experiments has already been reported by many authors. For completeness we show the results we obtain by using the solar neutrino fluxes given by Bahcall and Pinsonneault [2] in Fig. 2.1.

Given the experimental results R_j and their errors ΔR_j , we can calculate

$$\chi^2 = \sum_j \left(\frac{R_j - r_j}{\Delta R_j} \right)^2 \quad (2.1)$$

for any theoretical predictions r_j . The index j labels the different experiments. The experimental results R_j and their errors ΔR_j are given in Table 1. Minimization of χ^2 as function of Δm^2 and $\sin^2 2\theta$ defines our best fit values for the neutrino oscillation parameters, which we report in Table 2 together with the relative χ_{\min}^2 . We performed this exercise using fluxes from the solar model of Bahcall and Pinsonneault [2] (BPSM) and from the one of Turck-Chièze *et al.* [8] (TCL) to estimate the influence of SSM uncertainties. We believe that these two models well represent the whole range of reasonable theoretical predictions [9, 10]. Both values of χ_{\min}^2 indicates a good fit for 1 degree of freedom (3 experiments – 2 parameters). Under the assumptions that the experimental errors be normally distributed and that the model could be linearized around the best fit values, $\chi^2 - \chi_{\min}^2$

would be distributed as a χ^2 distribution with 2 degrees of freedom. In this case there would be a 90% probability that the true values of the parameters lay in the region defined by $\chi^2 \leq \chi_{min}^2 + 4.61$ and a 99% probability that they lay in the region defined by $\chi^2 \leq \chi_{min}^2 + 9.21$. These regions, together with the best fit points, are shown in Fig. 2.2 for both models. We point out that the plotted constant χ^2 curves are not ellipses, as they should be if the above assumption were correct. Moreover, three of the four selected regions in the parameters' plane are disconnected. We deduce that the model is definitely not linear in $\log(\sin^2 2\theta)$ and $\log(\Delta m^2)$. Nonetheless we still use χ^2 defined regions to characterize the "most likely" neutrino oscillation parameters and, for simplicity, refer to them as 90% and 99% confidence level (CL) regions, even if a precise assessment of the CL, *i.e.* the probability of finding the real parameters inside that region, would require a Monte Carlo simulation. In the literature, the part of the CL region that includes the best fit value, *i.e.* the point at which χ^2 has its absolute minimum, is referred to as the small angle (or nonadiabatic) solution of the SNP; the other one, when present, as the large mixing angle solution. We shall follow this convention. For reference, Table 2 reports, together to the absolute minima, the local minima found inside the large angle solution. We notice that the χ^2 values corresponding to the local minima indicate that their parameters are excluded at the 90% C.L. for 1 degree of freedom, but still allowed at the 99% C.L. For consistency we should disregard the large angle part of the 90% C.L. region present only for the BP model. However, because these C.L.'s have only a semi-quantitative validity, as previously discussed, we do not disregard this region, in spite of the fact that it is strongly disfavored. Finally let us remark that the large angle region disappears at the 87 % C.L. confirming its statistically marginal role.

The TCL predicts lower neutrino fluxes respect to the BPSM. This reduction is stronger for the ^8B neutrinos producing a less severe disagreement, relatively to the BPSM, with the Kamiokande experimental result compared to the other experiments. As a consequence, the large angle solution, which implies equally suppressed fluxes, is even less probable in the TCL than in the BPSM, as it is evident in Fig. 2.2. We also notice that the small angle solution is the most stable against changes of fluxes due to the steepness of the iso-SNU in that region.

The calculation of the iso-SNU contours, and consequently of the C.L. regions, is not trivial and computationally demanding, if one takes our approach and does not make any uncontrolled approximation at any stage. Several authors have performed similar calculations using various approximations that greatly simplify the task and are believed to reproduce the exact results within a few percents. We think worthwhile to compare our approach with a representative sample of the more recent such calculations [61-65]. To make the comparison more accurate, we repeated our computation of the C.L. regions in our approach by using in turns the solar models and the experimental results that have been used in the four computations under exam. In spite of the different inputs, the resulting C.L. regions (not shown) are similar one to the other. Moreover, the 90% confidence regions differ from the one shown in the top window of Fig. 2.2 mainly for their size: especially at large mixing angles they are bigger reflecting the use of older data with bigger errors.

The main points that distinguish the different calculations under exam are: the choice of the solution to the neutrino evolution equations on a given path, the average over the production region

and the handling of the regeneration inside the earth. We have tested several analytic solutions to the neutrino evolution [73] and found that it is indeed possible to find prescriptions that reproduce our numerical solution to within 5% for neutrinos that find monotonically decreasing densities as the ones that are produced at the center of the sun. Averaging over the neutrino production region is necessary not to overestimate the suppression and to correctly get a different average suppression of neutrinos that are produced over a larger region, *e.g.* pp -neutrinos, or over a smaller one, *e.g.* ${}^8\text{B}$ -neutrinos. This average implies that part of the neutrinos will find a non monotonical density and could resonate twice. It is not completely obvious to us that this part of the computation could be handled analytically with the same accuracy as the previous case. Finally, the main effect of neutrino propagation through the earth is to partially regenerate the ${}^8\text{B}$ neutrinos. On most of their path through the earth neutrinos find a density about 30 times smaller than they find in the sun, therefore resonating at values of $\frac{\Delta m^2}{4E}$ about 30 times smaller than in the sun: only the ${}^8\text{B}$ neutrinos have energies large enough that Δm^2 falls in a region not already excluded by the GALLEX result. At large angle the uniform suppression of ${}^8\text{B}$ and ${}^7\text{Be}$ is disfavored by the fact that Kamiokande sees a larger percentage of the SSM signal than the percentage seen by Homestake. Therefore, the smaller suppression of the ${}^8\text{B}$ neutrinos due to the earth regeneration increases the size and probability of the large angle solution to the SNP. This solution is still disfavored by the GALLEX result, and should disappear if GALLEX reduces its errors while keeping the reported value.

The calculation discussed by the GALLEX group [61] is the most similar to ours. The only differences are the method used to numerically solve the equations, the earth and sun density profiles (see remark in Sect. 2.1 on the insensitivity of the MSW suppression to densities changes) and the use of Monte Carlo method to perform the integrals over the production region, over the earth rotation and over the neutrino energy. We find almost identical intersections of the 2σ regions for the three experiments. The 90% CL region reported by the GALLEX group [61] is also in good agreement with the one we obtain by using the same SSM and experimental results they use. The only difference is in the large angle solution which we find slightly bigger. Given the agreement in the intersection of the 2σ regions, we ascribe the small difference to a different definition of the 90% CL region or to a different number of points in the parameter space that may affect the exact shape. Overall, we find reassuring, given the complexity of calculation, that two independently developed codes, which use different numerical algorithms, still provide very close results.

We are able to reproduce the small angle part of the 90% C.L. region found by Bludman *et al.* [62] with no theoretical uncertainties, but we disagree on the large mixing angle solution. They do not find this solution at the 90% C.L. when theoretical uncertainties are not included, while we find such solution using their input data, even if smaller than with the other inputs and that disappears at the 80% C.L. We think that the main cause of this discrepancy is the lack of earth effects in the discussion of Bludman *et al.*. In fact, a more recent computation by the same group [63] shows that including the earth effect enlarges the large mixing solution when theoretical uncertainties are included; even if they do not show there a calculation without theoretical uncertainties, we can assume that the effect would go in the same direction.

Calculations by Krastev and Petcov [64] of the intersection of the 68% and 95% C.L. regions for the Homestake, Kamiokande and GALLEX experiment (intersection that results in non- χ^2 -symmetric 31% and 86% C.L. regions) agree with our similar calculations in the small angle region. We do not find any large mixing intersection of the 68% C.L. regions, and they find a very small one. Our large mixing intersection of the 95% C.L. regions are qualitatively similar to theirs, but larger and shifted towards smaller angles: this discrepancy is most likely to be blamed on the lack of the earth regeneration.

We find the larger discrepancy with the work by Krauss *et al.* [65]. Even the small angle solution part of the 90% C.L. region, which seems to be the most stable in all calculations, is slightly shifted toward smaller mixing angles compared to our calculation that uses their same experimental numbers. Moreover, Krauss *et al.* [65] find a much wider large mixing angle solution, contrary to the previous cases, which all find smaller large mixing angle solutions: their solution extends from $\Delta m^2 = 7 \times 10^{-8}$ to $\Delta m^2 = 10^{-4}$, while ours goes from $\Delta m^2 = 3 \times 10^{-6}$ to $\Delta m^2 = 3 \times 10^{-3}$. We do not understand the reason of this relatively larger discrepancy.

In conclusion, we agree best with the one calculation [61] closer in method (numerical integration) and physical inputs (earth regeneration, annual and daily averages) to ours, find small and understandable differences with other two analytic calculations [62, [64]] and larger and less easily understandable differences with one calculation [65]. However, it is important to notice that most of the discrepancies are in the large mixing angle region, where iso-SNU are less steep and small changes of the experimental and/or theoretical data produce large changes of the confidence region. Moreover, this region has very little statistical weight, as already noticed it does not appear at the 90% C.L. using the TCL and disappear at the 87% C.L. using the BPSM, and seems doomed to disappear in the near future, if the next batch of GALLEX results confirm the actual ones.

We should mention that another effect of matter induced oscillations in the earth interior is the production of different day and night signals. The non observation of this effect excludes a portion of the parameter plane [14, 68]. The 90% C.L. excluded region is outside our 90% C.L. allowed regions and, therefore, we do not show it in our plots.

§2.3 Energy spectra

The MSW mechanism produces an energy dependent suppression of the solar neutrinos: experiments such as SNO [39] and Kamiokande [11, 12, 40], which provide information about the energy of the detected neutrino, should observe, given sufficient statistics, an energy spectra deformation that is independent of the overall flux and therefore of the SSM. We should remember that what is actually measured is the electron energy: in the charged current reaction at SNO little recoil energy is left to the much heavier nuclei, and the electron spectrum is almost equal to the neutrino one, shifted by the threshold energy, whereas in the neutrino-electron scattering the spectrum is smeared because of the neutrino recoil energy. Therefore, more stringent constraints on the oscillation parameters should come from the SNO spectrum information, given the same number of events. Fig. 2.3 shows

the theoretical electron spectra for the Sudbury experiment ($\nu_e + D \rightarrow e^- + p + p$) in the following cases: no mixing, parameters that produce the maximal spectral distortion, best fit, and the local χ^2 minimum for large mixing angles. Spectra for the same four cases are shown in Fig. 2.4 for the Kamiokande experiment. As already noticed, the figures show that the electron spectrum measured by Sudbury reflects directly the incident solar ν_e spectrum, while the electron spectrum measured by Kamiokande is smeared.

We report on the $\log(\sin^2 2\theta)$ vs. $\log(\Delta m^2)$ plane the information about the spectral deformation, so that it would be immediately evident for what range of parameters this information might help. To this end we find useful to characterize the deformation with the percentage variation of the moments of the electron energy spectrum from their standard value. Most of the relevant information is already present in the first of such moments: the average electron energy. We show results for the average energy over the scattered electron spectrum with a lower threshold of 5.5 MeV assuming 100% efficiency and no background.

We show in Fig. 2.5a the change in average energy that should be seen by SNO [39] because of the spectral deformation. The most useful constraints are along the nonadiabatic branch, where the average energy increases up to 14%, and along the adiabatic branch, where the average energy decreases as much as 20%; however, this last region is already excluded by the present experiments. The increase of the average energy along the nonadiabatic branch reflects the fact that the spectrum is depleted at lower energies; conversely, the spectrum is depleted at high energies in the adiabatic region and the average energy is consequently lower.

The change in average energy that can be measured by the neutrino-electron scattering gives its stronger constraints along the adiabatic branch for Δm^2 around 10^{-4} (eV^2) as shown in Fig. 2.5b. Again in this parameter region the spectrum is depleted at higher energies, and the average energy decreases to about 7% of its SSM value. The lower absolute variation respect to the corresponding measure at SNO reflects the smearing of the spectrum due to the recoil energy of the neutrino. The percentage deviation is much smaller in the nonadiabatic region ranging from 1% to 2%. However, the statistical analysis as discussed later show that even this small effect is not out of reach given the expected large statistics.

We remark that the change of the average neutrino energy depends only on the change of the shape of the spectrum and not on the possibly associated flux reduction, which is solar model dependent. To extract the maximal amount of information from the solar model independent spectral deformation and, therefore, to fully understand the quantitative impact spectral measurements we have performed the following more detailed analysis.

The spectra have been calculated in the whole region of the $(\Delta m^2, \sin^2 2\theta)$ plane which is concerned by the solar neutrino problem with the aim of identifying where the distortion is significant. We used a grid of 60 values of $\sin^2 2\theta$ logarithmically spaced between 10^{-4} and 1 times 100 values of Δm^2 logarithmically spaced between 10^{-7} and 10^{-3} eV^2 for a total of 6000 spectra. We consider these spectra between a threshold energy of 5.5 MeV (7.5 MeV) and an upper bound of 13.5 MeV, above which the signal is practically zero and experimental resolution and the smearing in energy are taken into account by histogramming the spectra with a bin width of 1 MeV: this produces 8 (6)

bins. Two experimental characteristics are not taken into account: the background which is not yet known in Sudbury, and which is hoped to be reduced in SuperKamiokande compared to the actual Kamiokande, and the fact that the efficiency is not 100 % above the threshold but increases from 50 % at 6.5 MeV to more than 90 % at 10 MeV [74]. For a fixed number of events N , typically 5000, let us define the following quantities: $n_i^{(0)}$ as the expected number of the events in the i th bin if the spectrum is not distorted and n_i as the actual number of the events found in the i th bin. If the spectrum under consideration is not distorted $\langle n_i \rangle = n_i^{(0)}$. Where we indicate with $\langle A \rangle$ the expected value of A . For each spectrum, we can generate by Monte Carlo an histogram $\{n_i\}$ and characterize its difference by the standard histogram $\{n_i^{(0)}\}$ by the function:

$$\chi^2 = \sum_{bin} \frac{(n_i - n_i^{(0)})^2}{n_i^{(0)}} \quad (2.2)$$

We can roughly say that a “large” χ^2 indicates a significant distortion. In the following, we shall call distorted (respect to the standard spectrum) a binned experimental spectrum $\{n_i\}$ for which χ^2 , as defined by Eq. (2.2), is greater than a fixed value $\chi_{99.5}^2$. The precise meaning of this definition is discussed in the Appendix.

For any given neutrino mixing angle and mass splitting we can compute theoretically the average $\langle \chi^2 \rangle$ in the limit of $\langle n_i \rangle \ll 1$. In Fig. 2.6 we report iso- χ^2 contours for $\chi^2 = 20(16.4)$, $40(34.6)$, $100(92.3)$ for a threshold energy of 5.5(7.5) MeV. These χ^2 isocontours have, roughly speaking, the following meaning: within this isocontours a spectral distortion, as defined above, should be detected with a statistic of about 5000, 2150 and 750 events respectively. We discuss in much more detail and in a more precise way the exact meaning of these statements in the Appendix. In Fig. 2.6a we plot the contours $\langle \chi^2 \rangle = 20, 40$ and 100 for the SuperKamiokande experiment assuming a 5.5 MeV threshold. Only the contours $\langle \chi^2 \rangle = 16.4$ and 92.3 are plotted for the same experiment with a 7.5 MeV threshold in Fig. 2.6b. We conclude that the SuperKamiokande experiment with a statistics of 5000 events should be able to test, via the spectral information alone, and independently of the SSM, the whole adiabatic region centered around $\Delta m^2 = 10^{-4}(\text{eV})^2$. If the SuperKamiokande experiment is able to achieve a lower threshold of 5.5 MeV, most of that region would already be excluded with only 1000 events. Moreover, the lower threshold experiment would be sensitive also to the nonadiabatic branch and in particular would cover the most likely region of the neutrino oscillation parameters given the present experiment and SSM’s. In any case less than two years of data taking for either SNO or SuperKamiokande should be sufficient to achieve a significant result, i.e. show or not a significant distortion of the measured spectrum.

In Fig. 2.6c and 2.6d we plot the contours $\langle \chi^2 \rangle = 20$ and 100 with respectively 5.5 MeV and 7.5 MeV thresholds for the SNO experiment. This experiment will be able to test the MSW hypothesis via the SSM independent spectral information over basically the whole interesting region of parameters including the actual best fit region of parameters. The lower threshold would imply that this result can be achieved already with the first 1000 events.

The results in Fig. 2.6 are perfectly consistent with Montecarlo simulation, we have chosen to display the $\langle \chi^2 \rangle$ only because it has a simpler visual interpretation.

For reference in Table 3 and Table 4 the expected $\langle \chi^2 \rangle$ for 5000 events is given at the best fit points, using respectively the BPSM and the TCL, for both experiments and thresholds. Notice that the $\langle \chi^2 \rangle$ we plot is only the expected value for the experimental quantity and statistical fluctuations of size described in Eq. (2.14) are indeed possible. Therefore, better discussed in the Appendix, we can conclude that the detection of spectral distortion for values of the neutrino oscillation parameter lying in the allowed 90 % C.L. region is only likely for the SuperKamiokande detector with the full 5000 event statistics. The same effect cannot be missed with the same statistics by the SNO detector. Let us remark that the chosen number of 5000 events is an extrapolation of the known Kamiokande result and it will be presumably obtained in about one or two years of operation, depending on the threshold.

The comparison of the results at different thresholds show that the detection threshold and efficiency near threshold will play a crucial role to determine the sensitivity of the spectral measurement. An higher threshold has a lower sensitivity due to both the lower statistics and the reduction in the number of points that define the shape of the spectrum, and consequently its distortion. In particular it seems that for a threshold of 7.5 MeV the nonadiabatic region might not be tested from Kamiokande and will require a large statistics at SNO.

As demonstrated by Figs. 2.6 the whole range of

$$10^{-8} \leq \Delta m^2 / eV^2 \leq 2 \cdot 10^{-4} \quad \text{and} \quad 10^{-8.56} (\Delta m^2 / eV^2)^{-1.08} \leq \sin^2 2\theta \leq 0.3 \quad (2.3)$$

will be explored by means of the spectral information only, covering almost four order of magnitude in Δm^2 (the actual upper limit in $\sin^2 2\theta$ is not so sharp as can be seen in figg. 2.5-2.6).

§2.4 Charged and Neutral Current Interaction

The detection of a ν_μ (or ν_τ) flux would provide a firm and SSM independent evidence of nonstandard neutrino properties. The possibility of distinguishing electron from other active neutrinos is provided by their different interactions with ordinary matter: electron neutrinos have both charged and neutral current interactions, while the other neutrinos can only interact with ordinary matter via neutral current at the relevant energies. We shall discuss two independent methods of extracting this important piece of information from future experiments.

A direct determination shall come from the SNO detector [39] that will be able to measure rates both of the charged current reaction $\nu_e D \rightarrow p + p + e^-$ and of the neutral current reaction $\nu_{e,\mu} D \rightarrow n + p + \nu_{e,\mu}$. The experimental rate for the first reaction is:

$$R_{\text{SNO}}^{cc} = \langle \Phi(E) P_{ee}(E) \sigma^{cc}(E, T) \rangle_{E, T} = \langle \Phi(T + \Delta^{cc}) P_{ee}(T + \Delta^{cc}) \bar{\sigma}^{cc}(T) \rangle_T \quad , \quad (2.4)$$

where E and T are respectively the energy of the incoming neutrino and the energy of the detected electron. We denoted the ^8B neutrino flux with $\Phi(E)$, the survival probability of electron neutrinos with $P_{ee}(E)$, and the charged current $\nu_e D \rightarrow p + p + e^-$ cross section with $\sigma^{cc}(E, T)$. (Notice that the ^8B neutrino flux is the only component of the total flux above the experimental threshold for

this reaction). We also denoted the integral over the neutrino and electron energy with $\langle \rangle_{E,T}$; this integral depends on the threshold energy for electron detection and on the detection efficiency, which in the following we shall assume equal to one. Since the kinematics is such that the final electron energy T is practically equal to the neutrino energy E minus the threshold energy Δ^{cc} for the charged current reaction, we defined $\bar{\sigma}^{cc}(T)$ such that $\sigma^{cc}(E, T) = \bar{\sigma}^{cc}(T)\delta(E - T - \Delta^{cc})$, and explicitly performed the integral over the neutrino energy in Eq. (2.4). Analogously, the experimental rate for the second reaction is:

$$R_{\text{SNO}}^{nc} = \langle \Phi(E)(P_{ee}(E) + P_{e\mu}(E))\sigma^{nc}(E) \rangle_E \quad , \quad (2.5)$$

where E is again the incoming electron energy, and no final particle energy is measured. We denoted the probability of electron neutrino conversion to muon neutrino with $P_{e\mu}(E)$, and the neutral current $\nu_{e,\mu}D \rightarrow n + p + \nu_{e,\mu}$ cross section with $\sigma^{nc}(E)$. Notice that $P_{ee}(E) + P_{e\mu}(E) = 1$ only if there are not oscillations in sterile neutrinos. We shall also use the symbols $(R_{\text{SNO}}^{cc,nc})_0$ for the corresponding quantities when $P_{ee}(E) = 1$ and $P_{e\mu}(E) = 0$. We extract a solar model independent physical information from the experimental quantities defined in Eqs. (2.4) and (2.5) through the following quantity:

$$R_{\text{SNO}}^{cc/nc} = \frac{R_{\text{SNO}}^{cc}}{R_{\text{SNO}}^{nc}} \left(\frac{R_{\text{SNO}}^{nc}}{R_{\text{SNO}}^{cc}} \right)_0 \quad . \quad (2.6)$$

Notice that the normalization factor is independent of the absolute value of the ${}^8\text{B}$ flux and, therefore, of the SSM. If electron neutrinos oscillate into muon or tau neutrinos, the ratio $R_{\text{SNO}}^{cc/nc}$ is less than one. However, this ratio could be different from one even when there are no muon or tau neutrinos, if the electron neutrino is converted into sterile neutrino with a energy dependent conversion probability. This spectrum deformation effect can be tested more effectively with the techniques discussed in the previous section and we shall assume only oscillations into active neutrinos.

We report in Fig. 2.7 the expected values of $R_{\text{SNO}}^{cc/nc}$ as function of the oscillation parameter for a lower threshold for electron detection of 5.5 MeV. We repeated the calculation for a threshold of 7.5 MeV finding no appreciable difference. In the same figures we report the 90% CL region (the exact definition of the region and the caveat about the meaning of 90% have been discussed in Sect. 2.2) coming from the present measures at Homestake [7], Kamiokande [14] and Gran Sasso [19, 20]: the overlap predicts the expected rate for the experiment. The predicted rates for the best fit values in the BP and TCL models are reported in Table 3 and Table 4, respectively. At the 90% C.L. the MSW solution of the SNP implies an effect larger than 50%, which should be clearly seen by the SNO experiment.

An alternative and complementary determination of the presence of active solar neutrinos other than the electron ones shall come from the comparison of the SNO and SuperKamiokande data. To our knowledge this is the first time that the following analysis of the experimental data is proposed. At SuperKamiokande ν_μ and ν_τ scatter off electrons through the neutral current interaction. This process has an averaged cross section which is, for threshold energies between 5 and 8 MeV about 15 % of the total ν_e scattering cross section. If we only look at the total cross section of the process, the oscillation of the ν_e into active neutrinos would be indistinguishable from the effect of a lower

neutrino flux. Nonetheless, it is possible to distinguish the two effects by comparing results from SNO and SuperKamiokande. From the SNO experiment, we shall have not only the total rate, but also the differential rate as a function of the electron energy:

$$\frac{dR_{\text{SNO}}^{cc}}{dT}(T) = \Phi(T + \Delta^{cc})P_{ee}(T + \Delta^{cc})\bar{\sigma}^{cc}(T) \quad , \quad (2.7)$$

where the symbols have been defined following Eq. (2.4). From this differential rate it is possible to derive $\Phi(E)P_{ee}(E)$ as function of the electron neutrino energy E for neutrino energy $E > T_{\text{th}} + \Delta^{cc}$, where T_{th} is the threshold electron energy for detection. Using this information, it is possible to isolate the contribution of the muon neutrinos to the Kamiokande signal. We define the ratio of this contribution to the total signal:

$$\mathcal{R}_{\text{Kam}}^{\mu} = \frac{\langle \Phi(E)P_{e\mu}(E)\sigma^{\mu}(E, T) \rangle_{E, T}}{\langle \Phi(E)(P_{ee}(E)\sigma^e(E, T) + P_{e\mu}(E)\sigma^{\mu}(E, T)) \rangle_{E, T}} \quad , \quad (2.8)$$

where $\sigma^{e,\mu}$ is the cross section for $\nu_{e,\mu}e^{-}$ scattering. It is also useful to define as R_{Kam} the total signal from the SuperKamiokande detector, which is nothing that the denominator of Eq. (2.8), and as $(R_{\text{Kam}})_0$ the corresponding signal expected if $P_{ee} = 1$ and $P_{e\mu} = 0$. It is a trivial exercise to obtain $\mathcal{R}_{\text{Kam}}^{\mu}$ from the known experimental quantities:

$$\mathcal{R}_{\text{Kam}}^{\mu} = 1 - \frac{(R_{\text{Kam}})_0 \langle W(E) \frac{dR_{\text{SNO}}^{cc}}{dT}(E - \Delta^{cc}) \rangle_E}{(R_{\text{SNO}}^{cc})_0 R_{\text{Kam}}} \quad , \quad (2.9)$$

where

$$W(E) = \frac{(R_{\text{SNO}}^{cc})_0 \langle \sigma^e(E, T) \rangle_T}{(R_{\text{Kam}})_0 \bar{\sigma}^{cc}(E - \Delta^{cc})} \quad . \quad (2.10)$$

$W(E)$ is a known function that depends on the threshold energy used to take the average over T , but not on the solar standard model. In Fig. 2.8c we plot $W(E)$: notice that it does not depend much on the energy in the relevant range. In the limit when $W(E)$ is constant, and equal to one because of chosen normalization, $\mathcal{R}_{\text{Kam}}^{\mu}$ reduces to:

$$\tilde{\mathcal{R}}_{\text{Kam}}^{\mu} = 1 - \frac{(R_{\text{Kam}})_0 R_{\text{SNO}}^{cc}}{(R_{\text{SNO}}^{cc})_0 R_{\text{Kam}}} \quad , \quad (2.11)$$

which is derived from the total rates only. Both $\mathcal{R}_{\text{Kam}}^{\mu}$ and $\tilde{\mathcal{R}}_{\text{Kam}}^{\mu}$ can be calculated from the experimental data and are independent of the solar standard model. The experimental error on the absolute value of $\tilde{\mathcal{R}}_{\text{Kam}}^{\mu}$ is smaller than the sum of the relative errors on R_{SNO}^{cc} and R_{Kam} , which is expected on the order of few percents. Moreover, we wish to point out that more information is in principle available: the possibility of comparing measurements as function of the electron energy will yield a differential measure of $\mathcal{R}_{\text{Kam}}^{\mu}$.

We report in Fig. 2.8a the expected values of $\mathcal{R}_{\text{Kam}}^{\mu}$ as function of the oscillation parameter for a threshold for electron detection at Kamiokande of 7.5 MeV. The choice of 7.5 MeV has been made, because it implies a threshold for electron at SNO lower than $7.5 - \Delta^{cc} \approx 6$ MeV, which should be achievable. In the same figures we report the 90% CL region coming from the present measurements.

The predicted rates for the best fit values in the BP and TCL models are reported in Table 3 and Table 4, respectively. At the 90% C.L. the MSW solution of the SNP implies an effect larger than 15%, which should be clearly seen. We report in Fig. 2.8b the expected values of $\bar{\mathcal{R}}_{\text{Kam}}^\mu$. The fact that there is almost no difference between Fig. 2.8a and Fig. 2.8b demonstrate that for all practical purposes $W(E)$ is one and it is enough to consider the information derived from the total rates.

§2.5 BOREXINO

The interest of the BOREXINO [41] experiment is that it is sensitive mostly to berillium neutrinos, and therefore supplements the chlorine measures [7], sensitive to boron and berillium neutrinos, the electron scattering experiments [13, 14] sensitive only to boron neutrinos, and gallium measures [20], sensitive to boron, berillium and pp neutrinos. The expected rate for this experiment is of a few 10^4 events per year. The ratio of the yield expected if the MSW mechanism is at work over the one expected without MSW as function of the square mass difference and of the mixing angle is shown in Fig. 2.9 together with the “90% CL region” from the present experiments. Tables 3 and 4 report the predictions for this experiment based on the available measures and on respectively the BPSM and the TCL.

This exercise teaches us that almost any value of the ratio from zero to one is compatible with the present experimental situation. This result reflects the fact that the berillium line has an energy close to the one for which nonadiabatic correction become important, and that a slight change of parameters can make the line fall in or out the suppression region. Conversely, if the steepness of the iso-ratio lines does not allow to make a prediction for this ratio, it is also true that an experimental measurement will pinpoint the neutrino oscillation parameters.

To better understand the impact of this measurement we have repeated the same plot assuming the experimental errors that should be available at the end of 1996, about the time when Borexino is expected to become operational, and by assuming three different central values, 77, 87 and 97 SNU for the gallium measurements. In fact, the gallium experiment is the only one which can have significantly different results and smaller errors at that time, both because of the increased statistics and of the better assessment of the systematic errors that shall follow the calibration of the detector. We should like to make two points here: *i*) the large angle solution is likely to disappear with increasing accuracy of the gallium experiments, *ii*) the prediction for Borexino will remain largely unfixed, even if one should notice that in the best fit point an almost maximal suppression is predicted for this experiment.

§2.6 Discussion and prospectives

i) We first addressed the calculation of the solar neutrino signals in the different detectors as a function of the neutrino square mass difference and of the mixing angle, using purely numerical

methods, without any approximation, in order to get the high accuracy necessary for the comparison of experimental data. We obtain a good fit to experimental data in the small angle region and a statistically marginally acceptable fit in the large angle region. We also notice that the small angle region is very stable against changes of fluxes. When comparing with other authors, we agree best with the one calculation closer in method and physical inputs to ours, find small and understandable differences with other two analytic calculations and larger and less easily understandable differences with one calculation. However, it is important to notice that most of the discrepancies are in the large mixing angle region, where iso-SNU are less steep and small changes of the experimental and/or theoretical data produce large changes of the confidence region. Moreover, this region has very little statistical weight and seems doomed to disappear in the near future, if the next batch of GALLEX results confirm the actual ones.

ii) Future measurements, of electron spectra (SNO, SuperKamiokande), will explore the region $10^{-8} \leq \Delta m^2/eV^2 \leq 2 \cdot 10^{-4}$ and $10^{-8.56}(\Delta m^2/eV^2)^{-1.08} \leq \sin^2 2\theta \leq 0.3$. In particular, the small angle solution will be tested certainly by SNO and likely also by SuperKamiokande.

iii) With respect to the no oscillation case, the ratio of charged to neutral current events in SNO would test unconventional neutrino properties in the range $10^{-8} \leq \Delta m^2/eV^2 \leq 2 \cdot 10^{-4}$ and $10^{-8} \cdot (\Delta m^2/eV^2)^{-1} \leq \sin^2 2\theta \leq 1.0$ (Fig. 2.7). This ratio is varied by at least 50 % for the MSW solution and should be clearly detected.

iv) We point out that the presence of muon neutrinos can be determined also by comparing the SNO charged current signal with the SuperKamiokande signal. We estimate that the essentially the same range of the previously discussed measurement will be explored. For the MSW solutions muon neutrinos contribute at least 15 /which should be clearly identified.

v) For ${}^7\text{Be}$ neutrinos, almost any suppression factor is compatible with MSW solutions (Fig. 2.9a). Even improved accuracy on the gallium measurement will not change this conclusion, (Fig. 2.9b-d). On the other hand, an accurate experimental determination of ${}^7\text{Be}$ flux will pinpoint the neutrino mixing parameters.

§2.7 Appendix

In this Appendix we give a more detailed discussion of the function χ^2 , which has been defined in Eq. (2.2), and of the information carried by its average value. This discussion supplements the qualitative description of Sect. 2.3 and, hopefully, clarifies the statements made there and conclusions drawn from Fig. 2.6.

Our first remark is that, even when the two underlying distributions are equal, *i.e.* $\langle n_i \rangle = n_i^{(0)}$, we still expect a χ^2 , as defined by Eq. (2.2), different from zero owing to statistical fluctuations. Under the hypothesis that the $\langle n_i \rangle \gg 1$ the distribution of the stochastic function defined in Eq. (2.2) are well approximated by the chi-square probability function with a number of degrees of freedom equal to the number of bins minus one, because the normalization imposes one constrain. A chi-square probability function with 7 (5) degrees of freedom yields an average $\langle \chi^2 \rangle$ of 5 (3)

and χ^2 values larger than $\chi_{99.5}^2 = 20.3$ (16.7) with a probability lower than 0.5%. Note that these numbers are independent of the total number of events and depend only on the number of bins. The first quantitative statement we are able to make is that if the experiment determines a χ^2 larger than $\chi_{99.5}^2 = 20.3$ (16.7) we can conclude that the spectrum is distorted at the 99.5% C.L. This explains our definition of distorted spectrum given in Sect. 2.3 as that spectrum that yields a $\chi^2 > \chi_{99.5}^2$. We could obviously have chosen a different CL for the definition.

The second quantitative statement we would like to make is the answer to the following question: will N events be enough to discriminate a given distorted spectrum from the standard one with the chosen C.L. or, equivalently, how many events are necessary to discriminate a given spectrum from the standard one. If the two spectra are not equal, the χ^2 , as defined by Eq. (2.2), has a probability distribution that is not anymore the chi-square probability function. Since we need this distribution to make quantitative statements, we can generate by Monte Carlo many histograms $\{n_i\}$ obtaining the distribution of the corresponding χ^2 's for each point in the MSW plane. Alternatively, we can assume that the distribution does not change much among points close to each other in the MSW plane and generate only one χ^2 for each point. An averaged (smeared) value among neighbouring points estimates the expectation for χ^2 , and the fluctuation between neighbouring points estimates the expected spread.

We find more instructive to follow a third approach. It is possible, even if tedious, to show, again under the hypothesis that the $\langle n_i \rangle \gg 1$ and dropping nonleading terms in $1/N$, that the expected value of χ^2 is:

$$\langle \chi^2 \rangle = \langle \chi_0^2 \rangle + Nf \quad , \quad (2.12)$$

where

$$f = \frac{1}{N} \sum_{bins} \frac{(\langle n \rangle - n_i^{(0)})^2}{n_i^{(0)}} \quad (2.13)$$

and the variance σ_{χ^2} of the χ^2 distribution is given by

$$\sigma_{\chi^2} = \langle (\chi^2 - \langle \chi^2 \rangle)^2 \rangle = 2Nf \quad . \quad (2.14)$$

Note that the function f depends only on the spectral distortion and does not depend on the normalization N . We have indicated with $\langle \chi_0^2 \rangle$ the value expected with no distortion. Under the reasonable hypothesis that there is about an equal probability of finding χ^2 larger or smaller than $\langle \chi^2 \rangle$, we can make the following statement. Given a theoretical distortion characterized by f the condition $\langle \chi^2 \rangle > \chi_{99.5}^2$ selects the values of N for which an experiment has a 50% probability of classifying the spectrum as distorted:

$$N > N_{50} = \frac{\chi_{99.5}^2 - \chi_0^2}{f} \quad . \quad (2.15)$$

For 8 (6) bins this formula yields $N > 15.3/f$ ($N > 13.7/f$).

Under the additional hypothesis that the χ^2 distribution is approximately gaussian with parameters given by Eq. (2.12-2.14) we can also make the following statement. Given a theoretical

distortion characterized by f the condition $\langle \chi^2 \rangle - 2\sigma_{\chi^2} > \chi_{99.5}^2$ selects the values of N for which an experiment has a 97.72% probability of classifying the spectrum as distorted:

$$N > N_{97.72} = \frac{4 + \chi_{99.5}^2 - \chi_0^2 + \sqrt{16 + 8(\chi_{99.5}^2 - \chi_0^2)}}{f} \quad (2.16)$$

For 8 (6) bins this formula yields $N > 31.1/f$ ($N > 28.9/f$).

All the above statements should be taken with a grain of salt. They are valid under the stated assumptions and become less and less quantitatively valid the more we go into the tails of the distributions. Our attitude is that Eqs. (2.15) and (2.16) do not define the precise boundaries within which the statements become valid at the claimed C.L., but they correctly represent the regions where those statements are valid. Moreover, it is possible to give different C.L. as the definition of distorted spectra and, given the definition, require different probabilities of seeing the distorted spectra in a given experiment. With this caveat in mind and with the hope of giving a simple picture of the possibility of this approach, we content ourselves with giving the contours of iso- χ^2 that are defined by $\langle \chi^2 \rangle = 20(16.4)$, $100(92.3)$ and, in some cases, $40(34.6)$ for an hypothetical experiment with a total number of events $N = 5000$ and a threshold of $5.5(7.5)$. The first contour delimits the MSW parameters that produce spectra that have a probability certainly larger than 0.5 of being detected as distorted. The other two contours delimit areas of MSW parameters with spectra that obviously have probability practically 1 of being detected as distorted, if we keep the number of events fixed to 5000. It is more interesting to read these other two contours as selecting spectra that have a probability certainly larger than 0.5 of being detected as distorted with total number of events $N < 1000$ and $N < 2500$.

TABLES

TABLE I. Comparison of experimental results (Experiment) to the theoretical predictions of the Bahcall and Pinsonneault [2] Solar Model (BP SM) and of the Turck-Chièze *et al.* [8] Solar Model (TCL SM). The BP SM is their best one with Helium diffusion from Ref. [2]. The TCL SM is their prediction from Table 8 of Ref. [8] (1993). Experimental errors are statistical $1\text{-}\sigma$ errors quadratically combined to the systematic ones. SM errors are $1\text{-}\sigma$ effective errors.

	Homestake (SNU)	Kamiokande ($10^6 \text{ cm}^{-2} \text{ s}^{-1}$)	GALLEX (SNU)
Experiment	$2.23 \pm 0.25^{\text{a}}$	$2.84 \pm 0.45^{\text{b}}$	$87 \pm 16^{\text{c}}$
BP SM	8.0 ± 1.0	5.69 ± 0.80	132^{+7}_{-6}
TCL SM	6.4 ± 1.4	4.4 ± 1.1	123 ± 7

^aRef. [7]

^bRef. [14]

^cRef. [20]

TABLE II. Best fit values of $\sin^2 2\theta$ and Δm^2 and corresponding absolute minima of χ^2 for the Bahcall and Pinsonneault [2] (BP) and for the Turck-Chièze *et al.* [8] (TCL) SM's. For reference we also report the values of $\sin^2 2\theta$, Δm^2 and χ^2 corresponding to the local minima found at large mixing angle.

	Small mixing (best fit)		Large mixing	
	BP	TCL	BP	TCL
Δm^2 (eV ²)	7.4×10^{-6}	7.4×10^{-6}	1.9×10^{-5}	3.0×10^{-5}
$\sin^2 2\theta$	5.8×10^{-3}	4.2×10^{-3}	6.3×10^{-1}	8.6×10^{-1}
χ^2 (1 d.o.f)	0.54	0.92	4.6	6.2

TABLE III. Predictions for the future neutrino experiments by using the Bahcall and Pinsonneault SM. The figure number next to each symbol refers to the relative caption for a description of the quantity considered. The first column reports the prediction corresponding to the best fit to the neutrino oscillation parameters (column labeled BP in Table II). The second and third columns report the range of allowed values at the 90% CL in the same model if we restrict the parameters to respectively the small and large mixing angle region (see top window in Fig. 2). The union of the two ranges gives the range allowed at the 90% CL

BP SM		Small mixing		Large mixing
		best fit	range	range
$R_{\text{SNO}}^{cc/nc}$	(Fig. 7)	0.35	0.20 – 0.45	0.20 – 0.30
$\mathcal{R}_{\text{Kam}}^{\mu}$	(Fig. 8)	0.20	0.15 – 0.35	0.25 – 0.35
Borexino	(Fig. 9)	0.27	0.22 – 0.80	0.45 – 0.70
$\Delta\langle E\rangle_{\text{SNO}}$	(Fig. 5a)	4.0%	2.5% – 5.5%	-0.3% – 1.5%
$\Delta\langle E\rangle_{\text{Kam}}$	(Fig. 5b)	1.4%	1.1% – 1.7%	-0.1% – 0.4%
$\chi_{\text{Kam}, 5.5 \text{ MeV}}^2$	(Fig. 6a)	27	20 – 38	5 – 8
$\chi_{\text{Kam}, 7.5 \text{ MeV}}^2$	(Fig. 6b)	13	9 – 21	3 – 4
$\chi_{\text{SNO}, 5.5 \text{ MeV}}^2$	(Fig. 6c)	150	90 – 360	5 – 34
$\chi_{\text{SNO}, 7.5 \text{ MeV}}^2$	(Fig. 6d)	50	30 – 130	3 – 18

TABLE IV. Predictions for the future neutrino experiments by using the Turck-Chièze *et al.* SM. The figure number next to each symbol refers to the relative caption for a description of the quantity considered. The first column reports the prediction corresponding to the best fit to the neutrino oscillation parameters (column labeled TCL in Table II). The second column reports the range of allowed values at the 90% CL in the same model. In this model there is no large mixing angle region allowed at the 90% CL (see bottom window in Fig. 2).

TCL SM		Small mixing	
		best fit	range
$R_{\text{SNO}}^{cc/nc}$	(Fig. 7)	0.45	0.25 – 0.60
$\mathcal{R}_{\text{Kam}}^{\mu}$	(Fig. 8)	0.13	0.10 – 0.30
Borexino	(Fig. 9)	0.27	0.22 – 0.85
$\Delta\langle E\rangle_{\text{SNO}}$	(Fig. 5a)	2.5%	1.7% – 4.5%
$\Delta\langle E\rangle_{\text{Kam}}$	(Fig. 5b)	1.1%	0.8% – 1.6%
$\chi_{\text{Kam}, 5.5 \text{ MeV}}^2$	(Fig. 6a)	20	12 – 36
$\chi_{\text{Kam}, 7.5 \text{ MeV}}^2$	(Fig. 6b)	9	6 – 18
$\chi_{\text{SNO}, 5.5 \text{ MeV}}^2$	(Fig. 6c)	80	30 – 260
$\chi_{\text{SNO}, 7.5 \text{ MeV}}^2$	(Fig. 6d)	30	20 – 90

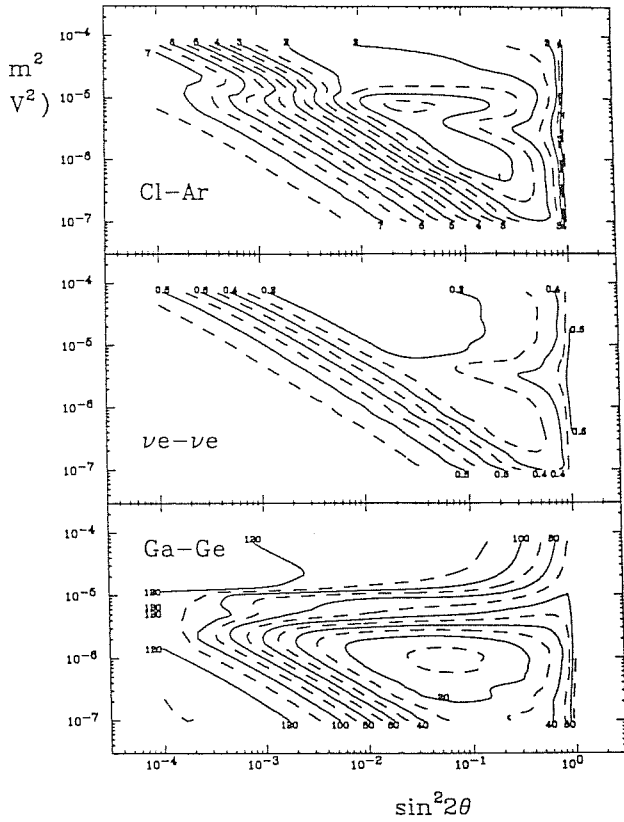


Fig. 2.1

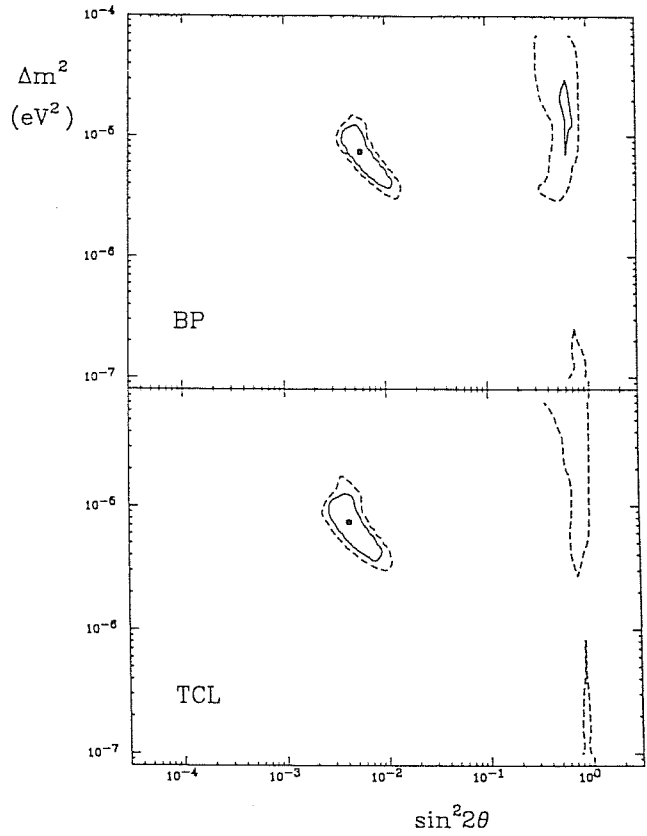


Fig. 2.2

Fig. 2.1 Iso-signal contours for the chlorine, electron scattering and gallium experiments. Results for the chlorine and gallium experiments are in SNU and have been obtained using neutrino fluxes from Ref. 2. Results for the electron scattering experiment are fractions of the no suppression result and the threshold energy for electron detection is 7.5 MeV. Labels refer to solid curves, dashed curves are half-way the solid ones.

Fig. 2.2 Confidence regions obtained using the Bahcall and Pinsonneault solar model [2] (BP) and the Turck-Chièze *et al.* solar model [8] (TCL). Solid curves delimit 90% CL regions, dashed curves 99% CL regions. Plotted points mark the best fit values for each of the two models.

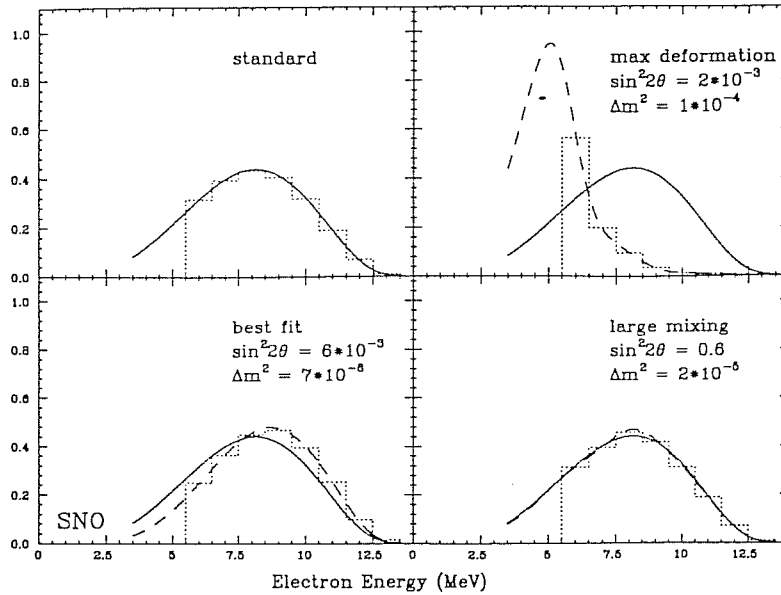


Fig. 2.3 Electron energy spectra as expected at SNO. Window labeled “standard” show the spectrum expected without neutrino oscillations and the corresponding binned histogram. The other three windows show as dashed curves the spectra expected for three choices of the MSW parameters: the top-right one corresponds to the maximal deformation, the bottom-left one to the best fit values and the bottom right one to the “large mixing” solution. We also plot the corresponding binned histograms and, for comparison, the standard spectrum as a solid curve. Spectra have been arbitrary normalized so that the integral between 3.5 MeV and 14.5 MeV is 2.5.

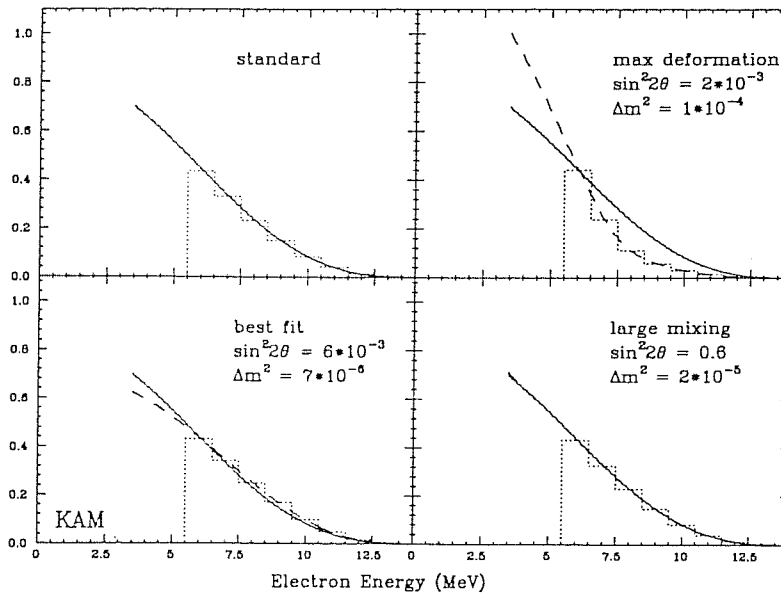


Fig. 2.4 Electron energy spectra as expected at Kamiokande. Window labeled “standard” show the spectrum expected without neutrino oscillations and the corresponding binned histogram. The other three windows show as dashed curves the spectra expected for three choices of the MSW parameters: the top-right one corresponds to the maximal deformation, the bottom-left one to the best fit values and the bottom right one to the “large mixing” solution. We also plot the corresponding binned histograms and, for comparison, the standard spectrum as a solid curve. Spectra have been arbitrary normalized so that the integral between 3.5 MeV and 14.5 MeV is 2.5.

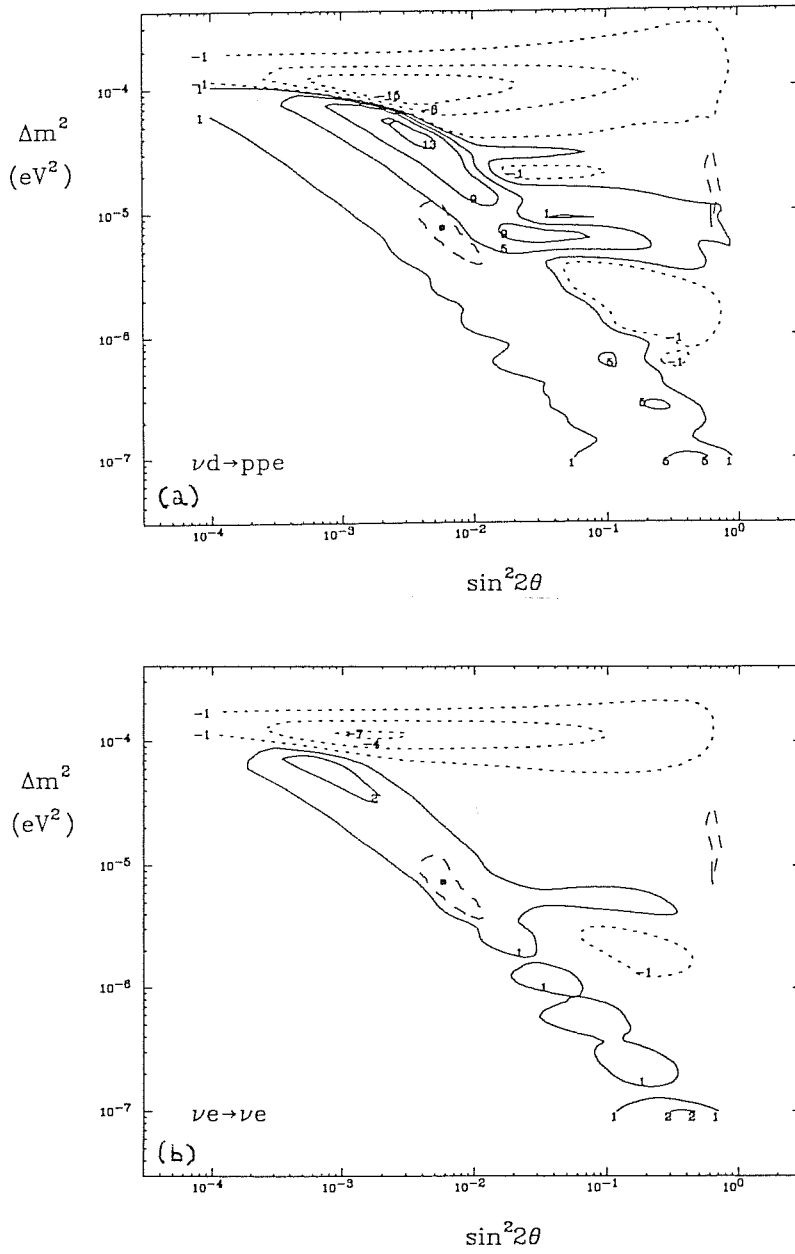
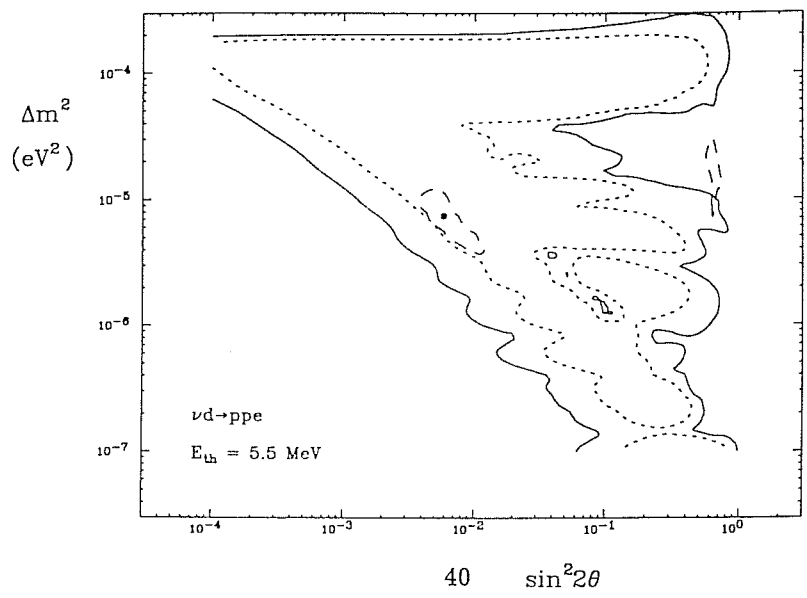
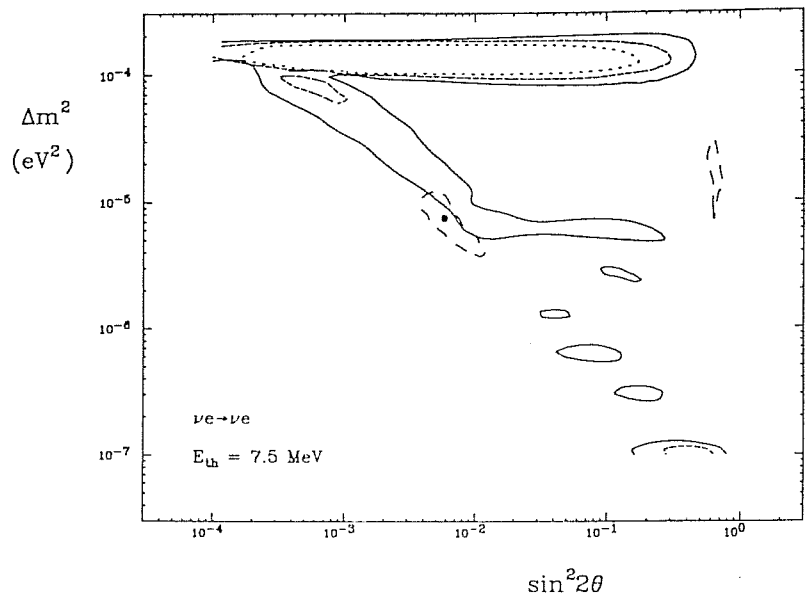
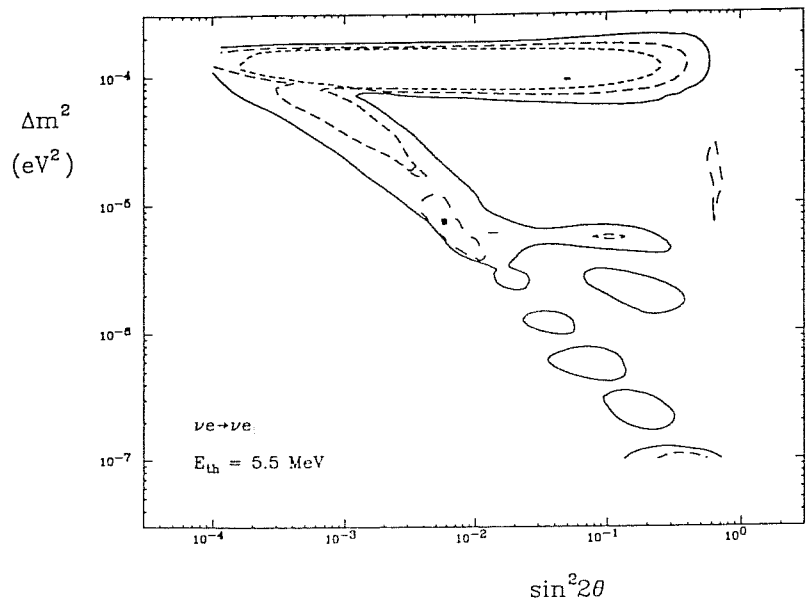


Fig. 2.5 Contours of iso-percentage-variation of the average electron energy expected at (a) SNO and (b) SuperKamiokande with a 5.5 MeV threshold. Solid curves denote positive variations, short-dashed curves negative variations. The 90% CL region (long-dashed curves) and the best fit to the experimental data as obtained in the BP SM (Fig. 2) are also superimposed. For SNO (a) the percentage variation ranges from -21.8% to 14.2% and the “standard” average electron energy is 8.42 MeV. For SuperKamiokande (b) the percentage variation ranges from -7.2% to 2.3% and the “standard” average electron energy is 7.44 MeV.



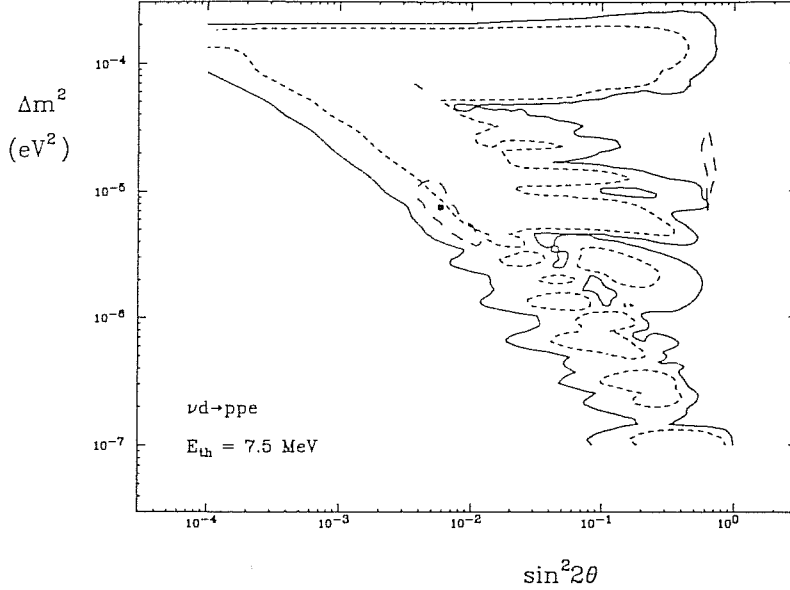


Fig. 2.6 Contours of the expected difference between the binned deformed electron spectra and the binned standard spectrum. The difference is measured by the $\langle \chi^2 \rangle$, with χ^2 defined in Eq. (2.1). All spectra are considered up to 13.5 MeV and from two lower thresholds for electron detection: 5.5 MeV (a) Kamiokande and (c) SNO, and 7.5 MeV (b) Kamiokande and (d) SNO. The bin size is one MeV yielding 8 bins for cases (a) and (c), and 6 bins for bins for cases (b) and (d). Solid curves delimit $\langle \chi^2 \rangle$ values larger than 20 for a sample of 5000 events for cases with 8 bins (a and c), larger than 17 for the same number of events for cases with 6 bins (b and d). Short-dashed curves delimit $\langle \chi^2 \rangle$ values larger than 82 (71) for the same sample size with 8 (6) bins or equivalently, as explained in the text, larger than 20 (17) for a sample of 1000 events. For cases (a) and (b) we also show curves (medium size dashes) delimiting $\langle \chi^2 \rangle$ values larger than 43 (37) for 5000 events or equivalently larger than 20 (17) for a sample of 2000 events. The largest values of $\langle \chi^2 \rangle$ (larger deformations) we found are: (a) 700 for $\sin^2 2\theta = 1.7 \times 10^{-3}$ and $\Delta m^2 = 1.1 \times 10^{-4}$ (enough 108 events to give a $\langle \chi^2 \rangle$ larger than 20), (b) 525 for $\sin^2 2\theta = 1.0 \times 10^{-3}$ and $\Delta m^2 = 1.3 \times 10^{-4}$ (enough 115 events to give a $\langle \chi^2 \rangle$ larger than 17), (c) 9500 for $\sin^2 2\theta = 1.9 \times 10^{-3}$ and $\Delta m^2 = 9.8 \times 10^{-5}$ (enough 8 events to give a $\langle \chi^2 \rangle$ larger than 20), (d) 3400 for $\sin^2 2\theta = 1.0 \times 10^{-3}$ and $\Delta m^2 = 1.3 \times 10^{-4}$ (enough 17 events to give a $\langle \chi^2 \rangle$ larger than 17). The 90% CL region (long-dashed curves) and the best fit to the experimental data as obtained in the BP SM (Fig. 2) are also superimposed.

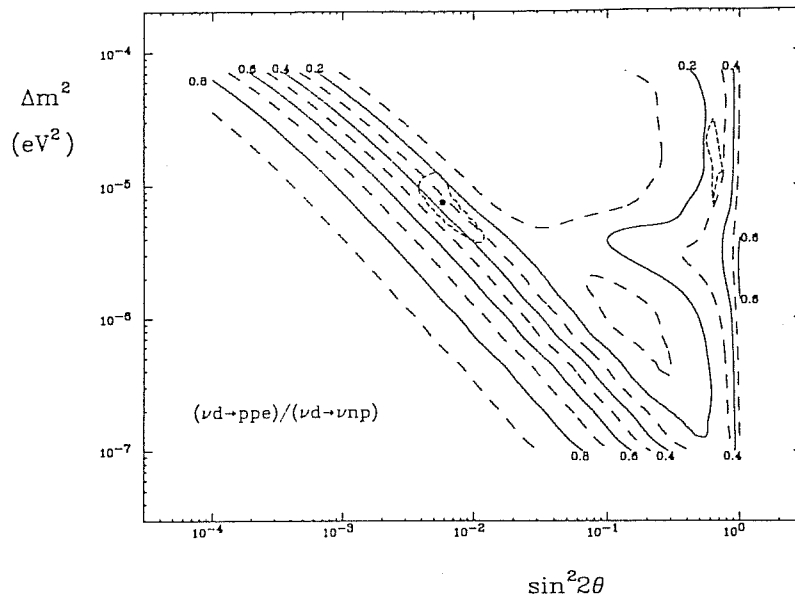
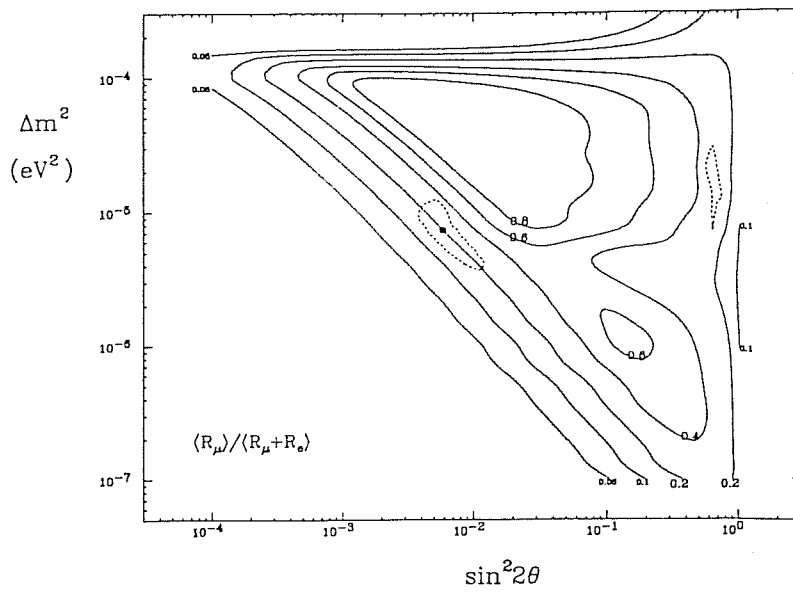


Fig. 2.7 Contours of iso-ratio of charged to neutral current reaction at SNO integrated from an electron threshold energy of 5.5 MeV; a threshold energy of 7.5 MeV produces no appreciable difference. The 90% CL region (long-dashed curves) and the best fit to the experimental data as obtained in the BP model (Fig. 2) are also superimposed.



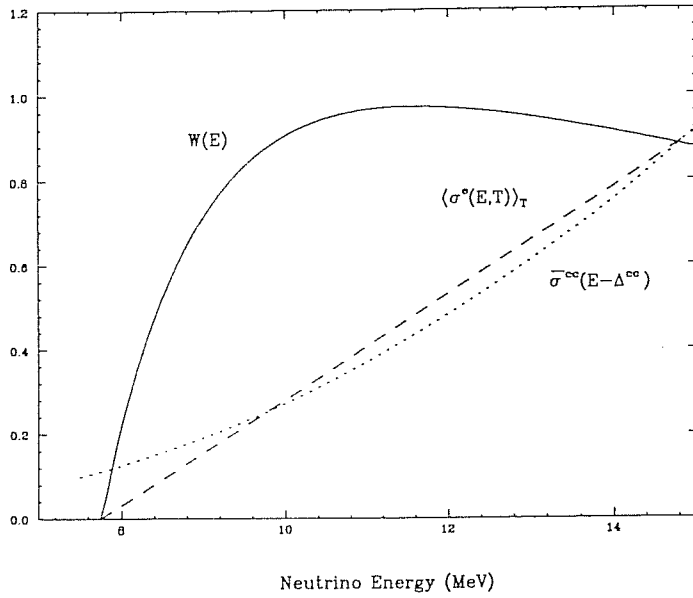
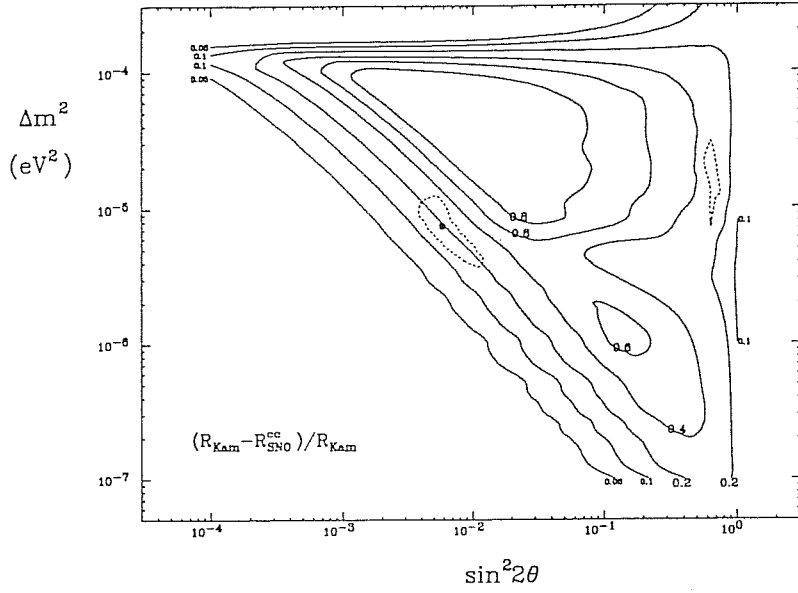
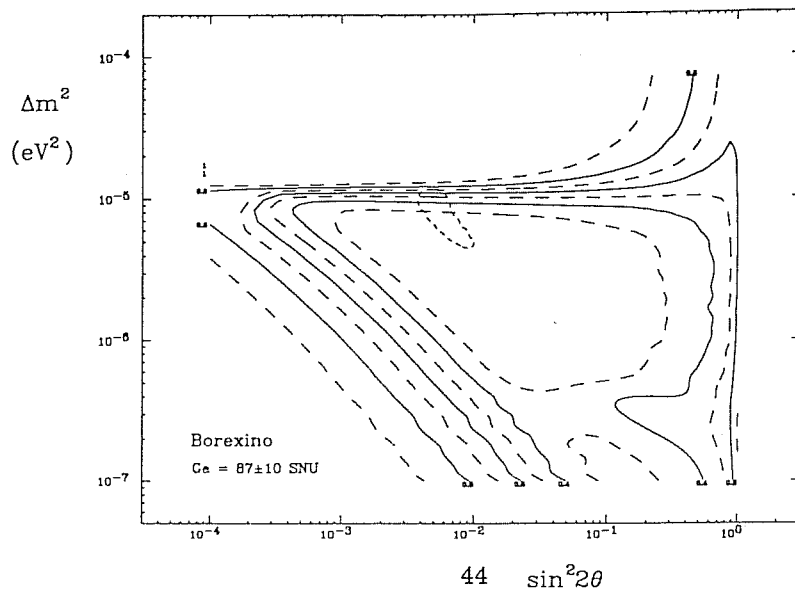
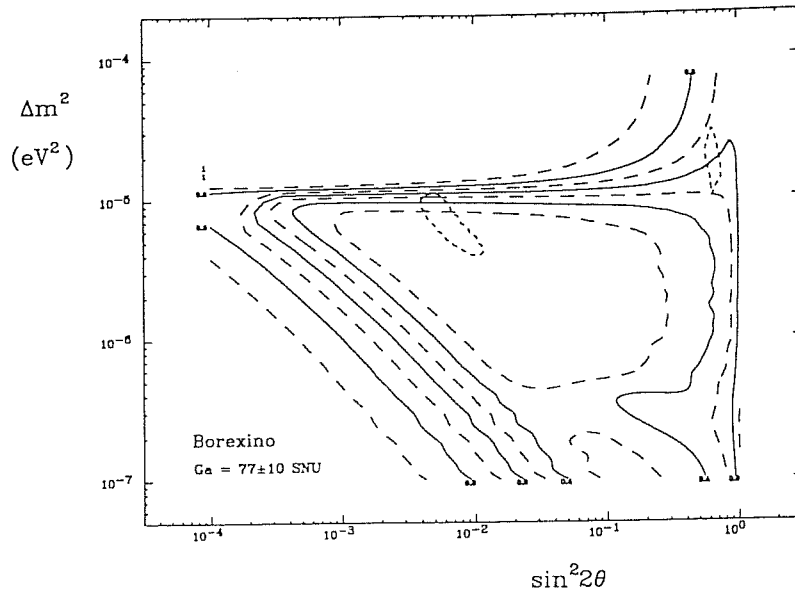
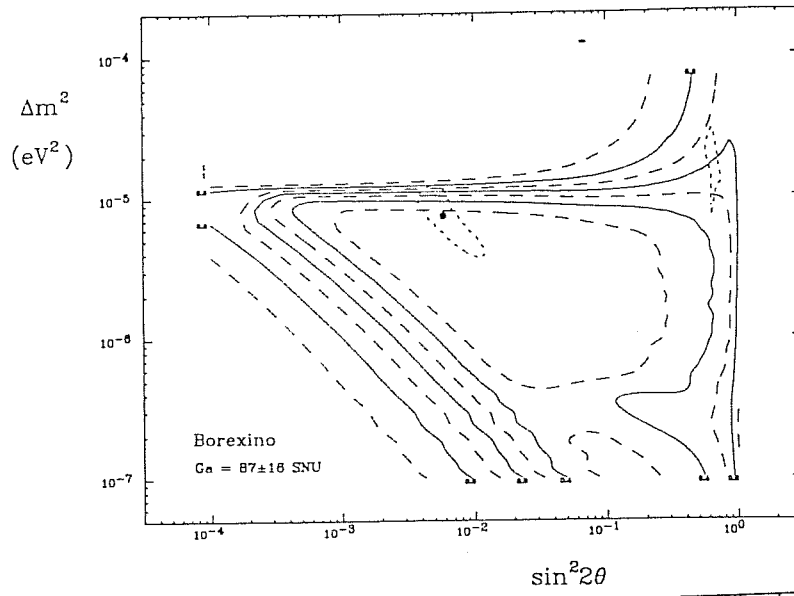


Fig. 2.8 Contours of iso-ratio of muon neutrino contribution to the total rate at Kamiokande as obtained comparing measurements at SNO and at Kamiokande by using (a) the exact formula Eq. (2.9) and (b) the approximation in Eq. (2.11). The 90% CL region (long-dashed curves) and the best fit to the experimental data as obtained in the BP SM (Fig. 2) are also superimposed. This approximation becomes exact in the limit that $W(E)$, as defined in Eq. (2.10), is constant in the relevant range. We plot (c) this function and the two cross sections whose ratio define $W(E)$; the y-scale is arbitrary.



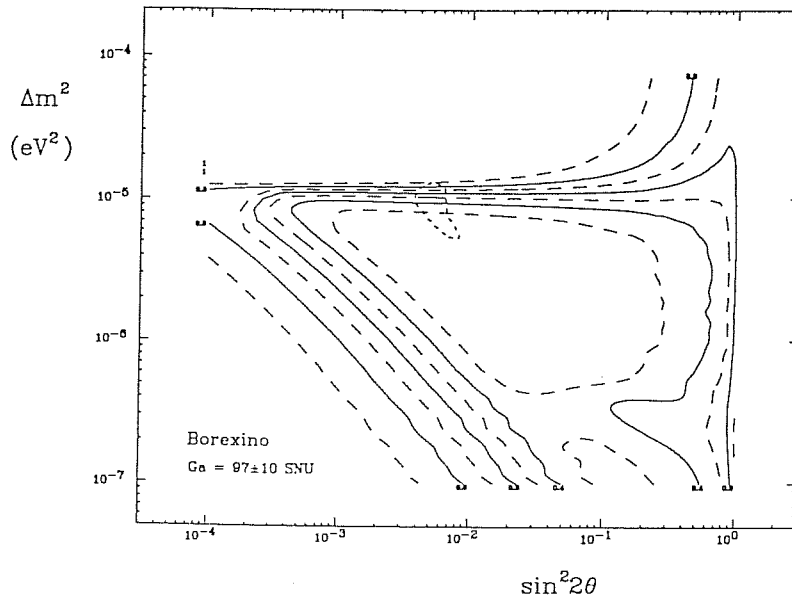


Fig. 2.9 Iso-signal contours for the Borexino experiment as fraction of the no suppression result. Labels refer to solid curves and dashed curves are half-way the solid ones. The 90% CL region (long-dashed curves) and the best fit to the present experimental data as obtained in the BP SM (Fig. 2) are also shown (a). We also show the 90% CL regions found using the present chlorine and Kamiokande experimental results but (b) a hypothetical GALLEX result of 77 ± 10 SNU, (c) a hypothetical GALLEX result of 87 ± 10 SNU, (d) a hypothetical GALLEX result of 97 ± 10 SNU.

CHAPTER 3

NEUTRINO SPIN PRECESSION IN A COHERENT MAGNETIC FIELD

The data of the Homestake detector do not seem to be constant in time and seem to be anticorrelated with the solar activity [7], the trend being that the signal is lower during the periods of stronger activity. The statistical significance of this time dependence does not allow definite conclusion, being at the 3σ level [75, 76]. One can therefore speculate over this possible anticorrelation and try to understand its origin. Since neutrinos are produced in the core of the sun, their production rate is independent from the solar activity in the convective region, and the only possibility to explain the eventual temporal correlation of the signal is to appeal to neutrino properties.

The ideas which have been proposed until now rely on non-standard neutrino electromagnetic properties which should allow non negligible interactions of neutrinos with the solar magnetic field. Observational data show the existence of a magnetic field at the surface of the sun whose magnitude is strongly correlated with the twentytwo years solar cycle.

It has also been postulated (without any experimental evidence) that a inner magnetic field can be present inside the most interior region of the sun, the "quiet" sun. This inner field, if it exists, however cannot be correlated with the solar activity in the convective region.

If we assume that neutrinos have unconventional electromagnetic properties, such as a neutrino magnetic moment, the coherent interactions of the neutrinos with the magnetic field origins new terms in the hamiltonian connecting left-handed neutrino states with right-handed, active or sterile, neutrino states. The effect of this interaction is to induce an effective mixing among right and left-handed states [27, 28]. Since this interaction connects neutrinos with opposite helicities (for ultrarelativistic neutrinos) we will usually call this effect neutrino spin-precession. If the interactions of neutrinos with the field of the convective region is strong enough, some correlation with the solar activity is expected [28]. This feature reproduces the claimed correlation of the Chlorine data with solar activity and motivates the large interest in this effect.

Up to now essentially two classes of models have been explored, namely either the original proposal [28] in which only spin-precession is postulated and the right-handed neutrino can be either the sterile right-handed partner of a Dirac neutrino or an active right-handed antineutrino (ZKM neutrinos [77]), or variants of the previous one in which both neutrino spin-precession and neutrino oscillations are supposed to be important. The models of this last class are usually referred as Hybrid models [29]. This second class of models seems to be more attractive since it provides naturally an explanation of the low signal also at periods of minimum solar activity when the magnetic field is supposed to be ineffective.

The evolution equation depends crucially on the magnetic field shape and strength. In particular it depends on the profile of the magnetic field and also on the relative direction of the magnetic field in the plane transverse to neutrino momentum as functions of neutrino positions. Whatever complicated is the spatial shape of the magnetic field, it results that the precession phase $\phi = \int \mu_\nu \mathbf{B} d\tau$ must be at least of the order of the desired spin-precession probability and therefore for

a magnetic field of 1 kG along the convective zone neutrino magnetic moment $\mu_\nu \sim 10^{-10} \mu_B$, μ_B being the Bohr magneton, are required. This value (even if, eventually allowing for a larger magnetic field, whose magnitude is unknown, it can be somehow lowered) is very close to the experimental bounds [78], and it is probably in conflict with limits coming from astrophysical considerations [79].

Such values for the neutrino magnetic moment would be a clear indication of physics beyond the standard model [36, 37]. In fact the most simple extension of the standard model, namely the assumption that the neutrino is a Dirac particle and its mass is less than 10 eV, as allowed by experiment, implies that $\mu_\nu \leq 10^{-18} \mu_B$, several order of magnitude lower than the required strength.

Together with the time dependence of the signal, the scenario including neutrino magnetic moment can have other peculiar phenomenological features. In particular hybrid models predict that a sizable fraction of the initial neutrinos oscillate in electron antineutrinos (unless forbidden by an exact symmetry, see the next chapter) whose detection would be an incontrovertible signal of non standard behaviour of the neutrinos, since there is no known process in the sun which can originate electron antineutrinos. This signature is extremely important since $\bar{\nu}_e$, detecting inverse beta decay process, can be distinguished experimentally from the other neutrinos and the cross section for the detection is much larger than the cross section for neutrino electron elastic scattering allowing the detection also for small fraction of antineutrinos. On the basis of the non observation of $\bar{\nu}_e$ signal in Kamiokande detector it is already possible to exclude hybrid models with large mixing angles and with the future detectors it will probably be possible to confirm or reject this class of models. Up to now it doesn't exist a complete analysis showing the consistence of these models with the data although many semiquantitative estimation show that, at least the hybrid models, can probably reproduce also the quantitative features of the data and possibly also the difference among the signal observed in the two detectors.

§3.1 Effective Lagrangean Accounting for Neutrino Electromagnetic Properties

Since neutrinos are electrically neutral, the most effective coupling (at low q^2 where q is the four momentum carried by the photon) of neutrinos to photons is of electric and magnetic dipole moment type. We are therefore induced to look for an effective lagrangean of the type

$$\mathcal{L}_{em} = \mu_{jk} \bar{\chi}_j \sigma_{\alpha\beta} \chi_k F_{\alpha\beta} + i d_{jk} \bar{\chi}_j \sigma_{\alpha\beta} \gamma_5 \chi_k F_{\alpha\beta} \quad (3.1)$$

where μ_{jk} and d_{jk} are the magnetic and electric dipole moment respectively, χ_j and χ_k are the fields of ν_j and ν_k neutrinos, and $F_{\alpha\beta} = \partial_\alpha A_\beta - \partial_\beta A_\alpha$.

If χ_j are four components Dirac fields the case $j = k$ in (3.1) is indeed possible and μ is the standard magnetic moment for the usual fermions.

If, on the contrary, χ_j are two components Majorana fields, due to the Majorana condition, $\chi_j = C \bar{\chi}_j^T$, $\chi_k = C \bar{\chi}_k^T$, we get

$$\begin{aligned} \bar{\chi}_j \sigma_{\alpha\beta} \chi_k &= -\bar{\chi}_k \sigma_{\alpha\beta} \chi_j \\ \bar{\chi}_j \sigma_{\alpha\beta} \gamma_5 \chi_k &= -\bar{\chi}_k \sigma_{\alpha\beta} \gamma_5 \chi_j \end{aligned} \quad (3.2)$$

and therefore diagonal magnetic and electric dipole moment are forbidden for Majorana neutrinos [80]. Usually non diagonal magnetic moments are called transitional magnetic moments.

In the following we shall assume that some new interactions give rise to the effective Lagrangean (3.1) and we consider the possible effects.

§3.2 Neutrino evolution equation in a coherent magnetic field

The interaction of the neutrino with the magnetic field can lead to two different consequences

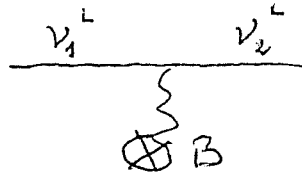
- a) neutrinos are scattered by the field \mathbf{B} which is present in the convective zone.
- b) Some interference effect of the same kind we have described in the previous chapter can hold.

We shall neglect *a* since it turns out that it requires unreasonable high value of μ and \mathbf{B} and we shall concentrate on *b*. Analogously to the weak interaction of neutrinos with matter, the interactions with a magnetic field modify the dispersion relations of the neutrino and affect its evolution.

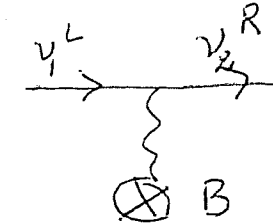
Exactly in the same manner as we got for the coherent weak interaction we get a contribution to the hamiltonian, due to the interaction of neutrino with the magnetic field; the coherent requirement leads exactly to the same condition: initial and final neutrino momentum must be equal.

In presence of a coherent magnetic field the evolution hamiltonian has non vanishing elements which connects ν_1^L and ν_2^L states with ν_2^R and ν_1^R states; therefore oscillations involving left handed and right handed components of both neutrino species are allowed.

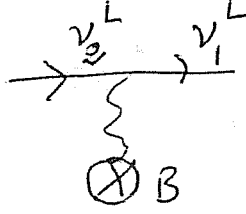
For a static magnetic field, again using the convention of appendix A we get the followings forward scattering amplitudes



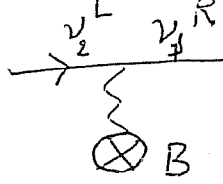
$$B_{1,2}^C = O\left(\frac{m}{E_\nu^2}\right) \frac{\mathbf{B} \cdot \mathbf{p}}{p} \mu_{1,2} \quad (3.3a)$$



$$B_{1,2}^F = 2B e^{i\beta} \left(1 + O\left(\frac{m}{E_\nu}\right)\right) \bar{\mu}^{i\delta} \quad (3.3b)$$



$$B_{2,1}^C = O\left(\frac{m}{E_\nu^2}\right) \frac{\mathbf{B} \cdot \mathbf{p}}{p} \mu_{1,2} \quad (3.3c)$$



$$B_{2,1}^F = -2B e^{i\beta} \left(1 + O\left(\frac{m}{E_\nu}\right)\right) \bar{\mu}^{i\delta} \quad (3.3d)$$

where $B e^{i\beta} = B_j + iB_k$, B_j and B_k being the components of the projection \mathbf{B}_\perp of the field \mathbf{B} in the plane transverse to neutrino momentum, and $\bar{\mu}^{i\delta} = \mu + id$. Including also this effect for the time evolution hamiltonian we get:

$$H_{TOT} = H_0 + \mathcal{V} + \mathcal{B} \quad (3.4)$$

where H_0 stands for the kinetic term, \mathcal{V} and \mathcal{B} account for the coherent interactions of neutrinos with matter and magnetic field respectively.

We shall discuss essentially two cases.

a) the magnetic moment is of Dirac type and neutrino oscillation are either absent or decoupled from spin precession.

In this case in eq. (3.4) the term H_0 is diagonal being left an right-handed neutrinos degenerate in mass and it is

$$H_{TOT} = \begin{pmatrix} \mathcal{V}_{1,2} & B_{1,2}^F \\ B_{1,2}^{F*} & -\mathcal{V}_{1,2} \end{pmatrix} \quad (3.5)$$

where $B_{j,k}^F$ have been defined in (3.3) and $\mathcal{V}_{1,2}$ is the level splitting induced by coherent interaction and depends on the flavour content of ν_j neutrino in (3.1).

b) The magnetic moment is of transitional type and we cannot decouple neutrino oscillations from neutrino spin precession. In this case, in the flavour bases, assuming, to be definite, that ν_j neutrinos in (23.1) are mass eigenstates and ν_e, ν_μ are superposition of ν_j neutrinos with mixing angle θ ,

$$H_{TOT} = \begin{pmatrix} \delta_c + V_1 & \delta_s & 0 & \beta \\ \delta_s & -\delta_c + V_2 & -\beta & 0 \\ 0 & -\beta^* & \delta_c - V_1 & \delta_s \\ \beta^* & 0 & \delta_s & -\delta_c - V_2 \end{pmatrix} \quad (3.6)$$

where $V_1 = \frac{G_F}{\sqrt{2}}(n_e(r) - n_n(r))$, $V_2 = -\frac{G_F}{\sqrt{2}}n_n(r)$, $\delta_c = \frac{m_1^2 - m_2^2}{4E} \cos 2\theta$, $\delta_s = \frac{m_1^2 - m_2^2}{4E} \sin 2\theta$, θ being the vacuum mixing angle and $\beta = \mathcal{B}_{1,2}^f$. In eqs. (3.5-3.6) we have neglected vanishing small terms of order m_ν/E_ν

§3.3 Neutrino Magnetic Moment and the Solar Neutrino Problem

There are two important issues to take into account in order to conclude if the occurrence of neutrino magnetic moment can be important for the solution of the SNP. First it is important to understand what are the values of μ_ν and \mathbf{B} which can significantly change the neutrino content in the sun and compare these values with the experimental bounds. Second one has to understand if models including neutrino magnetic moment effects are able to reproduce the observational data, namely a larger neutrino deficit in correspondence of stronger solar magnetic field intensity, a consistent deficit even for weak field intensity and possibly also some difference among Homestake detector which indeed observes such an anticorrelation and Kamiokande detector which, within large errors, observes no such an anticorrelation.

In the original proposal of Okun, Visotsky and Voloshin [28] it was considered the case of a diagonal magnetic moment of Dirac type and it was neglected the effect of coherent interactions. Under these assumptions, the equation of motion is exactly solvable and, for a solar magnetic field \mathbf{B} of about $\dagger 1 \text{ kG}$, a neutrino magnetic moments of order $10^{-10} \mu_B$, μ_B being the Bohr magneton, is needed in order that the conversion probability becomes appreciable. Subsequently it was noticed that, generally, the effect of coherent weak interaction is to induce terms in the evolution equation whose net effect is to suppress the spin-flip. As a result a magnetic moment five to ten times larger than the previous one is needed. This class of models suffers from two main difficulties: the experimental upper bound on μ_ν is very close to $10^{-10} \mu_B$ [78] and, moreover, astrophysical consideration from supernova and red giant cooling set limits of order $10^{-11} \div 10^{-13} \mu_B$ [79]; additionally, at least under the more conservative hypotheses that the inner magnetic field is absent or negligible, this model cannot explain the neutrino deficit at minima of the solar activity and probably cannot explain a depletion of the signal as large as the observed one.

To overcome partially these problems, 'Hybrid Models' were proposed [29], namely models with both neutrino magnetic moment of transitional type and neutrino mixing. In this class of models the mass splitting among the two neutrinos can compensate for the coherent weak interaction as discussed in the previous chapter and this allow for a somewhat lower μ_ν value (three to six times Bohr magneton). Additionally, in these models, since the magnetic moment induce transitions among states which are both active supernova limit is avoided. Finally these models, due to the contribution of neutrino oscillations, allow to reproduce the neutrino deficit at solar minima.

\dagger Here and below one has to remember that only the product $\mu_\nu \mathbf{B}$ is relevant for the problem, therefore if one wants to use different magnetic field the net effect is just a rescaling of μ_ν in all the following consideration

Subsequently it was noticed that the direction of the magnetic field along the neutrino path is not necessary constant. The effect of the twisting of the \mathbf{B}_\perp direction along neutrino path is to induce a dynamical phase in the evolution equation [81]. When this idea was proposed, it was claimed that a rapid twisting of the magnetic field can result in lowering the value of $\mu_\nu \mathbf{B}_\perp$, which is required to produce large $\nu_{eL} \rightarrow \nu_R$ conversion, by 3 ÷ 4 orders of magnitude [81]. Subsequently this result was shown to be incorrect [82, 83]. The twisting of the magnetic field can induce many new phenomena such as resonant spin flip even when ν_{eL} and ν_R are the components of a Dirac neutrino, the appearance of new resonant level crossing and also suppression of the precession, depending on the value of the corresponding parameter [82]. However, it results that, even for the "best choice" of parameters, the needed $\mu_\nu \mathbf{B}_\perp$ value, ensuring large $\nu_{eL} \rightarrow \nu_R$ conversion, can be lowered at most of a factor two [82]. Since the quoted analysis was carried out assuming a specific shape of the magnetic field and of the changing of the twisting of \mathbf{B}_\perp along neutrino path, the question of what is the minimal value of $\mu_\nu \mathbf{B}_\perp$ which can induce large neutrino spin precession assuming arbitrary \mathbf{B}_\perp and twisting of \mathbf{B}_\perp along the neutrino path, still remains open.

§3.3.1 The Region of Parameters Relevant for the Solar Neutrinos

We now try to understand what are the values of $\mu_\nu \mathbf{B}$, which can indeed be of some relevance for the solar neutrino problem. Looking at the evolution hamiltonians (3.5) one can easily trust that the spin-flip probability goes to zero in the limit $\mathcal{B}_{1,2}^f \sim 0$. Additionally in the case of time independent hamiltonian the evolution equation can be exactly solved and it is well known that the effect of diagonal terms in (3.5) is to dump the amplitude of the precession. Therefore one can guess that the limit of vacuum oscillation in presence of constant magnetic field give a good estimation of the values of parameters $\mu_\nu \mathbf{B}$ required to induce a spin-flip probability of order one. However since we do not have exact solution for the problem for a time dependent hamiltonian and in view of the claim of the possibly strong effect of the twisting of the field it is important to have a rigorous bound on the effect which can be induced by a given $\mu_\nu \mathbf{B}$.

In the following we shall demonstrate that for a general two level quantum system the maximum precession efficiency is reached when diagonal terms are absent. In this case the evolution equation is straightforwardly solved and one obtain as a general results that the value of the precession phase $\phi = \int \mu_\nu \mathbf{B} d\tau$ must be at least of the order of the desired precession probability. We briefly examine also the case of hybrid models, where neutrino oscillations and spin-flip precession are interfering and we found that this limit still holds.

§3.3.1.1 General Analyses

The evolution of a two-level quantum system in the case of an arbitrary, time dependent, hamiltonian is described by the equation

$$i\frac{d}{dt} \begin{pmatrix} a_1(t) \\ a_2(t) \end{pmatrix} = \begin{pmatrix} A(t) & D(t)e^{i\omega(t)} \\ D(t)e^{-i\omega(t)} & -A(t) \end{pmatrix} \begin{pmatrix} a_1(t) \\ a_2(t) \end{pmatrix}, \quad (3.7)$$

where $a_{1,2}(t)$ are the amplitudes of the probabilities that the system is in the state $|1\rangle$, $|2\rangle$ respectively; $A(t)$, $D(t)$, $\omega(t)$ are real functions and an inessential diagonal term in the evolution Hamiltonian was omitted. If we introduce the amplitudes

$$\begin{aligned} b_1(t) &= a_1(t)e^{-i\omega(t)/2}, \\ b_2(t) &= a_2(t)e^{i\omega(t)/2}, \end{aligned} \quad (3.8)$$

the probability to find the neutrino system in the state $|j\rangle$ is $P_j(t) = |a_j(t)|^2 = |b_j(t)|^2$ and eq. (3.7) becomes

$$i\frac{d}{dt} \begin{pmatrix} b_1(t) \\ b_2(t) \end{pmatrix} = \begin{pmatrix} C(t) & D(t) \\ D(t) & -C(t) \end{pmatrix} \begin{pmatrix} b_1(t) \\ b_2(t) \end{pmatrix}, \quad (3.9)$$

where $C(t) = A(t) + \dot{\omega}(t)/2$. Henceforth we shall discuss eq. (3.9) to which the more general eq. (3.7) can always be reduced.

Our aim is to determine the minimal value of $\varphi = \int_{t_i}^{t_f} dt D(t)$ which is needed to change the system from an initial state $|i\rangle = b_1(t_i)|1\rangle + b_2(t_i)|2\rangle$ characterized by the probabilities $P_j(t_i)$ to a final state $|f\rangle = b_1(t_f)|1\rangle + b_2(t_f)|2\rangle$ characterized by the probabilities $P_j(t_f)$.

Since the hamiltonian is hermitian the probability is conserved,

$$P_1(t) + P_2(t) = 1, \quad (3.10)$$

and it is enough to follow the evolution of P_2 .

Given the real and imaginary components of $b_{1,2}(t)$

$$\begin{aligned} b_1(t) &= x(t) + iy(t), \\ b_2(t) &= z(t) + iw(t), \end{aligned} \quad (3.11)$$

one can write the evolution equation for $P_2(t)$, which has the form

$$\frac{dP_2(t)}{dt} = 2D(t)\sigma(t), \quad (3.12a)$$

where

$$\sigma(t) = z(t)y(t) - w(t)x(t) \quad (3.12b)$$

From (3.12a) and (3.12b) it follows that

$$P_2(t_f) - P_2(t_i) = \int_{t_i}^{t_f} dt 2D(t)\sigma(t). \quad (3.13)$$

Using eq. (3.10) one can show that $|\sigma| \leq 1/2$. Consequently, to get a change ΔP_2 in the P_2 probability, according to (3.13), at least the following inequality must hold

$$\left| \int_{t_i}^{t_f} dt D(t) \right| \geq |\Delta P_2| \quad (3.14)$$

This bound can be further refined. One has to look for a path from t_i to t_f along which σ is maximal at each instant. For any given value of P_2 (which means for any given couple (z, w)) from eqs. (3.10) and (3.12) it follows that

$$\sigma = zy - w\sqrt{1 - P_2 - y^2}. \quad (3.15)$$

The maximal value of σ occurs for y_m such that $d\sigma/dy|_{y_m} = 0$. This value is given by

$$y_m(t) = \pm z(t) \sqrt{\frac{P_1(t)}{P_2(t)}}. \quad (3.16)$$

Therefore the minimal value of $D(t)$ of interest is obtained for a configuration of $D(t)$ and $C(t)$ for which condition (3.16) is satisfied. One can directly verify that for $C(t) = 0$ condition (3.16) is always fulfilled during the evolution of the system, if it is fulfilled for $t = t_i$. † Under these assumptions eq. (3.9) is straightforwardly solved and one gets an exact expression for $P_2(t)$:

$$\begin{aligned} \mathcal{P}_2(t) &= \mathcal{P}_2(t_i) \cos^2 \Omega + \mathcal{P}_1(t_i) \sin^2 \Omega \pm \sqrt{\mathcal{P}_2(t_i)\mathcal{P}_1(t_i)} \sin 2\Omega \\ \Omega &= \int_{t_i}^t dt D(t) \end{aligned} \quad (3.17)$$

where $\mathcal{P}_{1,2}(t)$ denote the probabilities $P_{1,2}(t)$ in the specific case when $C(t) = 0$. Therefore the bound in eq. (3.14) can be substituted by a stronger one. If we define by $\bar{\Omega}$ the minimal value of $|\Omega|$ for which $\mathcal{P}_2(t_f) - \mathcal{P}_2(t_i) = \Delta P_2$, then the bound (3.14) can be substituted by

$$|\Omega| \geq \bar{\Omega} \quad (3.18)$$

This result has a very simple meaning. The speed of the transition $|1\rangle \rightarrow |2\rangle$ is directly proportional to $D(t)$ and eq. (3.9) tells us just that this rate goes to zero in the limit $D(t) = 0$. Moreover, the effect of the term $C(t)$ is always to reduce the speed of the transition. The existence of resonance points t_r ($C(t_r) = 0$) just ensure the condition $C(t) = 0$, which is the most favourable for the transition, over a time interval $\Delta t \simeq B(t_r)/(dC(t)/dt|_{t_r})$.

† This condition can be verified to hold, in particular in the case of solar neutrino, in which we are mainly interested here.

§3.3.1.2 Neutrino Spin Flip in the Sun

We now come back to our original motivation, solar neutrino spin precession in the presence of a twisting magnetic field. If we consider an electron neutrino ν_{eL} with transition magnetic moment μ_ν which is crossing the convective zone of the sun and we assume for concreteness that $\nu_R \equiv \bar{\nu}_{\mu R}$, the evolution equation [29] of the system, taking into account also the possibility that \mathbf{B}_\perp can be twisting continuously on the way of the neutrino [81,82] is given by eq. (3.7), where now $t = r$, $|1\rangle = |\nu_{eL}\rangle$, $|2\rangle = |\nu_{\mu R}\rangle$, $a_1 = a_e$, $a_2 = a_{\bar{\mu}}$ (electron neutrino and muon antineutrino amplitudes), $A(r) = (G_F/\sqrt{2})(n_e(r) - n_n(r)) + (m_e^2 - m_\mu^2)/(4E)$ (G_F is the Fermi constant n_e , n_n are the electron and neutron densities), $D(r) = \mu_\nu \mathbf{B}_\perp(r)$, $\omega(r)$ describes the twisting of the magnetic field [82, 83] and we have neglected possible mixing among neutrino flavors. In order that the magnetic field induces a change $\Delta P_{\bar{\mu}}$ in the $\nu_{\bar{\mu}}$ content of the neutrino state the inequality (3.18) must hold, where now

$$\begin{aligned} P_1 &= P_e, \\ P_2 &= P_{\bar{\mu}}, \\ \Omega &= \int_{r_i}^{R_\odot} d\tau \mu_\nu \mathbf{B}_\perp(\tau), \end{aligned} \quad (3.19)$$

independently of $\omega(r)$ (we have denoted with r_i the point in which the electron neutrino is produced and with R_\odot the solar radius). This disproves the claim made in ref. [81]. We are just left with the vacuum spin-flip in presence of a non twisting field as an optimal case and the minimal value of the parameters which can induce a given spin-flip can be directly read from the results in this limit [28]. In this limit

$$P_{e\bar{\mu}} = \sin^2 | \bar{\mu}^{i\delta} \int_{R_i}^R dR B e^{i\beta} | \quad (3.20)$$

For $P_{e\bar{\mu}}$ to be significative we require

$$| \bar{\mu}^{i\delta} \int_{R_i}^{R_\odot} dR B e^{i\beta} | \geq 1 \quad (3.21)$$

Where R_i is the beginning of the convective zone and R_\odot is the solar radius. The length of the convective zone L_c is

$$L_c = \frac{3}{10} R_\odot \quad (3.22)$$

From (3.21-3.22) we get

$$\mu B \geq \frac{1}{L_c} \approx 10^{-15} eV \quad (3.23)$$

For magnetic field of order 1 up to 100 kG which seems possible inside the convective zone of the sun this mean.

$$\mu_\nu \geq 2 \cdot 10^{-12} \div 2 \cdot 10^{-10} \mu_B \quad (3.24)$$

where μ_B is the Bohr magneton.

The upper value for μ_ν is at the border of the present terrestrial limit [78]. Astrophysical bounds are more stringent $\mu_\nu \leq 10^{-12} \mu_B$ [79] even if some caution is needed. In any case, even being very optimistic about μ_ν and B values, from the experimental limit we get $\mu_\nu B \leq 10^{-14} eV$.

From the discussion of the previous section we can also infer what is the "best choice" for $\omega(r)$ (which, as \mathbf{B} , is unknown); we obtain the maximum precession efficiency for

$$\Lambda(r) = \frac{G_F}{\sqrt{2}}(n_e(r) - n_n(r)) + \frac{m_e^2 - m_\mu^2}{4E} + \frac{\dot{\omega}(r)}{2} = 0. \quad (3.25)$$

Condition (3.25) is probably unphysical in the sense that it would require a quite strange twisting of \mathbf{B}_\perp to be realized. However, from the previous discussion we can infer what is the condition which can be realized in the physical case and is the closest to eq. (3.25):

$$\Lambda(r_r) = 0, \quad \dot{\Lambda}(r_r) = 0. \quad (3.26)$$

In fact condition (3.26) would not only imply the occurrence of a resonance but also the widening of the resonance layer.

We shall now briefly describe the case of RSFP in which a nonzero mixing between ν_e and ν_μ is assumed. In this case the system of evolution equation has the form 29

$$i \frac{da_j(r)}{dt} = \mathcal{H}(r)_{jk} a_k(r). \quad (3.27)$$

In eq. (3.25) $j, k = e, \bar{e}, \mu, \bar{\mu}$ and $\mathcal{H} = H_{TOT}$ and H_{TOT} has been defined in eq. (3.26) It is convenient to introduce

$$\begin{aligned} b_j(t) &= a_j(t) e^{\epsilon_j \omega(r)/2} \quad \epsilon_j = 1, \text{ if } j = e, \mu; \quad \epsilon_j = -1, \text{ if } j = \bar{e}, \bar{\mu} \\ b_j(r) &= x_j(r) + iy_j(r). \end{aligned} \quad (3.28)$$

Only the β term can be responsible for the suggested time dependence of the signal in the Homestake experiment [7]. The net effect of this term is neutrino spin flip process which produces the change of the neutrino and antineutrino contents of the state. Let us define

$$P(r) = |b_e(r)|^2 + |b_\mu(r)|^2, \quad \bar{P}(r) = |b_{\bar{e}}(r)|^2 + |b_{\bar{\mu}}(r)|^2, \quad (P + \bar{P} = 1) \quad (3.29)$$

in order to study the efficiency of the neutrino spin-flip (which is the only effect which produce the time modulation), it is enough to follow the evolution of \bar{P} . From eqs. (3.26-3.29) one obtains

$$\begin{aligned} \frac{d\bar{P}(r)}{dr} &= \sigma_4(r) \mu_\nu \mathbf{B}_\perp(r) \\ \sigma_4(r) &= -x_{\bar{e}} y_\mu + y_{\bar{e}} x_\mu + x_{\bar{\mu}} y_e - y_{\bar{\mu}} x_e. \end{aligned} \quad (3.30)$$

The configuration for which neutrino spin flip proceeds with the highest speed at fixed $\mu_\nu \mathbf{B}_\perp$, corresponds to the maximum of σ_4 for any given \overline{P} (for any given $(x_{\bar{e}}, y_{\bar{e}}, x_{\bar{\mu}}, y_{\bar{\mu}})$). This implies that such configuration can be realized if the following conditions can be simultaneously fulfilled

$$\begin{aligned}
x_e y_{\bar{e}} + x_\mu y_{\bar{\mu}} &= 0, \\
x_e x_{\bar{e}} - y_\mu y_{\bar{\mu}} &= 0, \\
x_e x_{\bar{\mu}} + y_e y_{\bar{\mu}} &= 0, \\
\text{where } x_e &= \sqrt{1 - \overline{P} - x_\mu^2 - y_e^2 - y_\mu^2}
\end{aligned} \tag{3.31}$$

One can directly verify that if conditions (3.31) are fulfilled for $\tau = \tau_i$ and if all, but $\mu_\nu \mathbf{B}_\perp$, terms in (3.27) are zero, eqs. (3.21) are always fulfilled during the evolution of the neutrino system. So, also in the case of RSFP, condition (3.18) gives the correct estimate for the minimum size of $\mu_\nu \mathbf{B}_\perp$ which is needed to produce a given effect. Again in this case the diagonal terms suppress the transition amplitudes, moreover also the nondiagonal term δ_s suppresses the spin-flip transitions since it induces an energy splitting between the neutrino states which are connected by the magnetic moment term.

Two comments are in order: *i*) the above statement is correct only for spin flip transitions and it does not hold for the disappearance amplitude for ν_e , since also neutrino flavour transitions, induced by δ_s , contribute to this amplitude. However δ_s is present even if $\mathbf{B}_\perp \sim 0$ (the quiet sun) and it cannot provide any time dependence for the signal; *ii*) the case $\delta_s \neq 0$ has the attractive feature that it can provide lowering of the signal also in the periods of low solar activity and this is in agreement with the trend of experimental data [7].

§3.4 Implications of a large neutrino magnetic moment for the solar neutrino signal

We shall now turn to discuss the effect of the assumption that the neutrino has a magnetic moment large enough to affect the solar neutrino signal.

There are essentially two class of models: the original proposal to consider only spin-flip and the later proposal to include also neutrino oscillations.

It seems difficult to account for the depletion of the signal at the minimum of the solar activity in the case of neutrino spin-flip alone, the possible way out being either the assumption of a very strong magnetic field in the solar interior or the assumption of an extremely tuned shape and time dependence of the solar magnetic field. The only relevant phenomenological feature of this scenario is the correlation of the solar neutrino signal with the solar activity.

In the case of Hybrid models it is made the assumption that both neutrino spin-flip and neutrino oscillations are effective. In this way it is easier to explain the depletion of the signal at the minimum of the solar activity, moreover, in this class of models the occurrence of resonant crossing of energy levels is energy dependent and therefore some difference among experiments with different threshold energies is expected.

In addition to the time dependence of the signal for a wide class of hybrid models it is predicted a spectral distortion and the conversion of a fraction of the initial ν_e to $\bar{\nu}_e$. This last signature turns out to be extremely important since $\bar{\nu}_e$ are relatively easily detectable through inverse beta decay processes. In the following we discuss how it is already possible to exclude hybrid models with large mixing angles on the basis of the existent data.

Up to now it is possible to make only semiquantitative statements about this scenario since only partial or incomplete analysis have been performed. On the basis of the existent literature one can perhaps say that it's plausible to think that for some parameter regions the hybrid models fit the existent data better than the models which do not predict any time variation of the signal.

§3.4.1 The Main Feature of the Models

In the original proposal of Okun, Voloshin and Visotky [28] it was assumed that ν_1 and ν_2 were the four component of a Dirac neutrino. In this case both Δ and the vacuum mixing angle are zero and the evolution hamiltonian in the ν_{eL}, ν_{eR} basis (ν_{eL}, ν_{eR} evolution is decoupled from $\bar{\nu}_{eL}, \bar{\nu}_{eR}$ evolution) is given in equation (3.5) where $\mathcal{V}_{1,2} = G_F(N_e - N_n)/\sqrt{2}$ and the phase β in (3.5) was assumed constant along neutrino path.

This class of models is plagued with several difficulties. If one take the more conservative assumption that the magnetic field is present only in the convective zone, these models cannot account for any depletion at the minima of solar activity, in contrast with the phenomenological evidence. This difficulty can be overwhelmed only assuming a strong inner solar magnetic field of order 10^{-7} kG at the border of the values which are assumed possible.

Additionally these models can account for some difference among Homestake and Kamiokande detectors only for extremely large neutrino magnetic moment, namely

$$\mu_\nu = 4 \div 7 \times 10^{-10} \mu_B \quad (3.32)$$

since for these value of the magnetic moment elastic neutrino scattering mediated by a virtual photon contributes significantly to the detected signal in Kamiokande detector, while giving no contribution to the signal in Homestake detector.

Finally in these models the level splitting among L and R state induced by coherent interaction of neutrinos with matter have the tendency to dump the oscillations, therefore increasing the required $\mu_\nu \mathbf{B}$ value, as was noticed in [84].

This last problem however is not unavoidable. Assuming that the phase β in (3.5) is not constant along neutrino path inside the solar magnetic field, induces a new dynamical term in the evolution equation [81] which can compensate for the level splitting if $\dot{\beta} \sim -\mathcal{V}_{1,2}$ [82]. Evaluating $\mathcal{V}_{1,2}$ at the beginning of the convective zone one can see that if

$$\dot{\beta} \leq \frac{0.2}{R_\odot} \quad (3.33)$$

a resonant point will indeed occur in neutrino path. It is remarkable that the required values for β is just of the same order of the extension of the magnetic field and, therefore are very natural values.

We don't know of any detailed computation showing the possible consistence to these models with the observed time correlation and average suppression of the signal. Only qualitative and incomplete computation are at disposal, however it seems that to reconcile the difference among the detectors very large values of μ_ν are needed, very close to be excluded by terrestrial experiment and in strong conflict with astrophysical consideration, additionally to reproduce the average suppression of the signal one needs a very strong primordial inner magnetic field with which must be tuned in order to give an effect stronger than the coherent one and to provide just the observed one half suppression (roughly) during the periods of low solar activity during which only the inner field is assumed to be effective.

In view of the difficulties of these class of models it was natural to introduce the Hybrid models (3.6) in which both neutrino mixing and spin precession were operative.

We now study equation (3.6). Two situation can arise

- 1) some resonance can occur inside the convective zone
- 2) No resonance is crossed in neutrino travel.

In the following we shall show that 2 requires large mixing angle. This requirement leads to a large $\bar{\nu}_e$ production and conflict with experimental data.

If we assume that $m_2 > m_1$ and that adiabatic resonances indeed occur inside the convective zone of the sun this implies

$$5 \cdot 10^{-16} \text{eV} \leq \frac{m_2^2 - m_1^2}{4E} \leq 5 \cdot 10^{-15} \text{eV} \quad (3.34)$$

We observe that in their travel neutrinos crosses two resonances, the first when $H_{ee} = H_{\bar{\mu}\bar{\mu}}$ which implies

$$\frac{G}{\sqrt{2}}(N_e - N_n) = \frac{m_1^2 - m_2^2}{4E} \quad (3.35)$$

if the crossing is adiabatic we have $\nu_e \rightarrow \bar{\nu}_\mu$ conversion.

The second crossing is for $H_{ee} = H_{\mu\mu}$ which implies

$$\frac{G}{\sqrt{2}}N_e = \frac{m_1^2 - m_2^2}{4E} \cos 2\alpha \quad (3.36)$$

Again if adiabaticity holds we have $\nu_e \rightarrow \nu_\mu$ conversion.

However it turns out that in the convective zone N_n is quite small ($N_n \approx 1/6N_e$) and the two resonance are very near, this implies that even when adiabaticity is a good approximation equation (3.6) requires numerical investigation.

Due to the resonance (3.35-3.36) we expect a sizable amount of ν_μ and $\bar{\nu}_\mu$. In addition a small fraction of $\bar{\nu}_e$ is expected since it is not forbidden by any conservation law. It can be due to the following process

$$\nu_e \xrightarrow{\text{spin flip}} \bar{\nu}_\mu \xrightarrow{\text{oscillation}} \bar{\nu}_e$$

$$\nu_e \xrightarrow{\text{oscillation}} \nu_\mu \xrightarrow{\text{spin flip}} \bar{\nu}_e \quad (3.37)$$

since in both process one step is not resonant the $\bar{\nu}_e$ fraction is expected indeed small if the mixing angle is small.

Some numerical investigation of (3.6) has been carried out [85] and it seems that this idea can reproduce experimental data accounting also for the observed difference between the two experiments. However due both to the incompleteness of this investigation and to our ignorance of magnetic field shape and size we still lack a quantitative knowledge of the allowed region for the parameters ($\mu_\nu, B, \alpha, \Delta m^2$) and of the $\bar{\nu}_e$ flux.

In particular a better understanding of the following problems is needed:

- a) The region of m and α which can reproduce the data.
- b) The dependence of the solution on the magnetic field shape.
- c) The relevance of the inner magnetic field
- d) The stability of the behaviour of the system for small changement of the input parameters (expecially $B(R)$).

§3.5 Do $\bar{\nu}_e$ Come out from the Sun?

In the frame of the class of hybrid models we have described up to now some production of $\bar{\nu}_e$ is expected. Free proton rich detectors like kamiokande are very sensitive to $\bar{\nu}_e$ and it is a meaningful effort to investigate what bounds the kamioka data put on the $\bar{\nu}_e$ productions and how significative are for the hybrid models [43].

§3.5.1 Bounds on the solar $\bar{\nu}_e$ flux from Kamiokande background data

As is well known, the specific signature of $\bar{\nu}_e$ in materials containing hydrogen is through the reaction

$$\bar{\nu}_e + p \longrightarrow e^+ + n \quad (3.38)$$

which produces isotropically distributed monoenergetic positrons ($E_{e^+} = E_\nu - \delta m$, $\delta m = m_n - m_p$). For energies above a few MeV, the cross section is

$$\sigma(E_\nu) = 9.2 \times 10^{-42} \left[\frac{(E_\nu - \delta m)}{10 \text{MeV}} \right]^2 \text{ cm}^2 \quad (3.39)$$

The Kamioka water detector, which is sensible to the $\nu_e - e$ interaction with a much smaller cross section, is clearly also capable of detecting reaction (3.39) provided there is an appreciable flux of solar $\bar{\nu}_e$.

For the moment, we assume that the energy distribution of $\bar{\nu}_e$ is the same as that of ν_e apart for an overall factor $P_{e\bar{e}}$ denoting the probability of the $\nu_e \rightarrow \bar{\nu}_e$ transition. We also assume that the ν_e spectrum, $d\Phi/dE_\nu$, is that given by the standard solar model [3].

The average number of positron with energy larger than a threshold E_0 which are produced in the detector is

$$N(E_{e^+} \geq E_0) = P_{e\bar{e}} AT N_p \int_{E_0+\delta m} dE_\nu \frac{d\Phi(SSM)}{dE_\nu} \sigma(E_\nu) \quad (3.40)$$

where T is the measurement time ($T = 1040$ days), N_p is the number of free protons contained in the fiducial mass of the Kamioka detector (680 tons of water) and A , an overall factor accounting for the SSM uncertainty, ranges in the interval $0.7 \div 1.3$.

This number is shown in table 1 (last column) for several values of E_0 , by taking $A = 1$ and $P_{e\bar{e}} = 1$. (In the same table, the number of $\nu_e - e$, $\bar{\nu}_e - e$, $\nu_\mu - e$ and $\bar{\nu}_\mu - e$ interactions are also shown for comparison.)

E_0 [MeV]	$N(E_{e^+} > E_0)$				
	$\nu_e - e$	$\bar{\nu}_e - e$	$\nu_\mu - e$	$\bar{\nu}_\mu - e$	$\bar{\nu}_e - p$
5.30	2.08×10^3	3.59×10^2	3.16×10^2	2.45×10^2	6.65×10^4
6.30	1.42×10^3	2.13×10^2	2.13×10^2	1.63×10^2	5.68×10^4
7.30	9.05×10^2	1.20×10^2	1.34×10^2	1.01×10^2	4.48×10^4
8.30	5.29×10^2	6.32×10^1	7.77×10^1	5.83×10^1	3.17×10^4
9.30	2.76×10^2	3.03×10^1	4.02×10^1	3.00×10^1	1.93×10^4
1.03×10^1	1.23×10^2	1.26×10^1	1.78×10^1	1.32×10^1	9.40×10^3
1.13×10^1	4.34×10^1	4.25	6.25	4.62	3.13×10^3
1.23×10^1	1.06×10^1	1.00	1.52	1.12	5.13×10^2
1.33×10^1	1.37	1.27×10^{-1}	1.96×10^{-1}	1.44×10^{-1}	2.24×10^1

TABLE 1. Average number of interactions taking place within Kamiokande II fiducial volume during $T=1040$ d. with energy of e^\pm in excess of E_0 by assuming for each neutrino species the same differential flux $d\Phi/dE_\nu$ as given by the SSM for ν_e and by taking $\sin^2 2\theta_{11} = 0.23$.

If we take $E_0 = 9.3$ MeV, the detection efficiency for e^- exceed 90 % [12]. We assume the efficiency for e^+ to be the same, thus the average number of detected positrons is

$$N^{det}(E_{e^+} \geq E_0) \geq AP_{e\bar{e}} \times 1.7 \times 10^4 \quad (3.41)$$

These events, being isotropically distributed, contribute to the flat background detected by Kamioka in the angular distribution. On the other hand, the total background for 1040 days at $E_0 = 9.3$ MeV is about 1160 counts, see fig. 3 of Ref. [13]. This provides a bound on $N_{det}(E_{e^+} \geq E_0)$ and thus on $AP_{e\bar{e}}$:

$$A\langle P_{e\bar{e}} \rangle \leq 7.7\% \quad (\text{at } 99\% \text{ CL}) \quad (3.42)$$

where the average refers to the data taking period January 1987 - April 1990.

More detailed information can be obtained by looking at the energy distribution of the Kamiokande events, see fig. 3 (vertical bars) from ref [86], corresponding to the period June 1988 - April 1989. The

number of positrons which are produced inside the detector in the energy interval $E_{e^+} \div E_{e^+} + \Delta E$ in time Δt is given by

$$\frac{\Delta N_{e^+}}{\Delta E \Delta T} = N_p \sigma(E_\nu) \frac{d\Phi_{\bar{\nu}}}{dE_\nu} \quad (3.43)$$

where $E_{e^+} = E_\nu - \delta m$ and $d\Phi_{\bar{\nu}}/dE_\nu$ is the flux of $\bar{\nu}$ which we want to determine. Again by assuming a detection efficiency better than 90% and requiring that the number of detected positrons does not exceed the observed signal, we get the upper bound for $d\Phi_{\bar{\nu}}/dE_\nu$ shown in fig. 3.1 (diamonds).

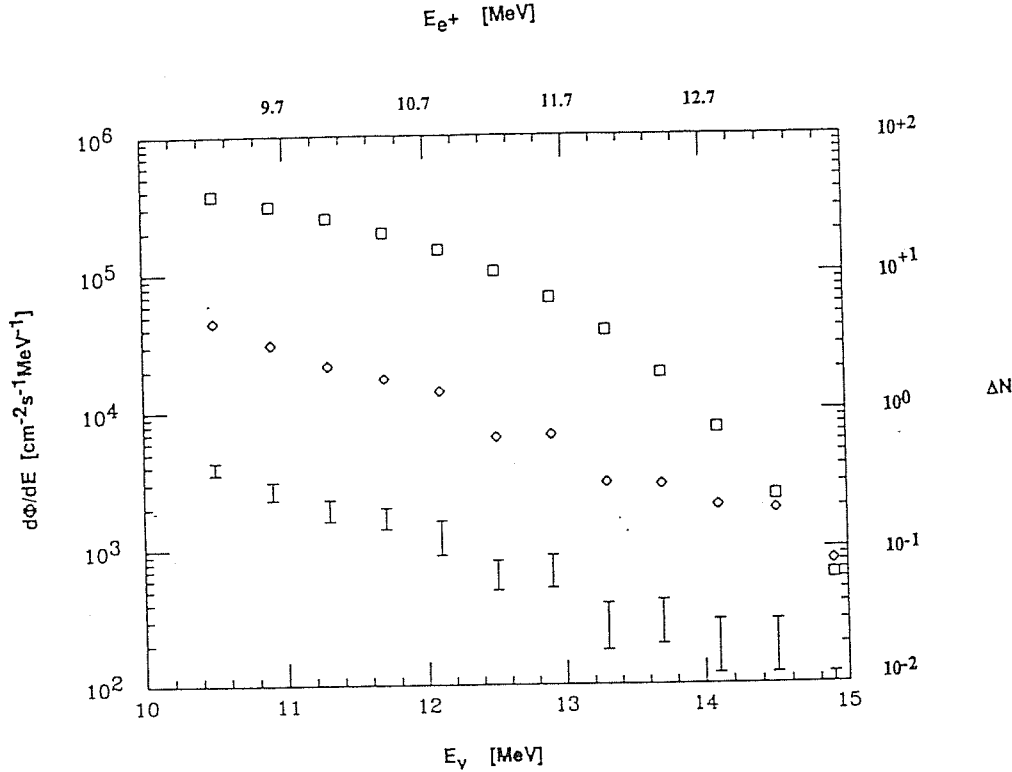


Fig. 3.1 The background spectrum in the Kamiokande II experiment for the period June 1988 - April 1989 86, in units of counts ΔN per day per energy interval of 0.4 MeV (vertical bar, right of the electron or positron energy E_{e^\pm} (top scale)). The corresponding upper bound on the $\bar{\nu}_e$ flux (diamonds, left scale), differentiated with respect to neutrino energy E_ν (bottom scale), fixed at $E_\nu = E_{e^\pm} + \delta m$. For comparison, the differential flux of ν_e predicted by the SSM is also shown (squares).

We derive that the total flux of $\bar{\nu}_e$ in the energy region of interest to us is severely bound,

$$\Phi_{\bar{\nu}}(E_\nu \geq 10.6\text{MeV}) \leq 6.1 \times 10^4 \text{cm}^{-2}\text{s}^{-1} \quad \text{at 99\%CL} \quad (3.44)$$

in comparison with the $\bar{\nu}_e$ flux predicted by the SSM in the same region $\Phi(SSM)(E_\nu \geq 10.6\text{MeV}) = A \times 6 \times 10^5 \text{cm}^{-2}\text{s}^{-1}$.

We remark that the bound in eq. (3.44) does not depend on assumptions about the spectrum of the antineutrinos. A more stringent bound can be derived if one assumes, as above, the spectrum to be the same as for ν_e . One finds in this way

$$A\langle P_{e\bar{e}} \rangle \leq 6\% \quad (\text{at } 99\% \text{ CL}) \quad (3.45)$$

§3.5.2 Hybrid models with large mixing angles and solar $\bar{\nu}_e$ flux

With the aim of appreciating how severe are the bounds we presented, we discuss as a concrete example a simple hybrid model, were we assume:

a) validity of the SSM

b) a squared neutrino mass difference $\delta m^2 = 10^{-9} \text{eV}^2$, so that the oscillation length $\lambda = 4\pi E_\nu / \delta m^2$ is much larger than the solar radius and much smaller than the sun earth distance ($E_\nu \simeq 10 \text{MeV}$)

c) a $\nu_e \rightarrow \bar{\nu}_\mu$ transition magnetic moment, $\langle \nu_e | \mu | \bar{\nu}_\mu \rangle$, and a transverse magnetic field B in the convective zone of the Sun such that, when the solar activity is high, the magnetic interaction energy $E_M = \mu B$ is the dominant term of the neutrino evolution hamiltonian in the convective zone:

$$E_M \gg \frac{\delta m^2}{E_\nu} \quad E_M \gg G n_e \quad (3.46)$$

where n_e is the electron density and G is the Fermi constant.

Independently of E_ν for each ν_e produced in the core of the sun the probabilities of emerging from the surface of the sun as ν_e and $\bar{\nu}_\mu$ are respectively

$$P_S(\nu_e) = \cos^2 \beta, \quad P_S(\bar{\nu}_\mu) = \sin^2 \beta \quad (3.47)$$

where $\beta = \mu \int dr B(r)$ and the integral is between the beginning and the end of the convective zone. It is natural to take B to be proportional to the square root of the sunspot number N_{ss} [76], so that

$$\beta = f \sqrt{N_{ss}} \quad (3.48)$$

In the trip from the sun to the earth a flavour transition can occur with an average probability $\sin^2 \theta$, which can be written in terms of the vacuum mixing angle α as

$$\sin^2 \theta = \frac{1}{2} \sin^2(2\alpha) \quad (3.49)$$

In conclusion, the arrival probabilities of the different neutrino species can be written as

$$\begin{aligned}
P(\nu_e) &= \cos^2 \theta \cos^2(f\sqrt{N_{ss}}) \\
P(\bar{\nu}_e) &= \sin^2 \theta \sin^2(f\sqrt{N_{ss}}) \\
P(\nu_\mu) &= \sin^2 \theta \cos^2(f\sqrt{N_{ss}}) \\
P(\bar{\nu}_\mu) &= \cos^2 \theta \sin^2(f\sqrt{N_{ss}})
\end{aligned} \tag{3.50}$$

We can now get information on the two parameters θ and f by analysing the experimental data of the Kamioka experiment.

For high electron energy threshold (E_0 close to the kinematical bound) the cross section of $\nu_e - e$, $\bar{\nu}_e - e$ and $\bar{\nu}_\mu - e$ are about 1/9 of the $\nu_e - e$ cross section (within 20%), see for example table 1. In the Kamioka experiment, the ratio R_K of the electron signal in the direction opposite to the sun to the expectation of the SSM can be written as

$$R_K = A\{P(\nu_e) + \frac{1}{9}[1 - P(\nu_e)]\} = A[\frac{8}{9} \cos^2 \theta \cos^2(f\sqrt{N_{ss}}) + \frac{1}{9}] \tag{3.51}$$

For simplicity, and without affecting the results in any significant way, we make a two parameter fit of these data by assuming

$$R_K = \frac{8}{9} C \cos^2(f\sqrt{N_{ss}}) + \frac{1}{9} \tag{3.52}$$

where $C = A \cos^2 \theta$

The available data on R_K correspond to five time intervals in the period 1987 - 1990, see fig. 2 of ref. 13. Fig. 3.2 shows in the plane (C, f) the results of the best fit (diamond) and the 99% CL contour (dashed curve).

The Chlorine experiment can be analyzed in the same way. The ratio of the observed number of Ar^{37} atoms to the expectation of the SSM is

$$R_{Cl} = C \cos^2(f\sqrt{N_{ss}}) \tag{3.53}$$

By analysing the Chlorine data for the period 1970 - 1990 (and by treating the quoted errors as if they were up - down symmetrical) we find as best fit value the point denoted by the cross in fig. 3.2 and at the 99% CL the area inside the dot - dashed curve. The shaded area denotes the area in the (C, f) plane consistent with both experiments.

By using eq. (3.50), the upper bound on the fraction of $\bar{\nu}_e$ given in eq (3.45) can be written as

$$(A - C)\langle \sin^2(f\sqrt{N_{ss}}) \rangle_{88-89} < 6\% \tag{3.54}$$

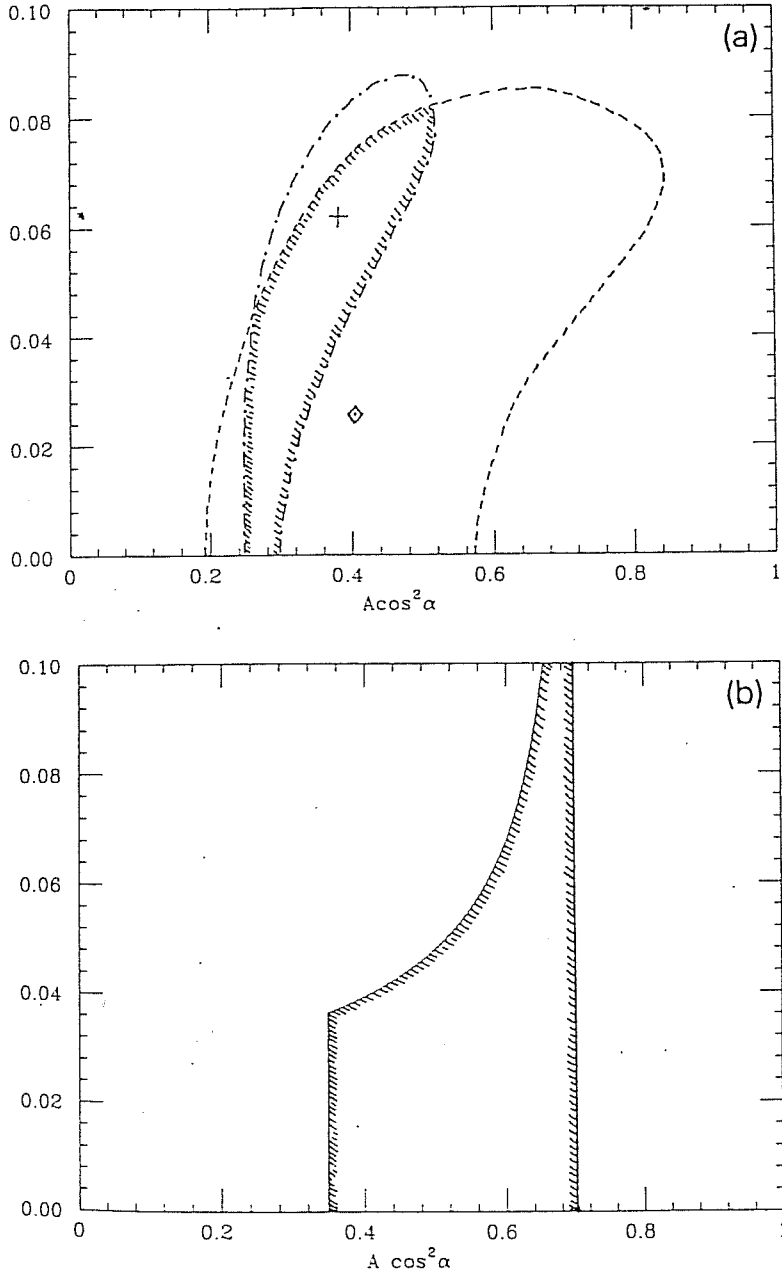


Fig. 3.2 In the plane $(C = A \cos \alpha, f)$ we show (a) the best fit for Kamiokande II electron signal R_K in the period 1987 - 1990 (diamond) and the allowed region (inside the dashed curve), the best fit of the Ar^{37} signal R_D in the period 1970 - 1990 (cross) and the allowed region (inside the dot-dashed curve), and we show the region which is consistent with the above constraint within the shaded curve. All curves correspond to 99 % confidence level. (b) The boundary of the region corresponding to the upper bound on the $\bar{\nu}_e$ flux (full curve), calculated for $A = 0.7$, the constraint $0.5 < \cos^2 \theta < 1$ (vertical lines) and the region consistent with the above constraints (shaded area).

No region of parameter space is left which is consistent both with the signal in the Chlorine experiment and in the Kamioka experiment as well as with the indirect information on the $\bar{\nu}_e$ flux. Choosing a value of A greater than 0.7 would worsen the situation.

The discussion of the simple model given above shows that, when building a consistent hybrid model, one has to avoid overproduction of $\bar{\nu}_e$. This can be accomplished, perhaps, by exploiting resonant phenomena induced by matter effects, for a suitable choice of parameters of the model [29]. Alternatively, a complete suppression of $\bar{\nu}_e$ can be achieved in a class of hybrid models where a suitable combination of lepton numbers (e.g. $L_e + L_\mu - L_\tau$) is conserved. We will come back to this last possibility in the next chapter.

Other mechanism of $\bar{\nu}_e$ production occur in a class of models where a heavy neutrino decay into a lighter one and in a pseudoscalar $\nu_2 \rightarrow \bar{\nu}_1 + M$. The most characteristic feature of all neutrino decay scenarios (including the matter induced decay) is that the $\bar{\nu}_e$ takes a smaller fraction of the initial neutrino energy, typically 1/3. The data we have discussed (corresponding to a threshold energy of 9.3 MeV) are clearly poor for giving information on the decay process. On the other hand, interesting information could be obtained with a significantly lower detection threshold.

CHAPTER 4

NEUTRINO OSCILLATION AND MAGNETIC MOMENT TRANSITION IN A MODEL WITH A CONSERVED LEPTON NUMBER

As we have already stressed the hybrid models proposed up to now, in our opinion, present two unpleasant features: they require two vastly different mass scales and they lead to the production of $\bar{\nu}_e$, which are severely restricted by data. A natural way of avoiding both these problems consists in considering all the three standard neutrino flavors ν_e , ν_μ and ν_τ and assuming a suitable nonstandard lepton number to be conserved:

$$L_\pm = L_e \pm L_\mu \mp L_\tau \quad (4.1)$$

This conservation law implies just one mass scale, the mass spectrum consisting of one massive Dirac neutrino and one massless Weyl neutrino [87, 88]. An unquenched magnetic transition can take place between the two helicity states of the Dirac neutrino and, on the other hand, the fact that the mass eigenstates are linear superposition of the different neutrino flavors gives rise to a flavour oscillation. In other words by considering all the three neutrino flavors one can have flavour oscillations even in the presence of a Dirac neutrino state in the spectrum.

§4.1 The model

For definiteness, we take L_+ as a conserved quantum number. The most general mass term which is consistent with this constraint is

$$\mathcal{L}_m = -m\bar{\nu}_{\tau R}^C(\nu_{eL} \cos \alpha + \nu_{\mu L} \sin \alpha) + h.c. \quad (4.2)$$

This lagrangean describes one Dirac neutrino with mass m

$$\psi_{mL} = \nu_{eL} \cos \alpha + \nu_{\mu L} \sin \alpha, \quad \psi_{mR} = \nu_{\tau R}^C \quad (4.3)$$

and a massless Weyl neutrino

$$\nu_0 = -\nu_{eL} \sin \alpha + \nu_{\mu L} \cos \alpha \quad (4.4)$$

For a sizeable values of the mixing angle α , experiment at nuclear reactors yield [89] $m \leq 0.1$ eV. Since significant magnetic moments call for high masses, we will explore the region near this upper bound

$$m \approx 10^{-2} - 10^{-1} \text{ eV} \quad (4.5)$$

In this range of masses the existing data from accelerator experiments on $\nu_e \rightarrow \nu_\mu$ ($\bar{\nu}_e \rightarrow \bar{\nu}_\mu$) do not impose any constraint on α .

The most general magnetic moment effective lagrangean, consistent with the conservation of L_+ , has the form

$$\mathcal{L}_\mu = -\frac{1}{2}\mu\nu_{\tau R}^C\sigma_{\lambda\phi}F_{\lambda\phi}(\nu_{eL}\cos\beta + \nu_{\mu L}\sin\beta) + h.c. \quad (4.6)$$

The Hamiltonian H which determines the evolution of the ν_e state in the sun

$$i\frac{\partial}{\partial\tau}|\nu(r)\rangle = H(r)|\nu(r)\rangle \quad (4.7)$$

where $r = ct$, is immediately obtained from eqs. (4.2) and (4.6), including the coherent neutrino weak interaction with matter [25]. We observe that due to the conserved lepton number the hamiltonian decouple into two sub-hamiltonians each couplings only three states. In the mass eigenstates basis ($|\nu_o\rangle, |\psi_{mL}\rangle, |\psi_{mR}\rangle$) one has

$$H(r) = \begin{pmatrix} G_F n_e \sqrt{2} \sin^2 \alpha - \frac{G_F n_n}{\sqrt{2}} & -G_F n_e \sqrt{2} \cos \alpha \sin \alpha & \mu B \sin(\beta - \alpha) \\ -G_F n_e \sqrt{2} \cos \alpha \sin \alpha & \frac{m^2}{2E} + G_F n_e \sqrt{2} \cos^2 \alpha - \frac{G_F n_n}{\sqrt{2}} & \mu B \cos(\beta - \alpha) \\ \mu B \sin(\beta - \alpha) & \mu B \cos(\beta - \alpha) & \frac{m^2}{2E} + \frac{G_F n_n}{\sqrt{2}} \end{pmatrix} \quad (4.8)$$

where n_e and n_n are the electron and neutron densities respectively, G_F is the Fermi constant and $B = B(r)$ is the transverse component of the solar magnetic field.

In the convective zone ($r \geq R_B = 0.7R_\odot$, where $R_\odot = 7 \times 10^5$ km is the solar radius) we assume $n_n = 1/6n_e$ and the density profile to be given by [3]

$$n_e \approx n_0 \exp\left(\frac{-r}{L_m}\right) \quad (4.9)$$

with $L_M \approx 0.1R_\odot$, and $n_e(R_B) \approx 0.16 N_A \text{cm}^{-3}$, N_A being the Avogadro number.

Concerning the magnetic field, we will assume that it is confined within the convective zone. In the absence of detailed information on the shape of the field, we use the following parameterization:

$$B(r) = \theta(r - R_B)B_0\left\{1 - \exp\left[\frac{-r + R_B}{L_B}\right]\right\} \quad (4.10)$$

The starting point R_B is taken at the beginning of the convective zone. The raising length L_B (some fraction of the convective zone) and the plateau value B_0 are kept as free parameters. B_0 varies during the solar cycle, from $B_0 \approx 0$ at the solar minima up to a value B^{max} in correspondence of the maxima of the solar activity.

Note that according to (4.10), in the very outer region of the sun the field does not fall (as fast) as the coherent weak interaction. In fact we expect the magnetic field to decrease with some power of the distance, whereas the density profile is exponentially decaying.

It is useful to introduce a magnetic energy term,

$$\epsilon(r) = \mu B(r) \cos(\beta - \alpha) \quad (4.11)$$

and a magnetic energy plateau ϵ_0 which is obtained from (4.11) for $B = B_0$. For the values of interest to us ($\mu \approx 10^{-10} \mu_B$, $B_0^{max} \approx 1 T$) one has $\epsilon_0^{max} \approx 2\theta/R_\odot$ for $\cos(\beta - \alpha) = 1$.

§4.3 Flavour oscillations and spin flip in the absence of coherent weak interaction

As a first stage of the discussion, we neglect in eq. (4.8) the coherent weak interactions. For the values of interest to us, one has $m^2/2E \gg \mu B$ and consequently the $|\nu_0\rangle$ state is decoupled from the others.

One also has $(m^2/2E)R_\odot \gg 1$ and so the oscillating terms of argument $(m^2/2E)R_\odot$ can be replaced by their average values. In these hypothesis, the arrival probability $P(\nu_x)$ of the originally ν_e state are

$$\begin{aligned} P_{ee} &= \sin^4 \alpha + \cos^4 \alpha \cos^2 \Phi \\ P_{e\mu} &= \frac{1}{4} \sin^2 2\alpha (1 + \cos^2 \Phi) \\ P_{e\bar{\tau}} &= \cos^2 \alpha \sin^2 \Phi \\ \Phi &= \mu \cos(\beta - \alpha) \int dr B(r) \end{aligned} \quad (4.12)$$

The main phenomenological features of the model are immediate from the equations given above:

a) Let us assume that the spectrum of neutrinos produced in the core of the sun dF/dE , is correctly given by the standard model, apart from a factor A accounting for the SSM uncertainties:

$$\frac{dF}{dE} = A \frac{dF^{SSM}}{dE}, \quad A = 0.7 \div 1.3 \quad (4.13)$$

In this case, the ratio of the signal in the Chlorine experiment to the expectation of the SSM is simply

$$R_C = AP_{ee} \quad (4.14)$$

The signal deficit at solar minima ($\Phi = 0$) calls for a large value of the vacuum mixing angle. Indeed from eqs. (VII) and (4.12) at the 1σ level, one gets

$$2\left(1 - \frac{0.61}{A}\right) \leq \sin^2 2\alpha \leq 2\left(1 - \frac{0.45}{A}\right) \quad (4.15)$$

In the case $A = 1$ this yields

$$0.78 \leq \sin^2 2\alpha \leq 1 \quad (4.16)$$

Note that the same result hold for $\Phi = 0$ also in the case that coherent weak interactions are included. In other words, the signal deficit at solar minima always implies a large vacuum mixing angle.

b) A significant depletion of the signal in correspondence of the solar maxima can be achieved only for Φ_{max} close to $\pi/2$. In fact, smaller values of Φ_{max} yield a too small time dependence,

whereas for larger values the signal oscillates with a frequency larger than that of the solar cycle. As remarked in [90] this condition requires a fine tuning of the parameters (μ and B) which are involved.

c) Even for the best case, $\Phi_{max} = \pi/2$, a significant depletion of the signal at the solar maxima calls for large vacuum mixing angle. From (VII) one has

$$\frac{\langle R_D \rangle_{max}}{\langle R_D \rangle_{min}} = 0.19 \pm 0.07 \quad (4.17)$$

By using eq (4.12) with $\Phi_{max} = \pi/2$ and $\Phi_{min} = 0$ we get, at the 1σ level

$$\sin^2 2\alpha = 0.79 \pm 0.20 \quad (4.18)$$

d) In the Kamioka experiment, in addition to ν_e , both ν_μ and $\bar{\nu}_\tau$ can scatter off electrons. For the Kamioka experiment one has

$$R_K = A[P_{ee} + W_\mu(E_{th})P_{e\mu} + W_\tau P_{e\bar{\tau}}] \quad (4.19)$$

where the factors $W_x(E_{th})$ depend on the threshold energy and on neutrino flavour (for $E_{th} = 9.3$ MeV $W_\mu = 1/7$ and $W_\tau = 1/9$. For the present model one obviously have $\langle R_K \rangle > \langle R_D \rangle$, in agreement with the trend of the experimental data. Also, the time modulation comes out to be weaker in Kamioka. As an example, by assuming $\Phi_{max} = \pi/2$ and $\Phi_{min} = 0$ at solar maxima and minima respectively, for α as in (4.18) and threshold energy $E_{th} = 9.3$ MeV we get a modulation $\langle R_K \rangle_{max}/\langle R_K \rangle_{min} = .34 \pm .06$

§4.4 Inclusion of coherent weak interaction

The neutrino evolution corresponding to the full hamiltonian given in eqs (4.8) has to be studied numerically. In this section we shall investigate two opposite limiting cases, which can be discusses analytically and yield a qualitative understanding of the complete solution.

For the values of masses we are considering (see (4.5)) both Gn_e and Gn_n are (almost) negligible in comparison with the energy splitting, $m^2/2E$. The same holds true for the μB term for the values of interest to us. In these circumstances, the massless neutrino component $|\nu_0\rangle$ is piratically decoupled from the others.

The problem thus simplifies to the study of a two state system, $|\psi_{mL}\rangle$ and $|\psi_{mR}\rangle$. For this system the relevant part of the hamiltonian (i. e. apart from terms proportional to the identity) is

$$h(\tau) = \begin{pmatrix} \Delta(\tau) & \epsilon(\tau) \\ \epsilon(\tau) & -\Delta(\tau) \end{pmatrix} \quad (4.20)$$

where

$$\Delta(\tau) = \frac{G(n_e \cos^2 \alpha - n_n)}{\sqrt{2}} \quad (4.21)$$

Note that, since the magnetic moment couples the left and the right components of the same Dirac neutrino, there are no mass terms inhibiting the spin flip transition.

We recall that we assume a large mixing angle $\cos^2 \alpha \approx 1/2$ and in the convective region we use eq. (4.9). We note that, as a consequence of the large vacuum mixing angle, $\Delta(r)$ never vanishes in the convective zone. A non zero value of $\Delta(r)$ clearly inhibits spin flip transitions [84], with respect to the case without coherent weak interactions.

The term $\epsilon(r)$ is defined by means of eqs. (4.10) and (4.11)

$$\epsilon(r) = \theta(r - R_B)\epsilon_0\left\{1 - \exp\left[-\frac{-r + R_B}{L_B}\right]\right\} \quad (4.22)$$

We shall investigate the solution of the problems in terms of the field raising distance L_B and the interaction energy plateau ϵ_0 which, we recall, varies during the solar cycle from $\epsilon_0 \approx 0$ at solar minima up to a maximum value ϵ_0^{max} at solar maxima.

Qualitatively, for the solution of the problem, one can distinguish three different regions:

a) in the inner part of the sun (say $r < R_1$) weak coherent effects dominate ($\Delta(r) \gg \epsilon(r)$) and the solution is immediate. For a state which is $|\psi_{mL,R}\rangle$ at $r = 0$ one has

$$r < R_1 : \quad |\psi_{mL,R}\rangle \rightarrow |\psi_{mL,R}\rangle \exp(\pm i \int_0^r ds \Delta(s)) \quad (4.23)$$

b) In the outer part (say $r > R_2$) the magnetic moment interactions dominates ($\Delta(r) \ll \epsilon(r)$). Also in this case the analytical solution is immediate. For a state which can be described as $|\psi_{mL,R}\rangle$ at $r = R_2$ one has

$$\begin{aligned} r > R_2 : \quad & |\psi_{mL}\rangle \rightarrow |\psi_{mL}\rangle \cos \xi(r) - i |\psi_{mL}\rangle \sin \xi(r) \\ & |\psi_{mR}\rangle \rightarrow -i |\psi_{mL}\rangle \sin \xi(r) + |\psi_{mR}\rangle \cos \xi(r) \\ & \xi(r) = \int_{R_2}^r ds \epsilon_B(s) \end{aligned} \quad (4.24)$$

c) In the intermediate region $R_1 < r < R_2$, Δ and ϵ are comparable. The behaviour of the solution in this intermediate region (and consequently of the entire problem) depends crucially on the shape of the magnetic field. One can envisage two limiting situations, corresponding respectively to an adiabatic or a sudden transition between regions *a* and *b*. We investigate the region of validity of the two approximations in the plane (ϵ_0, L_B) and then we discuss the appropriate solution for both cases.

§4.4.1 The adiabatic and the sudden region

The transition between the two regions can be taken as adiabatic or sudden depending on the value of the function

$$g(r) = \frac{|\epsilon\Delta' - \epsilon'\Delta|}{2(\epsilon^2 + \Delta^2)^{3/2}} \quad (4.25)$$

For $g \ll 1$ ($g \gg 1$) the adiabatic (sudden) limit is realized. One has to verify such condition close to the point $r = r^*$ where $\epsilon(r^*) = \Delta(r^*)$. The curves shown in fig. 4.1 correspond, for $\cos^2 \alpha \approx 1/2$, to $g(r^*) = 1$, i. e. they denote the transition between the two regimes.

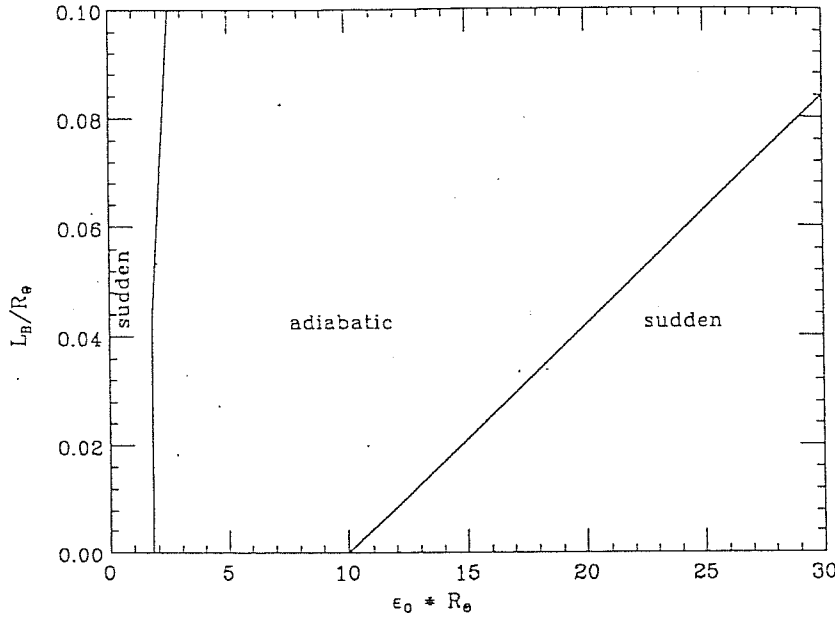


FIG. 4.1 In the plane (ϵ_0, L_B) we show the borders of the adiabatic and the sudden regimes, defined as $g = 1$, see eq. (4.25). ϵ_0 is the plateau value of the magnetic interaction energy and L_B is its raising length. R_\odot is the solar radius.

The main features of fig. 1.1 can be understood from the following considerations. Note that g is the sum of two positive functions, $g = g_1 + g_2$, where

$$g_1(r) = -\frac{\epsilon\Delta'}{2(\epsilon^2 + \Delta^2)^{3/2}} \quad g_2(r) = -\frac{\epsilon'\Delta}{2(\epsilon^2 + \Delta^2)^{3/2}} \quad (4.26)$$

At $r = r^*$, $g_1 = [4\sqrt{2}L_M\epsilon(r^*)]^{-1}$ and one has $g_1 \geq 1$ for $\epsilon_0 \leq (4\sqrt{2}L_M)^{-1}$. This explains the region of small fields where the sudden limit is achieved.

For intermediate values of the field, $(4\sqrt{2}L_M)^{-1} \leq \epsilon_0 \leq \Delta(r_B) \approx 10/R_\odot$, g_1 is smaller than unity. Also, the magnetic interaction ϵ approaches its plateau value ϵ_0 before r^* and $g_2(r^*)$ tend to

zero. Consequently the adiabatic condition can be satisfied. For even larger fields ($\epsilon_0 \geq \Delta(r_B) \approx 10/R_\odot$) r^* is reached while the magnetic interaction energy ϵ is raising and the adiabatic condition is fulfilled only for sufficiently large values of L_B .

§4.4.2 The adiabatic and the sudden solution

If the transition between regions a and b is adiabatic, the (instantaneous) eigenstates of region a go into the corresponding ones of the region b . After traversing the sun the probabilities of the different neutrino flavors are

$$\begin{aligned} P_{ee} &= \sin^4 \alpha + \frac{1}{2} \cos^4 \alpha \\ P_{e\mu} &= \frac{3}{8} \sin^2 2\alpha \\ P_{e\bar{\tau}} &= \cos^2 \alpha \end{aligned} \quad (4.27)$$

where oscillating terms of argument $(m^2/2E)R_\odot \gg 1$ have been averaged. If the transition is sudden, when crossing the intermediate region ($R_1 < r < R_2$) the $|\psi_{mL,R}\rangle$ states do not change. Beyond R_2 , coherent interactions are irrelevant and the time evolution is the same as discussed in the previous section.

The arrival probabilities are thus given again by eqs. (4.12), where the phase Φ is now given by

$$\Phi = \mu \cos(\beta - \alpha) \int_{R_2} ds B(s) \quad (4.28)$$

This means that the magnetic field contributes to the phase only in the region where it overwhelms the coherent weak interaction.

§4.4.3 Discussion

On these grounds we can discuss the arrival probabilities P_{ex} during the different phases of the solar cycle.

For any L_B , at the solar minimum ($\epsilon_0 \approx 0$) one is in the sudden limit. The solution is given by eqs (4.12) with $\Phi = 0$. As discussed in section (4.3) a significant depletion of the neutrino signal can be obtained for large mixing angles, as given in eq. (4.16).

As the field raises, different regimes (adiabatic, sudden, or intermediate) can be reached depending on the value of ϵ_0^{max} and L_B .

From the phenomenological point of view, the most important features of the adiabatic regime are:

a) The results do not depend on the precise value of μ and B_0^{max} . Thus a significant modulation of the signal, anticorrelated with the solar cycle, can be obtained without a fine tuning of the magnetic field and magnetic moment, provided that ϵ_0^{max} and L_B .

b) Note that the lowest values of ϵ_0^{max} which satisfy the adiabatic condition (and thus provide a significant time modulation) are of order $\epsilon_0^{max} \approx 5/R_\odot$, (the inverse of the convective zone dimension). Whichever mechanism one is invoking, one cannot do better, in the sense that for a significant spin flip probability the phase $\Theta = \epsilon_0 D$ where D is the depth of the convective zone, has to exceed unity.

c) On the other hand, the minimum value of P_{ee} is 1/3, which is at the border of the region allowed by the Chlorine data. Also, the signal modulation in the Chlorine experiment $\langle R_C \rangle_{max} / \langle R_C \rangle_{min}$ cannot be smaller than one half, which looks in disagreement with (VII).

In the case that sudden regime is reached, the same phenomenological consideration as for the "vacuum" case hold. In addition, we note that only the region of high fields ($\epsilon_0 > 10/R_\odot$) is relevant for getting a significant phase Φ . In comparison with the adiabatic limit, the sudden case requires ϵ_0^{max} appreciably larger in order to achieve a significant time modulation. On the other hand, the amplitude of the modulation can be much larger, as previously remarked.

In summary, the inclusion of matter effects does not alter drastically the picture. One can choose the available parameters so as to reproduce the main feature of experimental results. Furthermore, if adiabaticity holds, one has a natural suppression of the signal at the solar maxima, which does not require a fine tuning of the neutrino magnetic moment and the solar magnetic field.

So far we restricted the magnetic field to the convective zone. On the other hand, the existence of a primordial field in the core of the sun, B_{in} is not excluded. Of course B_{in} is decoupled from the eleven years solar semicycle. Before closing this section we note a peculiarity which occurs for $B_{in} \neq 0$. For $\cos^2 \beta < 1/2$, $\Delta(\tau)$ reverses its sign in the core of the sun. If the resonance is crossed adiabatically all $|\psi_{mL}\rangle$ transform into $|\psi_{mR}\rangle$. In the convective zone, if the field is high enough, the $|\psi_{mR}\rangle$ transform back into $|\psi_{mL}\rangle$. Thus a positive correlation with the magnetic field would occur.

§4.4.4 Conclusions

We have developed a phenomenological model with both neutrino flavour oscillations and spin flip transitions, characterized by a lepton number conservation law $L_\pm = L_e \pm L_\mu \mp L_\tau$. This implies a massless Weyl neutrino and one massive Dirac neutrino. The main consequences of this class of models are:

i) There is a large mixing angle between ν_e and ν_μ or ν_τ depending on the choice of the conserved lepton number (L_+ or L_-).

ii) The mass difference Δm coincides with the mass of the Dirac neutrino. As such it cannot be too small, in order to allow for a sizable magnetic moment. A value of order $10^{-1} \div 10^{-2}$ eV is consistent with bounds from reactor experiments. We note that $\nu_e - \nu_\mu$ oscillation with a large mixing angle and similar Δm may be indicated by the recently reported atmospheric neutrino flux anomaly [91].

iii) We have seen that the model can account for both the experimental data of the Chlorine and kamiokande II experiment, for a large mixing angle. The difference between the results of the two experiment can be understood on the basis that in the former only ν_e are active, whereas in the latter all the neutrino states contribute to the signal. Our discussion was qualitative in that only two limiting cases (the adiabatic and the sudden solution) have been explored.

iv) Obviously the model predict no $\bar{\nu}_e$ signal from the sun. This is supported by the stringent upper bound on solar $\bar{\nu}_e$ flux from the results of the Kamioka experiment. *v)* The suppression of the neutrino signal with the SSM prediction comes out to be independent of the neutrino energy. Thus we expect the Gallium experiment to give the same modulation as the Chlorine experiment.

CHAP. 5

NEUTRINO DECAY

We now turn to study the possibility that neutrinos are unstable particles. This possibility was first considered in connection with the SNP by Bahcall Cabibbo and Jahill [30]. Since electron neutrino is almost massless it can decay only in a lighter neutrino and an almost massless scalar or vector particle (we don't consider the possibility of three body decay in three lighter neutrino or similar channels since due to the much smaller phase space they cannot play any role for solar neutrinos).

The most natural candidates for the decay product are pseudo-goldston bosons and gauge vector bosons which are massless due to symmetry considerations. Since it turns out that neutrino decay into a photon cannot play any role in solar neutrino decay we devote our attention to the case of neutrino decay into a lighter neutrino and a majoron, namely a pseudo-goldstone boson arising as a consequence of the spontaneous breaking of lepton number conservation.

We first discuss the possibility that the neutrino decay in the path from the sun to the detector and we show that this is still a viable solution to the SNP (although strongly disfavoured from the recent Gallex results). Then we discuss the impact of matter effects when a strong enough neutrino majoron coupling is assumed. The effect of weak interaction of neutrinos with a medium is to induce additional effective mass splitting therefore modifying the phase space for the decay. One unique feature of neutrino decay in matter is the appearance of an effective mass splitting among a neutrino and its own antineutrino allowing also the decay in this channel which is forbidden in vacuum due to the mass degeneracy of this two states. Neutrino decay in matter, in the simplest models, cannot play a significant role for the solution SNP, however the detection of the decay of a neutrino into a lighter neutrino and a majoron would be of enormous interest independently of the SNP and therefore we study in detail the perspective for the detection of this signal. In addition it has recently been noticed that when also additional, strong enough, interaction of tau neutrino are included in the model the matter induced neutrino decay can be a plausible candidate to the solution of the SNP.

§5.1 The Neutrino Decay Solution to the SNP

One of the possible solutions of the solar neutrino problem (SNP) appeals to the possibility of neutrino decay during the flight from sun to earth [30, 48]. Since the fast radiative decay is excluded both from particle physics and astrophysical arguments, one has to consider fast invisible decay modes of the neutrino. This idea can be proposed in the context of majoron models [92, 93]. In order that the decay $\nu_2 \rightarrow \nu_1 + M$ occurs during the neutrino transit time $t_{\odot} \simeq 500s$, the majoron M should have sufficiently strong off-diagonal couplings ($g > 10^{-4}$) with the neutrino mass eigenstates $\nu_{1,2}$. (The existence of tree level off-diagonal couplings requires non-trivial symmetry properties distinguishing among the lepton families, as was emphasized in [94]). As well known, the most

familiar candidate, the triplet majoron [92], has been ruled out by LEP data on Z-boson invisible width [95], whereas the "see-saw" singlet majoron [93] is very weakly coupled to neutrinos. However, a variety of new singlet (or predominantly singlet) majoron models can be considered, in which the scale of lepton number violation can be sufficiently low as to provide coupling constants in the proper range (see [96] and references therein). In addition, if the 17 KeV neutrino [97] will be confirmed, it can be considered as one of the strongest arguments in favour of the existence of such a majoron: only the fast majoron decay can make the 17 KeV neutrino compatible with recent cosmological and astrophysical restrictions [98].

The observation of the $\bar{\nu}_e$ pulse from SN1987A [11, 46] rules out the neutrino decay solution of SNP with negligible neutrino mixing [30], which requires a ν_e decay length adjusted to the sun-earth distance. However, the case [47, 48] when the neutrino mixing angle θ is substantial remains open. Even if only the component ν_1 reaches earth owing to the fast decay of ν_2 , the ν_e signal is not vanishing and it directly measures the neutrino mixing angle: $\cos^4 \theta \simeq N_{Davis}/N_{SSM} \simeq 0.3$ [47, 48]. This is quite compatible with the SN1987A bound $\cos^4 \theta \geq 0.1$ [48].

We now revisit the majoron decay solution of SNP. We show that this scenario can reconcile the Homestake and the Kamiokande results and does not conflict with astrophysical constraints and terrestrial experiments. Definite predictions for Ga-Ge experiments are also given.

The central feature of this scenario is the appearance of a substantial flux of solar $\bar{\nu}_e$. We show that future low threshold real time detectors like Borexino/Borex [41] will be quite sensitive to this signal so as to confirm or rule out the ν decay solution.

As another solution [29] to SNP, the interplay of Majorana neutrino oscillations and spin-flavour precession due to neutrino magnetic moment can also provide a mechanism for solar $\bar{\nu}_e$ production [29, 99]. However, in the case of neutrino decay the $\bar{\nu}_e$ energy spectrum is degraded in a specific way with respect to the initial ν_e flux, whereas hybrid models generally lead to a much less degraded spectrum. Note that in the latter case the $\bar{\nu}_e$ flux can be strongly bounded [44] on the basis of Kamiokande data, whereas for the former one this bound does not apply. We will show that detectors like Borexino/Borex can clearly discriminate between these models of $\bar{\nu}_e$ production.

We remark that the study of solar $\bar{\nu}_e$'s can be of interest also independently of SNP, i.e. in the context of possibilities which by themselves are not capable to account for the solar neutrino deficit. Flux of solar $\bar{\nu}_e$ could appear due to matter induced neutrino decay $\nu_e \rightarrow \bar{\nu}_e + M$ [47], due to MSW transition $\nu_e \rightarrow \nu_\mu$ with forthcoming decay $\nu_\mu \rightarrow \bar{\nu}_e + M$ [100], or due to decay of a 17 KeV neutrino $\nu_{17} \rightarrow \bar{\nu}_e + M$ which, if it exists, should be unavoidably produced in the sun being a small admixture ($\sin \theta \simeq 0.1$) to the ν_e . Of course the last possibility could be applied to any Majorana neutrino with large mass and a small ν_e component. We briefly discuss these possibilities, which generally lead to a weaker antineutrino signal.

§5.1.1 Neutrino Decay with Majoron Emission

We assume the minimal CP conserving phenomenological Lagrangean for two Majorana neutrinos $\nu_{1,2} = C\bar{\nu}_{1,2}^T$, with mass term

$$\mathcal{L}_m = \frac{1}{2}(m_1\bar{\nu}_1\nu_1 + m_2\bar{\nu}_2\nu_2), \quad m_2 > m_1, \quad (5.1)$$

and Yukawa coupling with the majoron field M

$$\mathcal{L}_{Yuk} = \frac{i}{2}M \sum_{i,j} g_{ij}\bar{\nu}_i\gamma_5\nu_j, \quad g_{ij} = g_{ji}. \quad (5.2)$$

The inclusion of a third neutrino as well as of CP violating effects does not alter our discussion. In terms of the flavour eigenstates one has:

$$\nu_1 = c\nu_e - s\nu_x \quad \nu_2 = s\nu_e + c\nu_x, \quad (5.3)$$

where ν_x can be any active (ν_μ, ν_τ) or sterile (ν_s) neutrino and θ is the vacuum mixing angle ($c = \cos\theta, s = \sin\theta$). The g_{ij} in (2) are related with the majoron coupling constants in the flavour basis via

$$\begin{aligned} g_{11} &= c^2g_{ee} - csg_{ex} + s^2g_{xx} \\ g_{12} &= (c^2 - s^2)g_{ex} + 2cs(g_{ee} - g_{xx}) \\ g_{22} &= s^2g_{ee} - csg_{ex} + s^2g_{xx}. \end{aligned} \quad (5.4)$$

In the lab frame the decay widths of ultrarelativistic ν_2 ($E \gg m_2 = m$) in the two channels $\nu_2 \rightarrow \nu_1 + M$ and $\nu_2 \rightarrow \bar{\nu}_1 + M$ ¹ are [101]:

$$\Gamma_\nu = \Gamma_{\bar{\nu}} = \frac{g^2 m^2}{32\pi E}, \quad g = g_{12} \quad (5.5)$$

Here and in the following we neglect the mass of ν_1 neutrino, assuming $m_2 \gg m_1$. The energy distributions (normalized to 1/2) of secondary ν_1 and $\bar{\nu}_1$ are respectively:

$$\begin{aligned} W_\nu(\epsilon, E) &= \tau(E) \frac{d\Gamma_\nu(\epsilon, E)}{d\epsilon} = \frac{\epsilon}{E^2} \\ W_{\bar{\nu}}(\epsilon, E) &= \tau(E) \frac{d\Gamma_{\bar{\nu}}(\epsilon, E)}{d\epsilon} = \frac{E - \epsilon}{E^2} \end{aligned} \quad (5.6)$$

where ϵ is the energy of the secondary neutrino and

$$\tau(E) = \tau_0 \frac{E}{m} = [\Gamma_\nu(E) + \Gamma_{\bar{\nu}}(E)]^{-1}, \quad \tau_0 = \frac{16\pi}{g^2 m} \quad (5.7)$$

¹ In our case of Majorana neutrinos we identify the states of neutrino ν and antineutrino $\bar{\nu}$ as states with negative and positive helicities, respectively.

is the ν_2 lifetime. Eqs. (6) show the strong degradation of the final state energy: for $\nu_2 \rightarrow \nu_1 + M$ and $\nu_2 \rightarrow \bar{\nu}_1 + M$ decays, typically 1/3 and 2/3 of the initial neutrino energy E is taken away by the majoron.

The following remark is in order. In some previous papers [48, 100, 102] the decay $\nu_2 \rightarrow \nu_1 + M$ was assumed to be strongly suppressed as compared to $\nu_2 \rightarrow \bar{\nu}_1 + M$, appealing to the approximate lepton number conservation. According to [102] the majoron should carry two units of lepton number, in order to avoid an unacceptably fast $\mu \rightarrow e + M$ decay. In this respect the uniqueness of the triplet majoron model was emphasized, which now is already ruled out by the LEP data.

A more careful analysis shows that in fact there is no straightforward contradiction between these points. The criticism of [102] does not apply to the wide class of the singlet majoron models considered in [96]. The majoron, being the imaginary part of some complex scalar S with two units of lepton number, can not carry a definite lepton number. From the Lagrangean (2) both $\nu_2 \rightarrow \nu_1 + M$ and $\nu_2 \rightarrow \bar{\nu}_1 + M$ decays are allowed and their widths are equal in the limit of massless ν_1 . This can be seen if one considers the decay of ν_2 state with fixed spin s in the rest frame. In this case the decay widths in both helicity states ν_1 and $\bar{\nu}_1$ are equal, but the angular distributions are different: for ν_1 ($\bar{\nu}_1$) it is peaked backward (forward) with respect to s direction. After a Lorentz boost to the lab frame, where $E \gg m$, both ν_1 and $\bar{\nu}_1$ are peaked forward with respect to the momentum of initial ν_2 (at least for $\epsilon > m$). However, due to the above reason, the energy spectrum of the $\bar{\nu}_1$ state is degraded more than that of ν_1 . In other words, in the lab frame the decay amplitudes $\nu_2 \rightarrow \nu_1 + M$ and $\nu_2 \rightarrow \bar{\nu}_1 + M$ are both proportional to m/E , the former due to chirality while the latter due to spin conservation.

The neutrino decay solution requires a large mixing angle ($\theta \gtrsim 45^\circ$) and a short lifetime $\tau \lesssim t_\odot$. Since $E = 10$ MeV is a typical energy of solar neutrinos, relevant for both the Homestake and Kamiokande experiments, in the following we will use the parameter t_\odot/τ_{10} where $\tau_{10} = \tau(10 \text{ MeV})$ is the lifetime of a 10 MeV neutrino. According to (7), this parameter can be written as

$$\frac{t_\odot}{\tau_{10}} = 5 \cdot 10^{-5} \frac{m[\text{eV}]}{\tau_0[\text{s}]} = 1.5 \cdot 10^9 g^2 m^2 [\text{eV}^2]. \quad (5.8)$$

Let us examine now the present bounds on the parameters of the Lagrangean which are relevant for the fast ν decay scenario.

A. Mixing angle. As already mentioned, the observation of the $\bar{\nu}_e$ signal from SN1987A excludes the possibility that ν_e is very close to the heavier unstable eigenstate ν_2 , yielding the limit on the mixing angle: $\theta \leq 50^\circ \div 60^\circ$ [48].

B. Neutrino mass. In the case of large mixing angle θ , the upper bound on $m^2 \simeq \delta m^2$ comes from the absence of $\bar{\nu}_e \rightarrow \bar{\nu}_x$ oscillations at reactors: for $\theta = 45^\circ$ one has $m^2 < 1.6 \cdot 10^{-2} \text{eV}^2$. If $\nu_x = \nu_\mu$ more severe limits ($m^2 < 1.5 \cdot 10^{-3} \text{eV}^2$) can be derived from atmospheric neutrino oscillations (for a recent review see [103]).

C. Majoron coupling constants. The upper bound on the constant g_{ee} coming from the $\beta\beta_{0\nu}$ majoron decay varies between $1.5 \cdot 10^{-4}$ and $3.3 \cdot 10^{-3}$ [104], depending on the evaluation of the nuclear

matrix elements. On the other hand, leptonic decays of K-mesons give the limit $g_{ee}^2 + g_{ex}^2 < 4.5 \cdot 10^{-5}$ [105]. Stronger restrictions are imposed by the SN1987A neutrino observation [11, 46]:

i) the $\nu\nu$ and νM scattering beyond the neutrinosphere will lead to an additional neutrino diffusion, resulting in a significant time spread of the $\bar{\nu}_e$ signal, unless $g_{ij} < 2 \cdot 10^{-3}$ [106];

ii) neutrino scattering off relic neutrinos and majorons in the way from LMC to earth could diminish the $\bar{\nu}_e$ energy spectrum below the observational threshold unless $g_{ij} < 1.4 \cdot 10^{-3}$ [107];

iii) for g_{ij} in the interval $10^{-6} \div 10^{-4}$ the emission of majorons produced in the supernova core due to neutrino annihilation and matter induced decay reduces significantly the duration of the diffusive cooling stage [108, 109]. As a consequence, the ν -signal is shortened and the energies of emitted neutrinos become smaller. Additionally, for the interval $5 \cdot 10^{-6} \div 2 \cdot 10^{-4}$, the effect of matter induced decay ($\bar{\nu}_e \rightarrow \nu_e, \nu_x$) leads to the disappearance of the $\bar{\nu}_e$ signal [109].

By taking into account the above restrictions, the range $10^{-4} \div 10^{-3}$ seems to be allowed for the neutrino-majoron coupling constants g_{ij} and, in particular, for the off-diagonal constant $g = g_{12}$. In fact, in this range majorons are strongly trapped inside the supernova core together with neutrinos and do not affect significantly the diffusive cooling stage. In addition this range is obviously consistent with laboratory restrictions.

We should note, however, that this range of neutrino-majoron coupling constants is not free of criticism. Firstly, in this case, due to the fact that majorons are in equilibrium with neutrinos inside the supernova core, the lepton number symmetry is restored, and the resulting deleptonization of the core [110] makes more difficult to expel the supernova envelope with the prompt shock wave mechanism. Furthermore, in the Early Universe majorons come in equilibrium with neutrinos before the nucleosynthesis epoch and thereby contribute effectively to the cosmological energy density as a 4/7 neutrino species. Thus the effective neutrino number becomes $N_\nu = 3.6$, to be compared with $N_\nu = 3.4$ [111], as derived from the abundance of primordial ${}^4\text{He}$. However, we do not consider these arguments as sharp indications against the quoted range of g_{ij} .

In conclusion, the resulting restrictions on the neutrino lifetime and mixing angle are depicted in Fig. 5.1. The bound on θ comes from the SN1987A neutrino signal, whereas the restriction on t_\odot/τ_{10} is derived as a combination of the astrophysical bound $g < 1.5 \cdot 10^{-3}$ and of the bound on δm^2 (as a function of θ) from $\nu_e \rightarrow \nu_x$ and $\nu_e \rightarrow \nu_\mu$ oscillations [103].

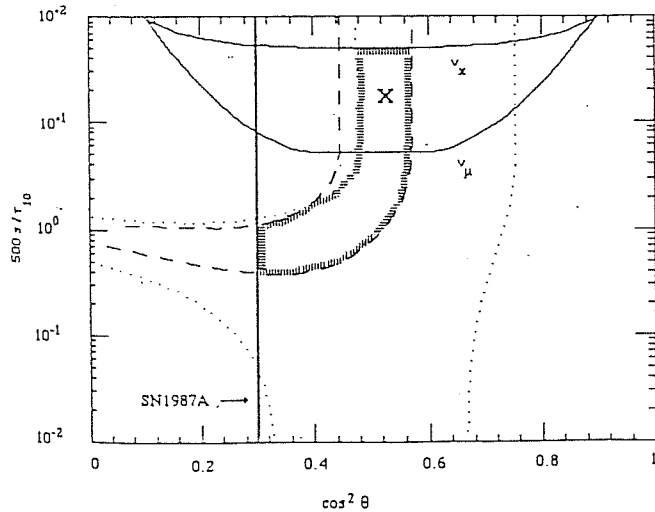


Fig. 5.1. In the plane of mixing angle and neutrino lifetime we present a) the region of $\cos^2 \theta$ excluded by the SN1987A dat (to the left of the solid vertical line); b) the region of τ_{10} excluded for arbitrary ν_x state (above the ν_x line); c) the region of τ_{10} excluded for $\nu_x = \nu_\mu$ (above the ν_μ line); d) the region allowed by the Homestake experiment, at the 2σ level (inside the dashed curve); e) the region allowed by the kamioka experiment, at the 2σ level (inside the dotted curves). The intersection between all constraints is within the shaded area. The subregion excluded for $\nu_x = \nu_\mu$ is denoted by X.

§5.1.2 The Neutrino Decay Solution for SNP Revisited

Let us analyse the fate of a solar ν_e being a mixture $c\nu_1 + s\nu_2$ of the mass eigenstates $\nu_{1,2}$ in the case of fast $\nu_2 \rightarrow \nu_1 (\bar{\nu}_1) + M$ decay. As far as $g^2 \ll 1$, the decay length $16\pi E/g^2 m^2$ is much larger than the oscillation length $4\pi E/m^2$. Therefore, one can average over the ν oscillations. Note that the secondary neutrinos produced in the decay are not coherent with the initial neutrino state. In conclusion, the fluxes of $\nu_e, \nu_x, \bar{\nu}_e, \bar{\nu}_x$ arriving on the earth are respectively:

$$\begin{aligned}\Phi_e(E) &= (c^4 + s^4 e^{-t_0/\tau(E)})\Phi(E) + c^2 s^2 \Phi_I(E) \\ \Phi_x(E) &= s^2 c^2 (1 + e^{-t_0/\tau(E)})\Phi(E) + s^4 \Phi_I(E) \\ \Phi_{\bar{e}}(E) &= s^2 c^2 \Phi_{\bar{I}}(E) \\ \Phi_{\bar{x}}(E) &= s^4 \Phi_{\bar{I}}(E),\end{aligned}\tag{5.9}$$

where $\Phi(E)$ is the differential ν_e flux expected from SSM [3] and $s^2 \Phi_{I,\bar{I}}(E)$ are the fluxes of secondary $\nu_1, \bar{\nu}_1$:

$$\Phi_{I,\bar{I}}(E) = \int_E^{E_{\text{end}}} dE' \Phi(E') [1 - e^{-t_0/\tau(E')}] W_{\nu,\bar{\nu}}(E, E').\tag{5.10}$$

From these equations one can compute the response of any solar neutrino detector as a function of τ_{10} and θ and compare with the experimental data. (The response of detectors sensitive to neutral currents depends also whereas ν_x is an active or sterile neutrino).

The ratio of ^{37}Ar production rate in the Homestake experiment ($N_{Davis} = 2.33 \pm 0.25$ SNU (1σ) [7]) to that expected from the SSM, averaging over the period 1970-1990, is:

$$\langle R_{Ar} \rangle_{70 \div 90} = 0.29 \pm 0.03.\tag{5.11}$$

(Note that the "3 σ " theoretical uncertainty in $N_{SSM} = 7.9 \pm 2.6$ SNU (3σ) [3] is not included in (11)). On the other hand, the signal to expectation ratio for the Kamiokande detector is considerably larger [13]:

$$\langle R_K \rangle_{87 \div 90} = 0.46 \pm 0.05 \pm 0.06.\tag{5.12}$$

We have computed the values of R_{Ar} and R_K as a function of τ_{10} and θ . The results can be represented in the following way:

$$\begin{aligned} R_{Ar} &= c^4 + s^4 F_e + 0.132c^2 s^2 F'_e \\ R_K &= c^4 + s^4 f_e + 0.127c^2 s^2 f'_e + 0.148c^2 s^2 (1 + f_x) Q_x + 0.019s^4 f'_x Q_x. \end{aligned} \quad (5.13)$$

For active (sterile) neutrinos $Q_x = 1(0)$. The functions F_e, f_e, f_x denote the contribution of the ν_2 flux surviving the decay, and F'_e, f'_e, f'_x are the contribution of secondary neutrinos. All these quantities depend on τ_{10} . The numerical values of these functions for different values of τ_{10} are given in Table 5.1.

τ_{10}	F_e	F'_e	f_e	f'_e	f_x	f'_x	G_e	G'_e
$\rightarrow 0$	0	1	0	1	0	1	0	1
500 s	0.28	0.71	0.38	0.55	0.38	0.64	0.07	0.96
1000 s	0.46	0.49	0.62	0.34	0.61	0.40	0.04	0.93
$\rightarrow \infty$	1	0	1	0	1	0	1	0

TABLE 5.1. The quantities F_e, f_e and f_x are the contribution of the ν_e and ν_x components which correspond to the ν_2 flux surviving the decay, for the calculation of the Homestake and Kamiokande signal, see (5.13). F'_e, f'_e and f'_x denote the similar quantities corresponding to secondary neutrinos, see again (5.13). Similarly G_e and G'_e are the contribution to the Ge-signal, see (5.14). τ_{10} is the lifetime of a 10 MeV neutrino.

In a range of parameters we can reconcile both the Homestake and Kamiokande data, provided that ν_x is an active neutrino. In Fig. 5.1 the 2σ contours are shown for both experiments. One can observe a large overlapping region (shaded) within the area allowed by the bounds considered in section 2. (In Figs. 5.2 and 5.3 the 1σ allowed region is also shown).

Some comments are in order:

a) for small lifetime, $\tau_{10} \ll t_\odot$, the signals depend only on the mixing angle θ since all solar ν_2 's decay before reaching the earth. In this regime (vertical branch of the shaded area in Fig. 5.1) the flux of secondary ν_e 's gives almost the same contribution to both experiments and the difference among the signals is provided mainly by the neutral current contribution for Kamiokande, corresponding to $\nu_x(\nu_\mu \text{ or } \nu_\tau)$ flux.

b) For lifetime $\tau_{10} \sim t_\odot$ (horizontal branch of the shaded area) more energetic neutrinos are less suppressed due to the Lorentz factor. This "just so" decay provides the main difference between the signals of these the two detectors due to the different energy thresholds.

c) If ν_x is a sterile neutrino the overlapping area for the two experiments is significantly reduced at the 2σ level (only the horizontal branch remains) and does not exist at 1σ level.

In order to understand the influence of the theoretical uncertainty we repeated the computation by considering 3σ deviations from the central value of the SSM prediction. It turns out that the neutrino decay scenario is incompatible with the data if we take the lower prediction for the flux $\Phi(E)$ (in this case the overlapping between 2σ contours appears in the area forbidden by SN1987A,

$c^2 < 0.3$). On the contrary, with increasing $\Phi(E)$ (at least within the SSM uncertainty) the 2σ allowed area is slightly increasing and the relevant region of parameters is not changed drastically: $\cos^2 \theta \simeq 0.3 \div 0.5$, $\tau_{10} \leq 1000s$.

We also computed the response of Ga-Ge detectors. The result can be expressed as

$$R_{Ge} = c^4 + s^4 G_e + 0.15c^2 s^2 G'_e \quad (5.14)$$

where the functions $G_e^{(j)}(\tau_{10})$ are tabulated in Table 5.1. In Fig. 5.2 the contours corresponding to different ratios of ^{71}Ge production rate with respect to the SSM central value (132 SNU) [3] are shown.

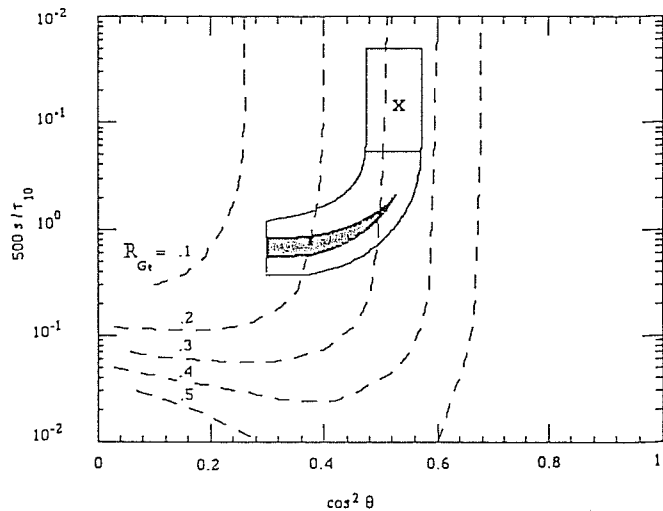


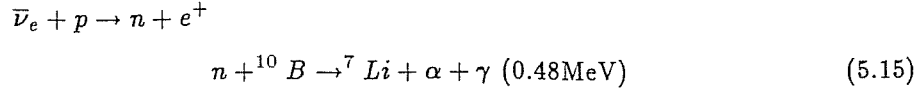
Fig. 5.2. The expectation for Gallium experiments. Isosignal curves corresponding to different values of R_{Ge} are shown. The area relevant for the SNP at 2σ level is within the solid curve. 1σ level region is also shown (shaded). The subregion excluded for $\nu_x = \nu_\mu$ is denoted by X.

Note that in the region of τ_{10} which is relevant for SNP the Germanium signal depends mainly on θ since low energy neutrinos are most important. In correspondence to the shaded area we have $R_{Ge} = 0.15 \div 0.36$. This is compatible with the preliminary results of the SAGE experiment $\langle R_{Ge} \rangle_{90 \div 91} < 72 \text{ SNU}$ (90% *c.l.*) [17].

§5.1.3 Solar Antineutrino Signal and SNP

As we have shown in the previous section, the range of parameters relevant for the solution of SNP corresponds to $c^2 = 0.3 \div 0.6$ and $\tau_{10} < 1000s$. In this case, according to eqs.(9,10), a substantial part ($\sim 10\%$) of solar neutrinos should decay into $\bar{\nu}_e$. The Kamiokande detector is not sensitive to this $\bar{\nu}_e$ flux due to the strong degradation of the energy spectrum (we remind that a secondary $\bar{\nu}_e$ takes typically about 1/3 of the initial neutrino energy). However, the planned low threshold, free

proton rich detectors like Borexino/Borex will be quite sensitive to this $\bar{\nu}_e$'s. The relevant reaction is



The coincidence of e^+ and γ signal provides a unique signature for $\bar{\nu}_e$.

As an example, we consider 100 tons of liquid scintillator corresponding to the fiducial volume of Borexino [41]. In Fig. 5.3 the total number of solar $\bar{\nu}_e$ reactions above the energy cutoff $E = 5$ MeV ($E_+ = 3.7$ MeV for the positron energy) is depicted as a function of θ and τ_{10} . As we see, for the region corresponding to SNP, about $10 \div 30$ interactions per year are predicted. We note that the reactor antineutrino contribution, which is considered as a main source of background, is very low ($\sim 3 \div 5$ reactions per year, see [41] and references therein).

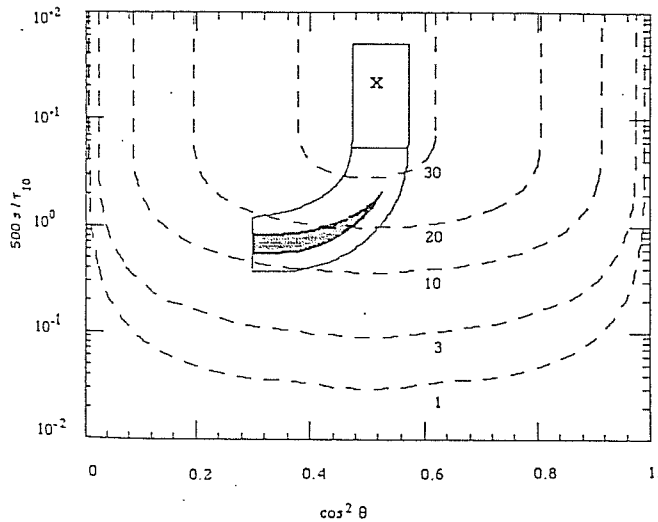


Fig. 5.3. Isosignal curves corresponding to the number of $\bar{\nu}_e + p \rightarrow n + e^+$ interactions per year in Borexino, for a fiducial mass of 100t and positron energy cutoff $E_+ = 3.7$ MeV. The area relevant for the SNP is within the solid line, same notation as in fig. 5.2

The appearance of solar antineutrinos is predicted also in the context of so called hybrid models as a result of the combined effect of resonant oscillations and spin-flavour precession of Majorana neutrinos [29, 99]. Such a possibility was suggested essentially for the explanation of the time variation of the solar neutrino flux in anticorrelation with solar magnetic activity. In this scenario the $\bar{\nu}_e$ energy spectrum should not be significantly altered as compared to the initial solar ν_e spectrum. Due to cancellation between the $\nu_e \rightarrow \nu_\mu \rightarrow \bar{\nu}_e$ and $\nu_e \rightarrow \bar{\nu}_\mu \rightarrow \bar{\nu}_e$ amplitudes, the ratio $\Phi_{\bar{\nu}_e}/\Phi_e$ is predicted at the level of few percents [99]. A rather conservative experimental upper bound, $\Phi_{\bar{\nu}_e}/\Phi_e < 6\%$, was derived from Kamiokande data by assuming that all the background is due to solar $\bar{\nu}_e$'s [44]. This bound could be improved by taking into account conventional background sources [112]. Note however, that $\Phi_{\bar{\nu}_e}/\Phi_e = 1\%$ corresponds to about 30 events/yr for Borexino.

Borexino sensitivity allows to discriminate clearly between these two solution of SNP. In Fig. 5.4 the energy distribution of $\bar{\nu}_e p$ interactions is shown for the antineutrinos from the decay and from the hybrid model, for some values of the parameters. The parameters have been chosen so as to give the same number of events in the two scenarios for a positron energy threshold $E_+ = 3.7$ MeV. The $\bar{\nu}_e$ energy spectra can be clearly discriminated. For comparison, the energy distribution of reactor $\bar{\nu}_e$ interactions is also shown.

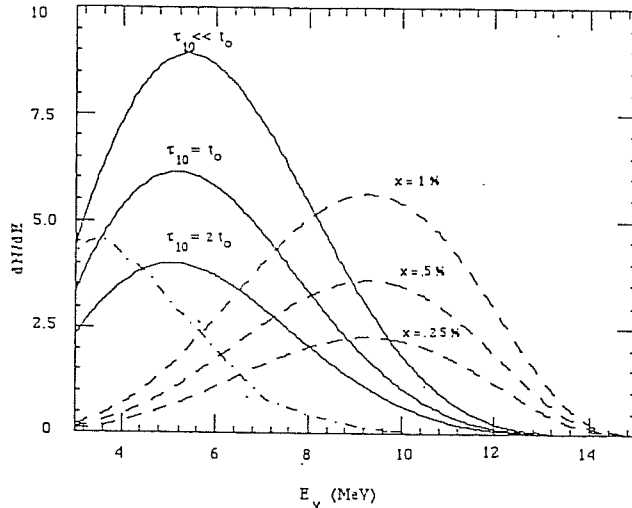


Fig. 5.4. Energy distribution of $\bar{\nu}_e + p \rightarrow n + e^+$ interactions per year in Borexino, for a fiducial mass of $100t$: a) due to reactor background (dot dashed line); b) due to solar $\bar{\nu}_e$ flux for the case that a percentage x of solar neutrinos are converted to $\bar{\nu}_e$ due to magnetic moment transition, dashed lines. Assuming $E_+ = 3.7$ MeV, the total number of interaction is 5 events for a, 32, 21 and 10 events respectively for the three curves in b and same for c.

We would like to remark that another important feature of the hybrid scenario is the prediction of direct correlation of solar $\bar{\nu}_e$ flux with solar activity. However, to establish this correlation large exposition time is required ($\sim 6 \div 10$ years).

Before concluding, the following comment is in order. The hybrid model will not produce $\bar{\nu}_e$ signal if the conservation of some lepton number takes place ($L_{\pm} = L_e \pm L_{\mu} \mp L_{\tau}$) [45]. The same holds for the case of neutrino decay. Even in this situation the decay scenario can be distinguished by other ones by looking at neutral current signals. The point is that, due to energy degradation of secondary neutrinos, one has a significantly weaker (by at least a factor two) neutral current signal, as compared to the oscillations and magnetic moment transition scenarios.

§5.1.4 Other Mechanisms of Solar Antineutrino Production

The study of solar $\bar{\nu}_e$'s can be of interest also independently of the solar neutrino deficit. In this spirit we discuss briefly some mechanisms of solar $\bar{\nu}_e$ production.

The 17 KeV Neutrino decay. If the 17 KeV neutrino [97] exists, it should be unavoidably produced in the sun with flux about 1% of Φ . If its lifetime is $\tau_0 < 1s$, the solar ν_{17} , according to (7), have to decay before reaching earth. The decay channel $\nu_{17} \rightarrow \bar{\nu}_e + M$ can occur, if it is not forbidden by conservation of lepton number $L_- = L_e - L_\mu + L_\tau$ as in popular models [88, 113]. Due to the small mixing angle ($\sin \theta \sim 0.1$) the response of Borexino to this signal should be weak: less than 1.5 events per year for $E_+ \geq 3.7$ MeV. For the cutoff $E_+ = 6$ MeV the signal to background ratio becomes one, however one expects less than one event per year. Due to small statistics, Borexino will not be able to discriminate the signal from background. However, the planned 2000 t Borex detector could observe such a signal and discriminate it from the background.

Similar considerations hold true for any heavy majorana neutrino and small mixing angle ($\sin^2 2\theta < 0.14$ [103]).

MSW catalized decay [100]. In the case of small mixing angle θ , i.e. $\nu_2 \simeq \nu_x$ and $\nu_1 \simeq \nu_e$, and small mass ($\delta m^2 \simeq m^2 \leq 10^{-4} \text{ eV}^2$), a flux of solar $\bar{\nu}_e$ could be produced via a MSW transition $\nu_e \rightarrow \nu_2$ and forthcoming decay $\nu_2 \rightarrow \bar{\nu}_e + M$, in the flight from sun to earth. In this case the $\bar{\nu}_e$ flux does not exceed $1/2(1 - R_{Ar})c^2\Phi_{\bar{\nu}_e}(E)$, where $\Phi_{\bar{\nu}_e}(E)$ is given in equation (10). This value is smaller than that given in [100] due to the fact that the branching ratio for $\nu_2 \rightarrow \bar{\nu}_e + M$ is 1/2, see section 2.

In this case, due to the restrictions on m and g , we have that $\tau_{10} > 3t_\odot$, which corresponds at most to 10 events per year in Borexino.

Matter induced neutrino decay [47]. In the inner part of the sun, the direct decay $\nu_e \rightarrow \bar{\nu}_e + M$ can occur due to matter induced level splitting, even in the absence of non diagonal neutrino coupling. For $g_{ee} = 1.5 \cdot 10^{-3}$ we get that a conversion probability of about 0.25%. In the case of small neutrino masses, the $\bar{\nu}_e$ spectrum is degraded as in the case of decay in vacuum, see eqs. (6). However, if the neutrino mass is larger than the effective mass splitting induced by coherent interaction with matter, the energy spectrum is not degraded and essentially repeats the spectrum of solar neutrinos. In the latter case, again for $g_{ee} = 1.5 \cdot 10^{-3}$ we get about 10 events per year in Borexino.

We finally would like to remark just two points of the above discussion:

- i) The neutrino decay solution of the solar neutrino problem can be definitely tested by future real time, low threshold solar neutrino detectors like Borexino/Borex;
- ii) also independently of the solar neutrino problem, the detection of neutrino decay with majoron emission is feasible. If successful it will be of major relevance for particle physics, establishing the idea of the spontaneous lepton number violation.

§5.2 Matter Induced Neutrino Decay and Solar Antineutrinos

As we have already discussed matter effects can be crucial for neutrino properties. It was shown in [47] that the presence of dense matter can drastically change the neutrino decay properties as well. For example in the simplest majoron models [92, 93], where all neutrinos have the same lepton

numbers, the majoron has only diagonal tree-level couplings with neutrinos [114], so that no neutrino decay occurs in vacuum with emission of the majoron. However, matter can induce the decay. The point is that the coherent interaction with the medium leads to an energy splitting between ν and $\bar{\nu}$ states, providing available phase space for the emission of the majoron χ through the decay either $\nu \rightarrow \nu' + \chi$ or $\nu \rightarrow \bar{\nu}' + \chi$, depending on the neutrino type and on the chemical content of matter [47]. In the general case, when neutrino mixing is non-vanishing, i.e. the flavour and the mass eigenstate are not the same, the diagonal (e.g. $\nu_e \rightarrow \bar{\nu}_e + \chi$) as well as non-diagonal (e. g. $\nu_e \rightarrow \bar{\nu}_\mu + \chi$) can occur. The properties of the ν decay in matter and its astrophysical implications were investigated in a number of papers [109, 115]. It was first emphasized in [47], that the sun can be a potential source of antineutrinos which could appear due to the decay of solar neutrino in vacuum [94] during the flight from sun to earth or due to the matter induced decay in the sun. The matter induced decay $\nu_e \rightarrow \bar{\nu}_x + \chi$ ($x = e, \mu, \dots$) is excluded to be a solution of the SNP because of the laboratory constraints on the majoron couplings. Nevertheless, the study of matter induced solar neutrino decay is interesting as a mean of investigating neutrino properties. This is really the spirit of this paper.

This solar $\bar{\nu}_e$ flux could be, in principle, detected and studied in future large volume solar neutrino detectors like Borex and Super Kamiokande. The matter induced decay of neutrinos, at least in principle, can be distinguished from other possible sources of solar $\bar{\nu}_e$'s. These are the decay in vacuum [47, 48, 49], and the resonant spin-flavour precession of Majorana neutrinos due to the off diagonal magnetic moment (provided the oscillation also occur) [99]. Spin-flavour precession does not alter significantly the ν_e energy spectrum (the solar $\bar{\nu}_e$ spectrum essentially reproduces the one for the ν_e 's) which, on the contrary, is degraded for the case of the decay. On the other hand, the matter decay, in principle, can be discriminated from the decay in vacuum due the unusual energy dependence of the decay probability which does not depend on the energy in the laboratory frame or even increase with energy, whereas the opposite occurs for the vacuum decay, where $\Gamma(E) \sim E^{-1}$. The paper is organized as follows. In sect. 1 we reexamine in some detail the dynamics of matter-induced decay for the cases of Majorana, Zeldovich-Konopinsky-mahmound and Dirac neutrinos. Then we study the effect of such decays for solar neutrinos (sect. 2) and discuss the possibility of the detection of the resulting $\bar{\nu}_e$ flux in the future underground detectors (sect. 4). Finally, in sect. 5 we draw our conclusions.

§5.2.1 Dynamics of Matter Induced Decay

Let us consider the propagation of neutrinos in matter. For the sake of definiteness we take the electron neutrino. The ν_e state is identified with the left-handed Weyl spinor, $\nu_e \equiv \nu_{eL}$, whereas the right-handed component can be specified as

- (a) electron antineutrino state: $\nu_R = C\bar{\nu}_{eL}^T$ (Majorana neutrino);
- (b) muon antineutrino state: $\nu_R = C\bar{\nu}_{\mu L}^T$ (ZKM neutrino) [77];
- (c) sterile state: $\nu_R = C\bar{\nu}_{sL}^T$ (Dirac neutrino).

In the majoron picture the neutrino mass appears due to the spontaneous violation of some lepton number symmetry, which is L_e for the case (a), $L_e + L_\mu$ for the case (b) and $L_e + L_s$ for the case (c). For the case (b) and (c), the symmetry violation occurs as $U(1)_e \oplus U(1)_\mu \rightarrow U(1)_{e-\mu}$ and $U(1)_e \oplus U(1)_s \rightarrow U(1)_{e-s}$ respectively, keeping $L_e - L_\mu$ and $L_e - L_s$ conserved.

As a consequence of this symmetry breaking, a Goldstone boson χ , called majoron, * appears. Its Yukawa coupling constant has to be $h = m/v$, where $\langle \sigma \rangle = v/\sqrt{2}$ is the non zero vacuum expectation value of some complex scalar field σ , violating the relevant lepton number symmetry. In order that the effects of χ - ν interaction are observable, a large enough coupling constant h is needed. Although the popular candidate for such a strong coupling, a triplet majoron model [92], is already ruled out by LEP data, a variety of singlet majoron models was suggested in which h can be as large as $10^{-2} \div 10^{-3}$ [96]. The interaction of neutrinos with the majoron cannot obviously provide the transition $\nu_L \rightarrow \nu_R \chi$ in vacuum due to vanishing phase space: ν_L and ν_R are two components of a massive four-component spinor $\nu \equiv \nu_L \oplus \nu_R$. However the background of dense matter, being CP asymmetric, distinguishes these two components and the decay becomes allowed.

The lagrangean relevant for the neutrino propagation and decay in matter has the form:

$$\mathcal{L} = \bar{\nu}_L(i\partial_\mu - \mathcal{V}_\mu^L)\gamma^\mu\nu_L + \bar{\nu}_R(i\partial_\mu - \mathcal{V}_\mu^R)\gamma^\mu\nu_R - m(\bar{\nu}_L\nu_R + \bar{\nu}_R\nu_L) + \frac{i}{2}h\chi(\bar{\nu}_L\nu_R - \bar{\nu}_R\nu_L) \quad (5.16)$$

where m is the neutrino mass, χ is the majoron field, \mathcal{V}_μ^L is the potential arising from the coherent forward scattering of ν_e off the matter constituents, and \mathcal{V}_μ^R is the same for the ν_R component. In the contest of the standard $SU(2) \otimes U(1)$ model, these potentials, in the rest frame of matter, take the form:

$$\mathcal{V}_\mu^L = \delta_{0\mu}\sqrt{2}G_F(n_e - n_n/2), \quad (5.17)$$

(where G_F is the Fermi constant, $n_{e,n}$ are the number density of electrons and neutrons respectively), and

$$\mathcal{V}_\mu^R = -\mathcal{V}_\mu^L \quad (5.18a)$$

in the case (a)

$$\mathcal{V}_\mu^R = \delta_{0\mu}\frac{1}{\sqrt{2}}G_F n_n, \quad (5.18b)$$

in the case (b) and

$$\mathcal{V}_\mu^R = 0 \quad (5.18c)$$

in the case (c).

Due to the presence of these potentials $\mathcal{V}_\mu^R \neq \mathcal{V}_\mu^L$, the dispersion relations for the propagation of the two helicity components L and R are different: **

$$p_0^2 = m^2 + \mathbf{p}^2 + 2\mathcal{V}^{L,R} |\mathbf{p}| + (\mathcal{V}^{L,R})^2 \quad (5.19)$$

* Actually the name majoron corresponds only to the case (a). The Goldstone boson of (b) in [113] was called flavon and the one of (c) diron [47].

** For ultrarelativistic neutrinos the + and - helicity states can be identified with ν_R and ν_L , so in the following we keep this notation.

Thereby a phase space for the decay either $\nu_L \rightarrow \chi + \nu_R$ or $\nu_R \rightarrow \chi + \nu_L$ is non vanishing (depending on whether $\nu^L > \nu^R$ or $\nu^R > \nu^L$), due to a non-zero energy level splitting. Formally the (5.19) means that in matter neutrinos acquire an additional (though somehow dependent on the momentum) mass term, so that the effective masses for ν_L and ν_R states are [109]:

$$(m_{L,R}^2)_{eff} = m^2 + 2\nu^{L,R} |\mathbf{p}|. \quad (5.20)$$

Let us assume that $\nu^L > \nu^R$. Then for $|\mathbf{p}| \gg \nu$, m the squared matrix element for the decay $\nu_L \rightarrow \chi + \nu_R$ is

$$|A(p, q)|^2 = \hbar^2 |\mathbf{p}| |\mathbf{q}| (1 - \cos \theta), \quad (5.21)$$

where \mathbf{p} and \mathbf{q} are the four-momenta of ν_L and ν_R respectively, and θ is the angle between \mathbf{p} and \mathbf{q} in the laboratory frame. The expression (5.21) coincides with the one for the non diagonal decay with helicity flipping in vacuum. Then the differential decay rate in the laboratory frame is:

$$\frac{d\Gamma(p_0, q_0)}{dq_0} = \frac{\hbar^2 m^2}{16\pi p_0^2} \left(1 - \frac{q_0}{p_0}\right) \left(\delta + 1 - \frac{p_0}{q_0}\right), \quad (5.22)$$

where

$$\delta = \frac{\Delta m_{eff}^2}{m^2} = \frac{2\Delta\nu |\mathbf{p}|}{m^2}, \quad \Delta\nu = (\nu^L - \nu^R), \quad (5.23)$$

is the parameter which characterize the phase space. The energy q_0 of the emitted ν_R is in the range:

$$\frac{p_0}{1 + \delta} \leq q_0 \leq p_0 \quad (5.24)$$

Then for the decay probability per unit length we obtain [115]:

$$\Gamma(p_0) = \frac{\hbar^2}{16\pi} \Delta\nu \left[\left(\frac{2 + \delta}{1 + \delta}\right) - \frac{2}{\delta} \ln(1 + \delta) \right]. \quad (5.25)$$

The energy distribution of the secondary ν_R ,

$$W(p_0, q_0) = \frac{1}{\Gamma(p_0)} \frac{d\Gamma(p_0, q_0)}{dq_0}, \quad (5.26)$$

is plotted on Fig. 5.5 for distinct values of δ .

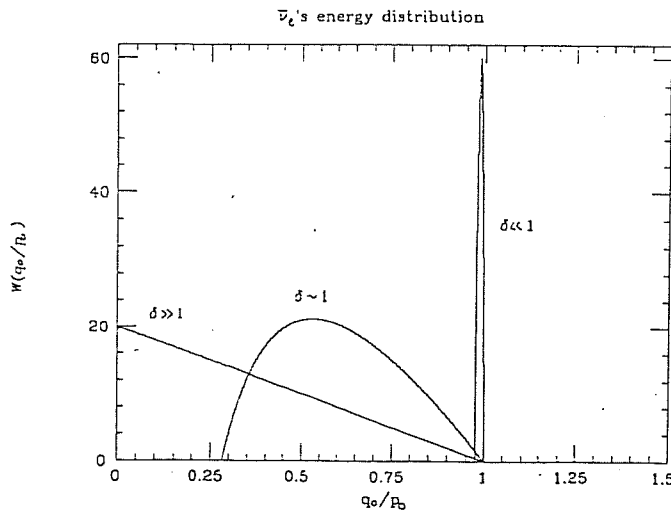


Fig. 5.5. The $\bar{\nu}$ energy distributions $W(p_0, q_0)$ due to the matter induced decay $\nu \rightarrow \bar{\nu} + \chi$ for different values of δ .

The magnitude of the parameter is clearly crucial. Considering the matter density as fixed it is interesting to distinguish different regimes

i) The "small mass" regime, $\delta \gg 1$, in which case the phase space is maximal. From a kinematical point of view this is the most profitable regime for the decay. We have

$$\Gamma(p_0) = \Gamma_0 \equiv \frac{h^2}{16\pi} \Delta \mathcal{V}. \quad (5.27a)$$

The energies of the secondary ν_R are strongly degraded: $\langle q_0 \rangle = \frac{1}{3}p_0$ (as well as in the case of vacuum decay $\nu_2 \bar{\nu}_1 + \chi$, with $m_2 \gg m_1$), since the bulk of energy is taken away from the majoron. Notice, that (5.27a) does not depend [47] on the parent neutrino energy p_0 , as distinguished from the case of decay in vacuum ($\Gamma_{vac} \sim p_0^{-1}$).

ii) The intermediate regime $\delta \sim 1$. In this case the energy of secondary ν_R is less degraded, but the decay probability is smaller. E. g. for $\delta = 1$ we have

$$\Gamma(p_0) \approx \frac{1}{9} \Gamma_0 \quad (5.27b)$$

iii) The "large mass" regime $\delta \ll 1$. In this case the energy of secondary ν_R is not essentially degraded $q_0 \simeq p_0$. However, the decay probability is substantially decreased:

$$\Gamma(p_0) = \frac{\delta^2}{3} \Gamma_0 = \frac{h^2 \Delta \mathcal{V}^3 p_0^2}{12\pi m^4} \quad (5.27c)$$

which clearly shows the unusual energy dependence: $\Gamma(p_0)$ is increased with neutrino energy. The angular distribution of ν_R is also of some interest, due to the peculiar properties of the decay. Due to the kinematical relativistic effect the angular distribution is sharply peaked forward, although the extremely forward direction $\cos \theta = 1$ is not allowed due to the conservation of angular momentum. The momentum of the final ν_R depends on the angle as follows:

$$|\mathbf{q}| = |\mathbf{q}'| \frac{1 + \frac{\delta}{2} \left(1 + \sqrt{1 - \frac{8p_0^2(1-\cos\theta)}{m^2\delta^2}}\right)}{1 + \delta + \frac{m^2\delta^2(1-\cos\theta)}{2\Delta\mathcal{V}^2}}, \quad (5.28a)$$

where the angle is constrained by

$$1 - \frac{m^2\delta^2}{8p_0^2} \leq \cos \theta \leq 1. \quad (5.28b)$$

From (5.28) we derive the angular distributions for the above regimes. For $\delta \gg 1$ we get

$$\frac{d\Gamma}{d\cos\theta} \simeq \frac{h^2 p_0^2 \Delta \mathcal{V}^2}{16\pi} \frac{1 - \cos\theta}{[p_0(1 - \cos\theta) + \Delta \mathcal{V}]^3}, \quad (5.29a)$$

which has a sharp maximum for $\cos \theta \simeq 1 - (\Delta \mathcal{V}/2p_0)$ (cf. [109]). In the opposite regime, $\delta \ll 1$ the momentum of the secondary ν_R is practically the same as that of the parent ν_L . We find:

$$\frac{d\Gamma}{d\cos\theta} \simeq \frac{h^2 p_0^2}{16\pi} \frac{1 - \cos\theta}{[\Delta \mathcal{V}^2 - 2m^2(1 - \cos\theta)]^{1/2}}. \quad (5.29b)$$

This distribution reaches the maximum at the lower extreme: $\cos\theta = 1 - 2(\Delta\mathcal{V}/2m)^2 < 1 - (\Delta\mathcal{V}/2/p_0)$.

The extremely forward peaked angular distribution makes the picture of matter induced decay self-consistent. In fact, the decay $\nu_L \rightarrow \nu_R + \chi$ can be treated as a coherent majoron production due to the neutrino scattering off matter components: $\nu_L + X \rightarrow \nu_R + X + \chi$ ($X = e, p, n$). This implies that the coherence length $r_{coh} \sim 1/p_0\theta^2$ is larger (or, at least of the same order order) than the refraction length $l_0 = 2\pi/\mathcal{V}$ [25], which is obviously the case since $\theta^2 l \Delta\mathcal{V}/p_0$.

§5.2.2 Neutrino Decay in Solar Medium

In view of discussing the potential detection of $\bar{\nu}_e$ flux produced in the solar interior, in what follows we shall mainly devote our attention to the matter induced decay $\nu_e \rightarrow \bar{\nu}_e + \chi$. The discussion can be straightforwardly extended to the other possible decays, $\nu_e \rightarrow \bar{\nu}_\mu$ or $\nu_e \rightarrow \bar{\nu}_s$. Now we consider the case in which neutrino propagates in a matter with varying density, as it takes place in the sun.

The full decay probability for a neutrino with energy p_0 , passing the sun from its center ($r = 0$) to the surface ($r = R$), is obtained taking into account the dependence of the potential $\mathcal{V}^{L,R} = \mathcal{V}^{L,R}(r)$ on the space coordinate r :

$$P(p_0) = \int_0^R dr \int_{q_0^{\min}}^{p_0} dq_0 \frac{d\Gamma}{dq_0}(r, p_0, q_0), \quad (5.30)$$

with $q_0^{\min} = \frac{p_0}{1+\delta(0)}$, where $\delta(0)$ is the value of δ at $r = 0$. For the most profitable case $\delta(r) > 1$, the probability of the decay $\nu_e \rightarrow \bar{\nu}_e + \chi$ can be rewritten as [109]:

$$P(p_0) = \frac{h_{ee}^2 d_{eff}}{4d_0}, \quad (5.31)$$

where $d_{eff} = m_n \int_0^R (n_e - \frac{1}{2}n_n) dr$ is the effective width of the matter traversed by the neutrinos, m_n is the nucleon mass and $d_0 = \sqrt{2}\pi G_F^{-1} m_n \equiv 1.6 \times 10^9 \text{g/cm}^2$ is the refraction width. As far as d_{eff} is a global characteristic of the sun, the possible value of P depends only on the majoron coupling constant. Concerning the existing bounds on the majoron coupling, we recall that

$$h_{ee} \leq 1.5 \times 10^{-4} \div 3.3 \times 10^{-3} \quad (5.32a)$$

$$\sum_x h_{ex}^2 \leq 4.5 \cdot 10^{-5} \quad (5.32b)$$

($x = e, \mu, \tau$ or s). Equation (5.32a), originated * from non observation of neutrinoless 2β decay with majoron emission [104], is relevant for the case (a) of Majorana neutrino. Equation (5.32b),

* This limit contain uncertainty of nuclear matrix elements of $2\beta_{0\nu}$ decay. The values shown in (5.32a) correspond to two ultimate estimations of matrix elements, given in [116] and [117] respectively.

derived from the limits on $\pi \rightarrow e\nu\chi$ and $K \rightarrow e\nu\chi$ decays [105], applies to the case (b) and (c) with $\nu_x = \nu_\mu, \nu_\tau$ and ν_s respectively.

Somewhat more stringent constraint follows from astrophysics. Namely, the observation of SN 1987A neutrino signal sets the bound: $h_{ee}, h_{ex} \leq 1.3 \times 10^{-3}$ [106, 107]. Bearing in mind this limit, in the following we will however base our conservative estimate on more direct laboratory limits (5.32a), (5.32b).

Just to get some numerical insight, it is useful to note that one has $\delta \approx 1$ in the solar core ($2\nu^L \approx 6 \times 10^{-12}$ eV) for $m \approx 10^{-2}$ eV, and $p_0 \approx 10$ MeV. Therefore, since the bulk of the decay of boron neutrinos occurs in the solar core, the small mass regime ($\delta \gg 1$) corresponds to $m \ll 10^{-2}$ eV. In the opposite case, $m \gg 10^{-2}$ eV we have the large mass regime ($\delta \ll 1$) for the solar interior.

We have calculated the decay probability P as a function of m^2/p_0 see Fig. 5.6. The profiles of electron and neutron densities in the sun are taken from [3].

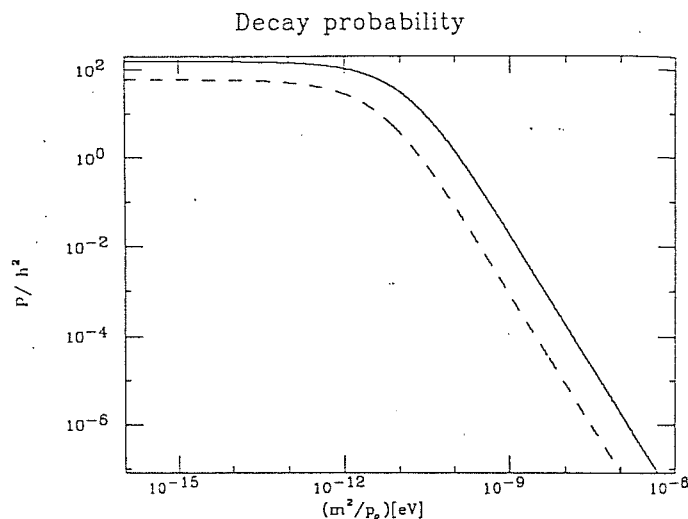


Fig. 5.6. The value of P/h_{ee}^2 for the decay $\nu_e \rightarrow \bar{\nu}_e + \chi$ (solid line) into the sun and $P/h_{e\mu}^2$ for the case $\nu_e \rightarrow \bar{\nu}_\mu + \chi$ (dashed line) versus the ratio m^2/p_0

The two cases are clearly distinguishable. For small m^2/p_0 values ($\delta \gg 1$), there is practically no dependence on the energy: $P/h_{ee}^2 \simeq 160$, whereas P is sharply decreasing with increasing energy m^2/p_0 in the regime $\delta \ll 1$. The numerical values for P (see Table 5.2) are obtained by taking h_{ee} at the maximal allowed value in (5.32a) and $p_0 \approx 10$ MeV.

m (eV)	P	$\Phi(\text{cm}^{-2}\text{s}^{-1})$	$\langle q_0 \rangle$	$N(3.7)$	$N(6.2)$	$N(7.2)$
10^{-4}	$2 \cdot 10^{-3}$	$9 \cdot 10^3$	2.5	4.4	1.7	1.0
10^{-2}	$3 \cdot 10^{-4}$	$1.3 \cdot 10^3$	5.2	3.0	1.4	0.8
$3 \cdot 10^{-2}$	$1 \cdot 10^{-5}$	55	7.7	0.4	0.3	0.2
$5 \cdot 10^{-2}$	$2 \cdot 10^{-6}$	8.4	8.2	$6.6 \cdot 10^{-2}$	$6 \cdot 10^{-2}$	$5 \cdot 10^{-2}$
10^{-1}	$2 \cdot 10^{-7}$	$6 \cdot 10^{-1}$	8.5	$5 \cdot 10^{-3}$	$4.4 \cdot 10^{-3}$	$4 \cdot 10^{-3}$

TABLE 5.2 Numerical estimates for the decay $\nu_e \rightarrow \bar{\nu}_e + \chi$. Assuming $h = 3.3 \cdot 10^{-3}$, we display for

different values of the neutrino mass: 1) The decay probability P for Boron neutrinos; 2) The total $\bar{\nu}_e$ flux Φ originated by the decay of Boron neutrinos (cf. $\Phi_{\text{ssm}} = 5.6 \cdot 10^6 \text{cm}^{-2} \text{sec}^{-1}$); 3) the average energy $\langle q_0 \rangle$ of $\bar{\nu}_e$'s in MeVs (cf. $\langle p_0 \rangle_{\text{ssm}} = 6.7$ MeV for Boron neutrinos). 4) The number N of positron events per year in 1000t fiducial mass of Borex, for different positron energy thresholds $E_{th} = 3.7, 6.2$ and 7.2 MeV (cf. the number of events from reactor background : 30, 2.3 and 0.1 respectively).

As we see in the most profitable regime in which matter effect is dominant ($m \ll 10^{-2}$ eV) about one or two of thousand solar ν_e 's can decay into $\bar{\nu}_e$ and χ . The case $m \simeq 10^{-2}$ eV ($\delta \simeq 1$) can be regarded as a transition regime and, it comes out, together with the small mass regime, to be relevant for solar $\bar{\nu}_e$ detection. The case of large masses ($m \gg 10^{-2}$ eV) is hopeless for $\bar{\nu}_e$ search due to the extremely small decay probability:

$$P(p_0) = \frac{h^2 p_0^2}{12\pi m^4} \int_0^R \Delta V^3 dr. \quad (5.33)$$

According to (5.31) and (5.27), the differential flux $\Phi(q_0) = d\Phi/dq_0$ of $\bar{\nu}_e$'s, resulting from the decay $\nu_e \rightarrow \bar{\nu}_e + \chi$ for the case $\delta \gg 1$ is:

$$\Phi(q_0) = \frac{h_{ee}^2 d_{\text{eff}}}{4d_0} \int_{q_0} \Phi_{\text{ssm}}(p_0) \left(1 - \frac{q_0}{p_0} \frac{dp_0}{p_0}\right), \quad (5.34)$$

where $\Phi_{\text{ssm}}(p_0)$ is the differential flux of ν_e 's expected from the Standard Solar Model [3]. The spectrum of antineutrinos appears to be strongly degraded at high energies: $\langle q_0 \rangle \simeq \frac{1}{3} \langle p_0 \rangle$. For the case $\delta \sim 1$ the $\bar{\nu}_e$ energy is not degraded practically (see Table 1): $\langle q_0 \rangle \simeq \langle p_0 \rangle$. In the limit of large mass, $\delta \ll 1$, we have

$$\Phi(q_0) \approx P(q_0) \Phi_{\text{ssm}}(q_0), \quad (5.35)$$

due to the unusual energy dependence of the decay probability (P increase with p_0 see (5.33)), the antineutrino spectrum is shifted towards higher energies so that the average energy $\langle q_0 \rangle$ is larger than the average energy $\langle p_0 \rangle$ of solar neutrinos. From (5.26c) and (5.35) one has:

$$\langle q_0 \rangle = \frac{\int_{q_0} dq_0 \cdot q_0 \Phi(q_0)}{\int_{q_0} dq_0 \Phi(q_0)} \approx \frac{\langle p_0^3 \rangle}{\langle p_0^2 \rangle} > \langle p_0 \rangle \quad (5.36)$$

Unfortunately there is practically no hope to observe this interesting effect, due to the extremely small decay probability in this regime (see Table 1).

In Fig. 5.7, the energy spectra of electron antineutrinos are plotted for different values of the mass, by considering the decay of ^8B neutrinos which are the only ones having energies high enough ($E \sim 10$ MeV) to make feasible the detection of solar $\bar{\nu}_e$'s.

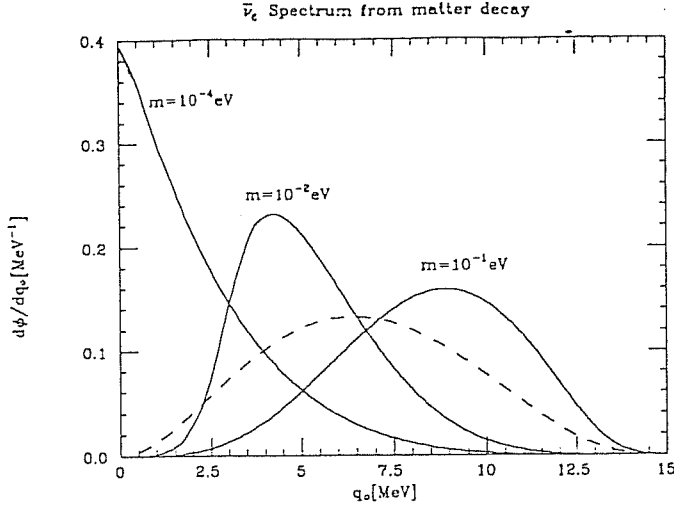


Fig. 5.7. The differential energy spectra of solar $\bar{\nu}_e$ flux produced due to matter-induced decay $\nu_e \rightarrow \bar{\nu}_e + \chi$ of the ^8B neutrinos for the three different regimes (solid lines). Notice that, in the case $m \ll 10^{-2}$ eV, the spectrum is strongly degraded compared to the "parent" spectrum of solar ^8B neutrinos (dashed lines), whereas for $m \gg 10^{-2}$ eV it is even enhanced to higher energies, since, in this regime, the more energetic neutrinos are decaying faster, quite the opposite to the case of decay in vacuum. All the spectra are normalized to unity.

In the above analysis we have confined ourselves only to the $\nu_e \rightarrow \bar{\nu}_e + \chi$ decay. Everything holds true for the $\nu_e \rightarrow \bar{\nu}_x + \chi$ decays as well ($x = \mu, \tau, s$), provided there is some conserved lepton number $L_e - L_x$. The antineutrinos appear not to be $\bar{\nu}_e$ if the lepton number $L_e - L_x$ is exact. This symmetry however, can be broken explicitly by Planck scale effects, leading to the mass splitting $\Delta m \simeq 10^{-6}$ eV between the two components [51, 118]. Then the $\bar{\nu}_x \rightarrow \bar{\nu}_e$ oscillations come into the game creating a $\bar{\nu}_e$ signal for the terrestrial detectors. Therefore, after the $\nu_e \rightarrow \bar{\nu}_x + \chi$ decay in the sun, in average a half of the produced $\bar{\nu}_x$ will oscillate into $\bar{\nu}_e$. (Notice, that for $m > 10^{-5}$ eV the neutrino mixing angle is practically 45° and the oscillation length $L_{osc} = 2\pi E/m\Delta m$ for Boron neutrinos is less than the sun-earth distance). The probability $P_{e\mu}$ of $\nu_e \rightarrow \bar{\nu}_{\mu(\tau)} + \chi$ for the sun density profiles is also shown on Fig. 5.6 (the probability of $\nu_e \rightarrow \bar{\nu}_x + \chi$ decay is practically the same). The $\bar{\nu}_e$ energy spectra are the same as that of Fig. 5.7.

§5.2.3 Antineutrino signal

Now we can discuss the possibility of detecting the electron antineutrino flux in future large volume real time detectors. The relevant reaction is the inverse β decay $\bar{\nu}_e + p \rightarrow n + e^+$. The spectrum of

positron events occurring in a detector is given by:

$$\frac{dN}{dE} = TN_p \Phi(E) \sigma(\bar{\nu}_e + p \rightarrow n + e^+), \quad (5.37)$$

where $E = q_0 - m_p + m_n$ is the positron energy, N_p is the free proton number contained in the fiducial volume, T is the detection time and $\sigma(\bar{\nu}_e + p \rightarrow n + e^+) \approx 9.2 \cdot 10^{-4} E^2 \text{ cm}^2$. The spectra of positrons are shown in Fig. 5.8 for distinct masses of neutrino.

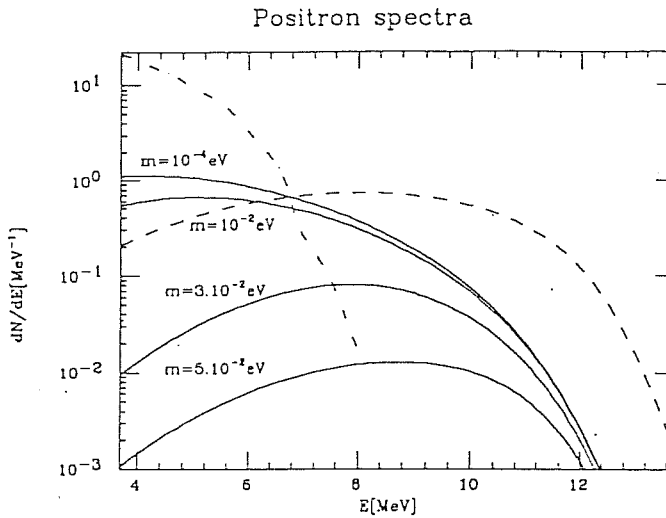


Fig. 5.8. We present the positron spectra resulting from $\bar{\nu}_e + p \rightarrow n + e^+$ interactions, for antineutrinos originated from matter induced $\nu_e \rightarrow \bar{\nu}_e + \chi$ decay, for different values of neutrino masses (solid lines). The background due to the reactor $\bar{\nu}_e$'s is given by the dot-dashed line. For the sake of comparison the positron spectra from $\bar{\nu}_e$'s due to spin-flavour precession is also given (dashed line). The $\bar{\nu}_e$ spectrum for the ν_e decay in vacuum is practically the same as that of matter-induced decay for $m < 10^{-4} \text{ eV}$. All the spectra are normalized to unity.

From this figure we see that there is at least in principle, some chance to discriminate from the alternative mechanisms of solar $\bar{\nu}_e$ production, as are the decay in vacuum [47, 48] and spin-flavour precession [29], provided high statistic and detection sensitivity are available. However, experimentally the situation is quite difficult and this can be understood by looking at the total number of detectable events N for one year running of 1000 t of Borex detector [41], for different energy thresholds E_{th} of positron energy. The results are displayed in Table 1, where the maximal upper bound of (5.33a) is assumed $h_{ee} = 3.3 \cdot 10^{-3}$. We see that the number of events depends crucially on the neutrino mass: only the regime of small masses $\leq 10^{-2} \text{ eV}$ could be relevant.

Constraints on the positron energy threshold arise, at least, from the presence of spurious terrestrial antineutrinos. The flux of antineutrinos due to the terrestrial radioactivity [119, 120] extends up to $E_{th} = 3.3 \text{ MeV}$ and it is about $10^7/(\text{cm}^2\text{s})$ that is some order of magnitude larger than the solar $\bar{\nu}_e$'s, which we may expect (see Table 1). Moreover, we must also take into account the external background due to nearby nuclear power reactors. It is estimated to be about 20-30

events/yr [121] for $E_{th} = 3.3$ MeV, in a 1000 t of fiducial volume of Borex detector [41], planned to be located at Gran Sasso, which few times exceeds the possible solar $\bar{\nu}_e$ signal. The reactor spectrum ends at $q_0 \simeq 10$ MeV so that one is forced to take higher thresholds. As we see from Table 1, the threshold $E_{th} > 6-7$ MeV could be enough to exceed the background. The background can also come from diffuse supernova neutrinos or from atmospheric neutrinos, which, in the energy range 10-15 MeV, can be estimated to be at the level of $N \sim 10^{-2}$ [120] which is less than the possible signal. Notice, that for $m > 10^{-2}$ eV the distributions of events reaches its maximum beyond the threshold. In the case of high statistics this could distinguish the matter-induced neutrino decay from the decay in vacuum. The spectrum in the latter case is essentially the same as the one of the matter decay in the small mass regime: $m \ll 10^{-2}$ eV. However, the extremely small rate of positron events (about one per year) is too small to be reliable for the identification of matter induced $\nu_e \rightarrow \bar{\nu}_e + \chi$ decay.

We have performed our calculations using the maximal allowed value $h_{ee} = 3.3 \cdot 10^{-3}$, which is not in fact too conservative from the present point of view. For the more reliable bound $h_{ee} < 10^{-4}$, the $\bar{\nu}_e$ signal would be two orders of magnitude less and therefore hopeless for the detection in the terrestrial installations. However, as it was mentioned in Sect. 3, the direct $\nu_e \rightarrow \bar{\nu}_e + \chi$ decay is not the only possibility for the creation of $\bar{\nu}_e$ signal. In the case of ZKM or Dirac neutrinos, the $\nu_e \rightarrow \bar{\nu}_x + \chi$ decay can occur, which provides $\bar{\nu}_e$'s due to the subsequent oscillation $\bar{\nu}_x \rightarrow \bar{\nu}_e$ during the travel from the sun to the earth. The majoron coupling constant in this case is constrained by (5.33b). However the relevant phase space is smaller in this case due to the fact that $\delta_{e\mu,\tau} \approx 1/3\delta_{ee}$ and $\delta_{es} \approx 1/2\delta_{ee}$. These relations, accounting also for the factor 1/2 due to oscillation, compensate what we could gain for the decay probability owing to the weaker bound on the coupling constant h_{ex} (5.33b). Thus the estimations given in Table 1 remain roughly the same.

§5.2.4 Conclusions

Our main goal in this paper was to investigate the possibility that the solar $\bar{\nu}_e$ flux can be created by the hypothetical matter induced decays in the solar interior: $\nu_e \rightarrow \bar{\nu}_e + \chi$ or $\nu_e \rightarrow \bar{\nu}_x + \chi$ with the subsequent oscillation $\bar{\nu}_x \rightarrow \bar{\nu}_e$ ($x = \mu, \tau, s$). For that reason we have reexamined the features of neutrino decay with majoron emission in the presence of matter background. Our results are not very optimistic. In the future free proton reach real time detectors (like Borex and SuperKamiokande), one can expect few events in one year for fiducial mass in the range of thousands of tons, for $m \leq 10^{-2}$ eV, and $h_{ee}^2 \approx 10^{-6}-10^{-5}$ for the majoron coupling constant. Besides, the analysis of the event spectrum could in principle, allow to discriminate the matter induced decay from other mechanisms of $\bar{\nu}_e$'s production for the special transition regime of $m \approx 10^{-2}$ eV.

However, in principle, the experimental data do not exclude that ν_τ or ν_s have an additional interaction as strong as the weak one. In this case the value of ΔV could be not so small and corresponding the decay probability could be of the order of 10^{-2} in which case the detection of solar $\bar{\nu}_e$ flux could be of experimental relevance. Let us notice that the existence of such interactions

is an unavoidable consequence of most of the models in [96], which could provide enough strong majoron coupling of singlet majoron with neutrinos.

Acknowledgments

It is a pleasure to acknowledge proff. R. Barbieri and S. T. Petcov for continuous encouragement and assistance in my research work and in the development of the present thesis. I would like also to acknowledge for collaboration and many stimulating discussions Z. Berezhiani, G. Fiorentini, M. Lissia, G. Mezzorani, A. Rossi and D. Vignaud with whom many of the results of this thesis have been derived.

- [1]D. D. Clayton, Principles of Stellar Evolution and Nucleosynthesis, 1983 (Chicago: University of Chicago Press)
- [2]J. N. Bahcall and M. H. Pinsonneault, Rev. of Mod. Phys. 64 (1992) 885
- [3]J. N. Bahcall *Neutrino Astrophysics* (Cambridge University Press, Cambridge 1989).
- [4]B. Pontecorvo, Chalk River Laboratory Report No PD-205
- [5]F. Reines and C. L. Cowan Jr., Phys. Rev. 92 (1953) 830.
- [6]R. Davis *et al.*, Phys. Rev. Lett. 20, 1205 (1968)
- [7]R. Davis, Proceedings of the second International Workshop on "Neutrino Telescopes", 1 (1990), ed. M. B. Ceolin;
K. Lande, Talk given at the 15th International Conference on Neutrino Physics and Astrophysics, Granada, Spain (1992)
- [8]S. Turk-Chieze *et al.*, Astrophys. J. 335 (1988) 415;
S. Turk-Chieze, Proceedings of the 15th International Conference on Neutrino Physics and Astrophysics, Granada, Spain (1992), Nucl. Phys. B (Proc. Suppl.) 31 (1993) 111;
S. Turk-Chieze and I. Lopes Astrophys. J. 408 (1993) 347.
- [9]J. N. Bahcall, R. K. Ulrich Rev. of Mod. Phys 60, 297 (1988);
R. B. Sienkiewicz *et al.*, Astrophys. J. 349 (1990) 641;
I. J. Sackman *et al.*, Astrophys. J. 360 (1990) 727;
G. Berthomieu *et al.*, Astron. Astrophys. 268 (1993) 775.
- [10]V. Castellani *et al.*, Astron. Astrophys., 271 (1993) 601.
- [11]K. S. Hirata *et al.*, Phys. Rev. Lett. 58 (1987) 1491;
K. S. Hirata *et al.*, Phys. Rev. D 38 (1988) 449.
- [12]K. S. Hirata *et al.*, Phys. Rev. Lett. 63 (1989) 16.
- [13]K. S. Hirata *et al.*, Phys. Rev. Lett. 65 (1990) 1297.
- [14]Y. Suzuki, talk given at the International Symposium on Neutrino Astrophysics, Takayama Kamioka, Japan, (1992), ICCR-Report-294-93-6
- [15]V. N. Gavrin *et al.*, Proceedings of "Inside the Sun" Conference, Versailles, ed. by G. Berthomieu and M. Cribier (Kluwer Academic, Dordrecht 1989) 201.
- [16]T. Kirstein *et al.*, Proceedings of "Inside the Sun" Conference, Versailles, ed. by G. Berthomieu and M. Cribier (Kluwer Academic, Dordrecht 1990) 187.
- [17]A. I. Abazov *et al.*, Phys. Rev. Lett. 67 (1991) 3332.
- [18]V. Gavrin *et al.*, in Proceedings of the XXVIth International Conference on High Energy Physics, Dallas, Texas.
- [19]Gallex Collaboration, Phys. Lett. B 285 (1992) 376.
- [20]Gallex Collaboration, Phys. Lett. B *in press*.
- [21]J. N. Bahcall and H. A. Behte, Phys. Rev. D (1993) 1299;
V. Castellani *et al.*, Phys. Lett. B 303 (1993) 68;
S. Bludman *et al.*, Preprint UPR-0572T University of Pennsylvania.
- [22]B. Pontecorvo, JETP (Sov. Fiz.) 33, 549 (1957);
B. Pontecorvo, JETP (Sov. Fiz.) 34, 247 (1958)

- [23]V. Gribov and B. Pontecorvo, Phys. Lett. B 82 (1969) 493;
- [24]S. M. Bilenky and B. Pontecorvo, Phys. Rep. 41 (1978) 225
- [25]L. Wolfenstein, Phys. Rev. D 17, 2639 (1978)
- [26]S. P. Mikheyev and A. Yu Smirnov, Yad. Fiz. 42, 1441 (1985);
S. P. Mikheyev and A. Yu Smirnov, Nuovo Cimento C 9, 17 (1986)
- [27]A. Cisneros, Astrophys. Space Sci. 10, 2634 (1979)
- [28]M. B. Voloshin and M. I. Vysotsky, Sov. J. Nucl. Phys. 44 (1986) 544;
L. B. Okun, Sov J. Nucl. Phys. 44 (1986) 546;
M. B. Voloshin *et al.*, Sov. J. Nucl. Phys. 44 (1986) 440;
- [29]E. Kh. Akhmedov, Yad. Fiz. 48 (1988) 599;
E. Kh. Akhmedov, Phys. Lett. B 213 (1988) 64;
C. S. Lim and W. J. Marciano, Phys. Rev. D 37 (1988) 1368.
- [30]J. N. Bahcall *et al.*, Phys. Rev. Lett. 28 (1972) 316;
J. N. Bahcall *et al.*, Phys. Lett. B 181 (1986) 369.
- [31]L. Wolfenstein, Phys. Rev. D 20 (1979) 2634.
- [32]M. M. Guzzo *et al.*, Phys. Lett. B 260 (1991) 155.
- [33]Roulet E. Phys. Rev. D 44 (1992) R935.
- [34]M. Gell-Mann *et al.*, in *Supergravity* edited by P. van Nieuwenhuizen and O. Friedman (North Holland Amsterdam 1979) p. 317;
T. Yanagida, in *Proceedings of the Workshop on Unified Theories and Baryon number in the Universe*, edited by A. Sawada and A. Sugamoto (KEK Tsuba 1979);
B. Stech, in *Unification of Fundamental Particle Interactions* edited by S. Ferrara, J. Ellis and P. van Nieuwenhuizen (Plenum, New York 1980).
- [35]A. Zee Phys. Lett. B 93 (1980) 389.
- [36]K. S. Babu and R. N. Mohapatra, Phys. Rev. Lett. 63 (1989) 228;
R. Barbieri and R. N. Mohapatra Phys. Lett. B 218 (1989) 225;
K. S. Babu and R. N. Mohapatra, Phys. Rev. Lett. 64 (1990) 1705;
H. Georgi and M. Luke, Nucl. Phys. B 347 (1990) 1;
H. Georgi and L. Randall, Phys. Lett. B 244 (1990) 196;
M. Leurer and M. Marcus, Phys. Lett. B 237 (1990) 81;
D. Chang *et al.*, Phys. Rev. D 42 (1990) 1559;
L. Wolfenstein, Nucl. Phys. B 345 (1990) 327.
- [37]S. M. Barr *et al.*, Phys. Rev. Lett. 65 (1990) 2626;
S. M. Barr and E. M. Freire, Phys. Rev. D 43 (1991) 2989.
- [38]J. Goldstone, Nuovo Cim. 19 (1961) 154.
- [39]G. Ewan *et al.*, Technical Report No. SNO-87-12 (unpublished).
- [40]T. Kajita, Report 185-89-2, ICCR (unpublished);
Y, Totsuka Report 227-90-20, ICCR (unpublished).
- [41]C. Arpesella *et al.*, in *BOREXINO proposal* edited by R. R. *et al.*, G. Bellini (University of Milano, Milano 1992), Vol. 1-2.

- [42]G. Fiorentini, M. Lissia, G. Mezzorani, M. Moretti and D. Vignaud, *Solar Neutrino Experiments and Determinations of the Neutrino Oscillation Parameters* (in preparation).
- [43]M. Moretti, Phys. Lett. B 293 (1992) 378.
- [44]R. Barbieri, G. Fiorentini, G. Mezzorani and M. Moretti, Phys. Lett. B 259 (1991) 119.
- [45]Z. Berezhiani, G. Fiorentini, M. Moretti and S. T. Petcov, Phys. Lett. B 264 (1991) 381.
- [46]R. M. Bionta *et al.*, Phys. Rev. Lett. 58 (1987) 1494.
- [47]Z. G. Berezhiani and M. I. Visotsky, Phys. Lett. B 199 (1987) 281.
- [48]J. A. Frieman *et al.*, Phys. Lett. B 200 (1988) 115.
- [49]Z. Berheziani, G. Fiorentini, M. Moretti and A. Rossi, Z. Phys. C 54 (1992) 581.
- [50]Z. Berheziani, M. Moretti and A. Rossi, Z. Phys. C 58 (1993) 423.
- [51]R. Barbieri *et al.*, Phys. Lett. B 90, 249 (1980).
- [52]V. Barger *et al.*, Phys. Rev. D 24 (1981).
- [53]S. M. Bilenky *et al.*, Phys. Lett. B 94 (1980) 495;
 J. Schechter and J. W. F. Valle Phys. Rev. D 22 (1980) 2227;
 I. Yu. Kobzarev *et al.*, Sov. J. of Nucl. Phys. 32 (1980) 823;
 M. Doi *et al.*, Phys. Lett. B 102 (1981) 323.
- [54]B. Kayser, Phys. Rev. D 24 (1981) 110.
- [55]S. Nussinov, Phys. Lett. B 63 (1976) 201;
 L. M. Krauss and F. Wilczek, Phys. Rev. Lett. 55 (1985) 122;
 A. Loeb Phys. Rev. D 39 (1989) 1009.
- [56]V. Barger *et al.*, Phys. Rev. Lett. 65, 3084 (1990);
 A. Acker *et al.*, Phys. Rev. D 43, R1754 (1991);
 V. Barger *et al.*, Phys. Rev. D 43 (1991) 1111;
 P. I. Krastev and S. T. Petcov, Phys. Lett. B 299 (1993) 99.
- [57]A. Halprin, Phys. Rev. D 34 (1986) 3462;
 P. D. Mannheim, Phys. Rev. D 37 (1988) 1935;
 A. J. Baltz and J. Weisner, Phys. Rev. D 37 (1988) 3364.
- [58]P. Langacker *et al.*, Nucl. Phys. B 282 (1987) 589.
- [59]W. C. Haxton, Phys. Rev. Lett. 57, 1271 (1986);
 S. J. Parke Phys. Rev. Lett. 57, 2232 (1986)
- [60]T. Kaneko Prog. Theor. Phys. 78, 532 (1987);
 S. Toshev, Phys. Lett. B 198, 551 (1987);
 S. T. Petcov, Phys. Lett. B 200, 373 (1988);
 M. Ito *et al.*, Prog. Theor. Phys. 79, 13 (1988).
- [61]GALLEX collab., Phys. Lett. B (1992) 390.
- [62]S. A. Blundman *et al.*, Phys. Rev. D 47 (1993) 2220.
- [63]N. Hata and P. Langacker, Preprint UPR-0570T, University of Pennsylvania.
- [64]P. I. Krastev and S. T. Petcov, Phys. Lett. B 299 (1993) 99.
- [65]L. M. Gauss *et al.*, Phys. Lett. B 299 (1993) 94.
- [66]Mikheyev and Smirnov, in Proceedings of Twelfth International Conference on Neutrino Physics

- and Astrophysics, edited by T. Kitagaki and H. Yuta (Singapore World Scientific, 1986) 177;
 E. D. Carlson, Phys. Rev. D 34 (1986) 1454;
 A. Dar and A. Mann Nature 325 (1987) 790;
 Hiroi et al, Prog. Theor. Phys. 78 (1987) 1428;
 A. J. Baltz and J. Weneser, Phys. Rev. D 35 (1987) 528.
- [67] J. M. Bouchez *et al.*, Zeit. fur Phys. C 32 (1986) 499;
 M. Cribier *et al.*, Phys. Lett. B 182 (1986) 89.
- [68] K. S. Hirata *et al.*, Phys. Rev. Lett. 66 (1991) 9.
 K. S. Hirata *et al.*, Phys. Rev. D 44 (1991) 2241.
- [69] K. S. Hirata *et al.*, Phys. Rev. Lett. 65 (1990) 1301.
- [70] J.-P. Poirier, *Introduction to the Physics of the Earth Interior* (Cambridge University Press, Cambridge 1991).
- [71] A. Garcia *et al.*, Phys. Rev. Lett. 67 (1991) 3654.
- [72] N. Tatare *et al.*, Phys. Rev. C 42 (1990) 1694.
- [73] M. Lissia and G. Mezzorani (unpublished).
- [74] K. Khiara, Ph. D Thesis, ICCR, 1992.
- [75] H. Minakata, preprint TMUP-HEL-9006 (1990);
 J. N. Bahcall, Proceedings of "Neutrino 90" Conference, Geneva 1990, Nucl. Phys. B 19 suppl. (1990);
 B. W. Filippone and P. Vogel Caltech preprint (1990).
- [76] G. Fiorentini and G. Mezzorani, Phys. Lett. B 253 (1991) 181.
- [77] Ya. B. Zeldovich, Dokl. Akad. Nauk. SSR 86 (1952) 505;
 E. J. Konopinsky and H. Mahmoud Phys. Rev. 92 (1953) 1045.
- [78] F. Reines *et al.*, Phys. Rev. Lett. 37 (1976) 315;
 A. V. Kyuldjiev, Nucl. Phys. B 243 (1984) 387;
 P. Vogel and J. Engel, Phys. Rev. D 39 (1989) 3378.
- [79] S. I. Blinnikov, Preprint Itep 88-19;
 G. Raffaelt *et al.*, Astrophys. J. 365 (1990) 559;
 R. Barbieri and R. N. Mohapatra, Phys. Rev. Lett. 61 (1988) 27;
 J. Lattimer and J. Cooperstein, Phys. Rev. Lett. 61 (1988) 23;
 D. Notzold, Phys. Rev. D 38 (1988) 1658.
 V. Castellani and S. Degl'Innocenti, Pisa University Preprint.
- [80] J. Schechter and J. W. F. Valle, Phys. Rev. D 24 (1981) 1883;
 B. Kayser Phys. Rev. D 26 (1982) 1662;
 J. F. Neives Phys. Rev. D 26 (1982) 3152.
- [81] J. Vidal and J. Wudka, Phys. Lett. B 249 (1990) 473.
- [82] A. Yu. Smirnov, Pis'ma ZhETF 53 (1991) 280; Phys. Lett. B 260 (1991) 161;
- [83] A. Aneziris and J. Schechter, Syracuse University preprint SU-4228-449, 1990.
 E. Kh. Akhmedov, A Yu Smirnov, P. I. Krastev Z. Phys. C 52 (1991) 701.
- [84] L. B. Okun et al., Sov. J. Nucl. Phys. 44, (1986) 1;

- R. Barbieri and G. Fiorentini, Nucl. Phys. B 304, (1988) 909.
- [85]E. Kh. Akhmedov, Nucl. Phys. A 527 (1991) 679;
 E. Kh. Akhmedov, Phys. Lett. B 257 (1991) 163;
 K. S. Babu *et al.*, Phys. Rev. D 44 (1991) 2265;
 Y. Ono and D. Suematsu, Phys. Lett. B 271 (1991) 165;
 M. Fukugita and T. Yanagida, Phys. Rev. Lett. 65 (1990) 1975.
- [86]K. S. Hirata *et al.*, ICR report 195-89-12 (1989).
- [87]S. T. Petcov, Phys. Lett. B 110 (1982) 245;
 C. N. Leung and S. T. Petcov, Phys. Lett. B 125 (1983) 461;
- [88]M. J. Dugan *et al.*, Phys. Rev. Lett. 54 (1985) 2302.
- [89]V. Zacek *et al.*, Phys. Rev. D 34 (1986) 2621;
 G. S. Vidyakin *et al.*, Sov. Phys. JETP 66 (1987) 243.
- [90]R. Barbieri and G. Fiorentini, Proceedings of the second International Workshop on "Neutrino Telescopes", 1 (1990), ed. M. B. Ceolin.
- [91]K. S. Hirata *et al.*, Phys. Lett. B 205 (1988) 416;
 D. Casper *et al.*, Proceedings of the third International Workshop on "Neutrino Telescopes", (1991), ed. M. B. Ceolin.
- [92]G. B. Gelmini and M. Roncadelli, Phys. Lett. B 99 (1981) 411;
 H. Georgi *et al.*, Nucl. Phys. B 193 (1981) 297.
- [93]Y. Chikashige *et al.*, Phys. Lett. B 98 (1981) 265; Phys. Rev. Lett. 45 (1981) 1926.
- [94]J. W. F. Valle, Phys. Lett. B 131 (1983) 87;
 G. B. Gelmini and J. W. F. Valle, Phys. Lett. B 142 (1984) 181.
- [95]F. Dydak, Proceedings of the XXV HEP Conference, Singapore, August 1990.
- [96]Z. G. Berezhiani *et al.*, Phys. Lett. B 291 (1992) 91.
- [97]J. J. Simpson, Phys. Rev. Lett. 54 (1985) 1891;
 J. J. Simpson and A. Hime, Phys. Rev. D 39 (1989) 1825, 1837;
 A. Hime and N. A. Jelley, Phys. Lett. B 257 (1991) 441;
 B. Sur *et al.*, Phys. Rev. Lett. 66 (1991) 2444.
- [98]E. W. Kolb and M. S. Turner, Phys. Rev. Lett. 67 1991 5;
 A. Hime *et al.*, Preprint OUTP 91-02P (1991);
 G. Gelmini *et al.*, Preprint UCLA/91/TEP/15.
- [99]E. Kh. Akhmedov, Phys. Lett. B 255 (1991) 84.
- [100]R. S. Raghavan, X. G. He and S. Pakvasa, Phys. Rev. D 38 (1988) 1317.
- [101]C. W. Kim and W. P. Lam, Mod. Phys. Lett. A5 (1990) 297.
- [102]S. Nussinov, Phys. Lett. B 185 (1987) 171.
- [103]F. Pierre, Preprint Saclay DPHPE-90-19 (1990).
- [104]M. Doi, T. Kotani and E. Takasugi, Phys. Rev. D 37 (1988) 2575.
- [105]V. Barger *et al.*, Phys. Rev. D 25 (1982) 907.
- [106]A. Manohar, Phys. Lett. B 192 (1987) 217.
- [107]E. W. Kolb and M. S. Turner, Phys. Rev. D 36 (1987) 2895.

- [108]K. Choi et al., Phys. Rev. D 37 (1988) 3225;
J. A. Grifols, E. Masso and S. Peris, Phys. Lett. B 215 (1988) 593;
K. Choi and A. Santamaria, Phys. Rev. D 42 (1990) 293.
- [109]Z. G. Berezhiani and A. Yu. Smirnov, Phys. Lett. B 220 (1989) 279.
- [110]G. B. Gelmini *et al.*, Nucl. Phys. B 209 (1982) 157;
E. W. Kolb *et al.*, Ap. J. Lett. 225 (1982) L57, Nucl. Phys. B 223 (1983) 532.
- [111]K. A. Olive et al., Phys. Lett. B 236 (1990) 454.
- [112]O. Ryazhskaya, in Proceedings of Gran Sasso conference on "Weak Interactions and Neutrino Physics", L'Aquila Italy-July 8-12, 1991, to be published.
- [113]R. Barbieri and L. Hall, Nucl. Phys. B 364 (1991) 27.
- [114]J. Schechter and J. W. F. Valle Phys. Rev. D 25 (1982) 774;
- [115]C. W. Kim, W. P. Lam, in TAUP 89, Proceedings of the Workshop, p. 333, A. Bottino, P. Monacelli, (eds.) L'Aquila, Italy 1989.
C. Giunti *et al.*, Phys. Rev. D 45 (1992) 1557.
- [116]K. Grotz and H. V. Klapdor, Nucl. Phys. A 460 (1986) 395; Phys. Lett. B 153 (1985) 1.
- [117]J. Engel *et al.*, Phys. Rev. C 37 (1988) 731.
- [118]E. Akhmedov *et al.*, Phys. Rev. Lett. 69 (1992) 3013.
- [119]L. M. Krauss *et al.*, Nature 310 (1984) 191.
- [120]R. S. Raghavan *et al.*, AT & Bell Labs. Tech. Memorandum 11121-910204-16, 1991
- [121]P. O Lagage, Nature 316 (1985) 420;
K. Schreeckenbach *et al.*, Phys. Lett. B 160 (1985) 325.